

EVALUATION OF DIFFERENT IN VITRO SURROGATES TO REPRESENT  
NONSPECIFIC BINDING FOR TISSUE: PLASMA WATER PARTITION  
COEFFICIENT PREDICTIONS

---

A Dissertation  
Submitted to  
the Temple University Graduate Board

---

In Partial Fulfillment  
of the Requirements for the Degree  
DOCTOR OF PHILOSOPHY

---

by  
Kimberly L Holt  
December 2019

Examining Committee Members:

Dr. Kenneth Korzekwa, Advisory Chair, Department of Pharmaceutical Science  
Dr. Swati Nagar, Department of Pharmaceutical Science  
Dr. Wayne Childers, Department of Pharmaceutical Science  
Dr. Carlos Barrero, Department of Pharmaceutical Science  
Dr. Christopher Gibson, External Member, Merck, West Point, PA

©  
Copyright  
2019

by

Kimberly Holt  
All Rights Reserved

## ABSTRACT

With the growing use of physiologically-based pharmacokinetic (PBPK) modeling to predict the pharmacokinetics of a drug, accurate prediction of the tissue: plasma water partition coefficients ( $K_{p,\mu}$ ) has become increasingly important. In these predictions, drug-lipid interactions have been traditionally described using the octanol: water partition coefficient ( $\log P$ ) and the vegetable: oil: water partition coefficient ( $\log P_{vo}$ ). However, the  $\log P$  does not fully represent all of the drug interactions with phospholipids, while the  $\log P_{vo}$  is calculated from the  $\log P$  and not determined experimentally. Partitioning into microsomes has been used as a potential surrogate for phospholipid partitioning in our previous steady-state volume of distribution prediction method. Microsomal partitioning is able to act as a total phospholipid partitioning term, representing both acidic and neutral phospholipid interactions. Partitioning into adipocytes potentially can provide an alternative surrogate for describing neutral lipid partitioning in adipose tissue, because of the large presence of neutral lipids in these cells. The purpose of this project is to use microsomal partitioning and adipocyte partitioning in  $K_{p,\mu}$  prediction equations to more mechanistically describe lipid interactions.

A  $K_{p,\mu}$  prediction equation utilizing microsomal partitioning ( $K_{p,mem}$ ) was compared with the Rodgers and Rowland (R&R) equations ( $K_{p,dPL}$ ) in its ability to describe the distribution of nineteen diverse drugs. Values for the fraction unbound in plasma ( $f_{up}$ ) and microsomes ( $f_{um}$ ) were determined experimentally using equilibrium dialysis. The steady-state volume of distribution ( $V_{ss}$ ) and concentration-time profile were predicted using both  $K_p$  prediction methods and PBPK modeling. Overall, the  $K_{p,mem}$  prediction method was able to predict the  $V_{ss}$  and simulate the concentration-time profiles with comparable

accuracy to the  $K_{p,dPL}$  method. When outliers were removed, there was no significant difference in the AAFEs between the two methods, and no significant difference in the average EOC between the methods. However, using microsomal partitioning to represent phospholipid partitioning allows for a more mechanistic prediction of drug distribution.

To represent neutral lipid partitioning in adipose tissue, drug partitioning into differentiated and undifferentiated 3T3-L1 fibroblasts was determined. The 3T3-L1 cells were cultured and differentiated into adipocyte-like cells and were characterized by using BODIPY intensity to represent neutral lipid content. Drugs were partitioned into both cell types, and the fold-difference in BODIPY intensity and partition coefficients was determined. There was a significant difference in the partition coefficient between the two cell types for two drugs (diclofenac and felodipine). However, the resulting partitioning ratios did not increase with an increase in fold BODIPY intensity. Initial modeling attempts were made to determine the influence of neutral lipid partitioning on the adipocyte partition coefficients measured. These attempts suggest that the partitioning into neutral lipids does contribute to the overall partitioning in the cells.

Chapter one describes the project background, rationale, and hypothesis, as well as an introduction to the specific aims. Chapter 2 elaborates on specific aim one and describes the experimental determination of the plasma protein binding and microsomal partitioning. Chapter 3 focuses on specific aim 2, where the two  $K_p$  prediction methods were used for the prediction of the  $V_{ss}$  and concentration-time profile. Chapter 4 explores the development of in vitro assays to describe neutral lipid partitioning in adipose tissue. Chapter five provides background, a summary for both the adipocyte and microsomal partitioning work, and future directions for the project.

## DEDICATION

To my fiancé, Christa, and my family, for their constant love and support.

## ACKNOWLEDGMENTS

Before I came to Temple University, I was attempting to figure out what I wanted to do with my life. I ultimately decided to go to graduate school to study pharmaceutical science, and it has been one of the best decisions I have ever made. This PhD has also been one of the hardest things which I have done. Despite that, I have learned so much over the last five years. Through all the preliminary exams, my proposal, and my many research struggles, I have been supported and encouraged by so many awesome people.

Dr. Ken Korzekwa has been my mentor and teacher throughout my time at Temple. Despite my struggles with writing, he has continuously encouraged me in finishing this dissertation. I also have him to thank for my understanding of PK. Many concepts which seemed entirely foreign to me when I started, have begun to make sense. I also need to thank Dr. Swati Nagar, who while not my advisor, has helped me time and time again. From what to wear to GRC, to how to ask questions, to understanding how we parameterized  $a/b$  in the  $K_p$  equation, she has served as a genuine model of how to be a successful female scientist.

I'd also like to thank the other members of my committee. Dr. Wayne Childers has been very supportive since my first semester at Temple. Dr. Carlos Barrero agreed recently to be on my committee and has never hesitated in his advice and help with my project. Also, I am grateful that Dr. Chris Gibson agreed to serve as my external committee member.

The Korzekwa/Nagar lab has slowly become my second family. Min Ye, Dr. Erickson Paragas, Tirtha Nandi, John Wang, Leonard Hridoy, and Casey Radice, you have all cheered me on this last year and given me so much support. I need to specifically thank,

Casey, Erickson, and John, for reading through all of my chapter drafts and providing valuable feedback and questions. Former lab-mates, Dr. Jaydeep Yadav, Dr. Priyanka Kulkarni, Dr. Aneesh Argikar, Alex Kim, and Dr. Chuong Pham, helped me learn PK and have fun along the way. I learned so much from them on how to be a successful graduate student and scientist. They were always so patient with me, and still give me their unconditional support.

Additionally, though not in our lab, Fang Wang has been vital to the experiments included herein and is one of the best people to have on your team. She helped me with the confocal imaging and moved around her schedule a million times, in order to help me run my cells. She was an awesome collaborator in the cell work, and I could not have done this without her.

So many other people in the School of Pharmacy were crucial to me finishing my work. Min Ye has been an awesome mentor to me from day one and has taught me so much about PBPK modeling and LC-MS/MS method development. I also need to thank Dr. Mario Rico, for always answering my cell culture questions. Truly, the entire faculty and staff of Temple School of Pharmacy has been instrumental in my completion of this project.

I have to thank my family-my mom, dad, brother, and sister. They've always known that I could do this and offered their support when I needed it. Further, none of this would be possible without my fiancé, Christa. She has listened to my presentations, read my chapters, listened to my frustrations, and come with me to the lab when I needed to work on weekends. I could not have finished this without her. Lastly, to my cats, Winnie, Minnie, and Dory, for keeping me company during the many hours of writing and occasionally helping me write (by walking and laying on the keyboard).

## TABLE OF CONTENTS

	page
ABSTRACT .....	iii
DEDICATION .....	v
ACKNOWLEDGMENTS .....	vi
LIST OF FIGURES .....	xii
LIST OF EQUATIONS .....	xiv
LIST OF TABLES .....	xv
ABBREVIATIONS AND DEFINITIONS .....	xvi
CHAPTER 1: INTRODUCTION .....	1
1.1: Background .....	1
1.1.1: Distribution .....	1
1.1.2: Steady-state volume of distribution prediction methods .....	4
1.1.3: Tissue: plasma partition coefficient prediction methods .....	7
1.2: Project Rationale .....	9
1.2.1: Biological lipids .....	9
1.2.2: Improving description method for drug-phospholipid interactions .....	11
1.2.3: Improving description method for drug-neutral lipid interactions .....	13
1.3: Hypothesis .....	14
1.4: Introduction to specific aims .....	15
CHAPTER 2: PLASMA PROTEIN BINDING AND MICROSOMAL PARTITIONING .....	16
2.1: Background/Rationale: .....	16
2.1.1: Background .....	16
2.1.2: Techniques to determine the $f_{up}$ and $f_{um}$ .....	17
2.1.3: Factors which influence measurement of the $f_{up}$ or $f_{um}$ using equilibrium dialysis .....	18
2.2: Materials .....	19

2.3: Methods .....	20
2.3.1: Development of quantification methods of probe drugs .....	20
2.3.2: Equilibrium dialysis .....	22
2.3.3: Determination of the $f_{up}$ and $f_{um}$ .....	23
2.4: Results.....	24
2.4.1: Quantitation methods .....	24
2.4.2: Microsomal partitioning and plasma protein binding.....	24
2.5: Discussion and conclusions .....	26
CHAPTER 3: PREDICTION OF TISSUE - PLASMA PARTITION COEFFICIENTS USING MICROSOMAL PARTITIONING .....	28
3.1: Background/Rationale: .....	28
3.1.1: Differential phospholipid $K_p$ prediction method.....	28
3.1.2: Simulations .....	29
3.1.3: Data analysis .....	31
3.2: Materials .....	32
3.3: Methods .....	32
3.3.1: Probe drug selection and data collection .....	32
3.3.2: Simulations .....	33
3.3.3: $V_{ss}$ predictions.....	38
3.4: Results.....	39
3.4.1: Data collection .....	39
3.4.2: Parameterization of a and b terms.....	40
3.4.3: Steady-state volume of distribution .....	41
3.4.4: Simulations .....	46
3.5: Discussion and conclusions .....	50
CHAPTER 4: REPRESENTING NEUTRAL LIPID PARTITIONING.....	55
4.1: Background/Rationale .....	55

4.1.1: Background.....	55
4.1.2: Cell source .....	56
4.1.3: Differentiation.....	57
4.1.4: Methods of characterization/quantification .....	58
4.1.5: Partitioning assay .....	58
4.2: Materials .....	59
4.2.1: Cell culture and differentiation .....	59
4.2.2: Confocal imaging.....	59
4.2.3: Partitioning.....	60
4.3: Methods .....	60
4.3.1: Cell culture and passaging .....	60
4.3.2: Differentiation of pre-adipocytes to adipocytes.....	62
4.3.3: Cell characterization/neutral lipid quantification.....	64
4.3.4: Partitioning assay .....	66
4.3.5: Data analysis and model development.....	67
4.4: Results.....	68
4.4.1: Confocal microscopy method optimization .....	68
4.4.2: Cell characterization/neutral lipid quantification.....	70
4.4.3: Partitioning.....	74
4.4.4: Initial model development .....	77
4.5: Discussion and conclusions .....	79
CHAPTER 5: SUMMARY AND FUTURE DIRECTIONS.....	81
5.1: Summary.....	81
5.2: Future directions .....	83
REFERENCES CITED.....	88
APPENDIX A: STRUCTURES OF COMPOUNDS .....	101
APPENDIX B: REPRESENTATIVE MASS SPECTROMETRY PARAMETERS.....	106
APPENDIX C: REPRESENTATIVE LC PARAMETERS .....	107

APPENDIX D: REPRESENTATIVE LC-MS/MS CHROMATOGRAMS AND STANDARD CURVES FOR PROBE DRUGS .....	110
APPENDIX E: COMPARTMENTAL MODELS .....	129
APPENDIX G: DRUG SPECIFIC PARAMETERS .....	132
APPENDIX H: CLINICAL DATA .....	134
APPENDIX I: DIFFERENTIAL EQUATIONS FOR PBPK MODEL .....	135
APPENDIX J: BODIPY QUANTITATION METHODS .....	137

## LIST OF FIGURES

	page
Figure 1: Tissue determinants of drug distribution (Holt et al., 2019a). .....	4
Figure 2: Schematic for Oie-Tozer equation. ....	6
Figure 3: Bicarbonate buffer system.....	26
Figure 4: Generic perfusion-limited whole body PBPK model.....	30
Figure 5: Observed versus predicted rat $K_{p,u}$ values from Equation 15.....	41
Figure 6: Observed $V_{ss}$ versus the Predicted $V_{ss}$ .....	42
Figure 7: Simulated concentration-time profiles for basic drugs.....	47
Figure 8: Simulated concentration-time profiles for neutral drugs.....	47
Figure 9: Simulated concentration-time profiles for acidic drugs. ....	48
Figure 10: EOC determination for verapamil. ....	48
Figure 11: Analyzed fields in each well. ....	65
Figure 12: Optimization of BODIPY concentration. Images are at 1 nM BODIPY using 20x magnification. Image on left is BODIPY alone, while image on right is with 2 $\mu$ M midazolam.....	68
Figure 13: Attempt on using BODIPY to identify lipid droplets (20x magnification and 1 nM BODIPY concentration was used). ....	69
Figure 14: Effect of incubation and wash with buffer on attachment of cells (1 nM BODIPY and 20x magnification was used). ....	70
Figure 15: 40x magnification of undifferentiated 3T3-L1 cells (left) and differentiated 3T3-L1 cells (right) (15 nM BODIPY was used).....	71
Figure 16: Quantification of BODIPY intensity in undifferentiated cells (left) and differentiated cells (right) (15 nM BODIPY and 20x magnification was used). ....	71

Figure 17: Heat map of the BODIPY signal in wells used for assay.....	72
Figure 18: Comparison of BODIPY intensity for each well. Q: quinidine, C: caffeine, F: felodipine, D: diclofenac, M: midazolam. ....	73
Figure 19: Comparison of average BODIPY intensity for different compounds. ....	73
Figure 20: Neutral lipid area comparison for different wells. ....	74
Figure 21: Comparison of average partition coefficient between differentiated and undifferentiated cells. ....	74
Figure 22: The fold difference in BODIPY intensity plotted against log of the adipocyte: buffer coefficient from differentiated cells. ....	75
Figure 23: Comparison of the logP and the log of the adipocyte partition coefficient. ....	76
Figure 24: Comparison of the logLKI and log of the adipocyte partition coefficient ratio.....	76
Figure 25: Experimental K <sub>p</sub> plotted against the predicted K <sub>p</sub> . ....	79

## LIST OF EQUATIONS

	page
Equation 1: Definition of volume of distribution. ....	2
Equation 2: Allometric equation. ....	5
Equation 3: Definition of $K_p$ . ....	6
Equation 4: Definition of $V_{ss}$ . ....	7
Equation 5: Tissue: plasma water partition coefficient definition. ....	7
Equation 6: Correction used to account for use of dilutions in assay. ....	23
Equation 7: Correcting for different microsomal protein concentration. ....	24
Equation 8: Determination of the $\log P_{vo}$ from the $\log P$ . ....	33
Equation 9: Determination of the extraction ratio (ER). ....	34
Equation 10: $K_{p,dPL}$ equation for moderate to strong bases. ....	35
Equation 11: The $K_{p,dPL}$ equation for acids, weak bases, and neutrals. ....	35
Equation 12: Association constant for red blood cells. ....	36
Equation 13: $K_{p,u}$ for red blood cells. ....	36
Equation 14: Relationship between the $K_p$ and $K_{p,u}$ . ....	36
Equation 15: $K_{p,mem}$ equation. ....	37
Equation 16: Determination of LKl. ....	38
Equation 17: EOC determination. ....	38
Equation 18: Equation for $V_{ss}$ predictions. ....	39
Equation 19: Determination of the fold error. ....	39
Equation 20: AAFE determination. ....	39
Equation 21: Determination of the adipocyte: buffer partition coefficient. ....	67
Equation 22: Initial model developed to describe lipid interactions. ....	77

## LIST OF TABLES

	page
Table 1: Lipid or lipid surrogate characteristics. ....	10
Table 2: Experimental $f_{up}$ and $f_{um}$ . ....	25
Table 3: Absolute average fold error for $V_{ss}$ predictions using both $K_{p,mem}$ and $K_{p,dPL}$ prediction methods. ....	43
Table 4: Fraction of drugs whose predictions were less than 1.5-, 2-, and 3-fold error.....	44
Table 5: Fold decrease in $V_{ss}$ upon a 2-fold decrease in the $f_{up}$ .....	45
Table 6: Observed and predicted $V_{ss}$ and EOC values for both methods .....	49
Table 7: Differentiating agents. ....	63
Table 8: Comparison of partition coefficients. ....	75
Table 9: Parameter estimates. ....	78
Table 10: Correlation matrix.....	78
Table 11: Structures of probe drugs and internal standards.....	101
Table 12: Representative MS parameters. ....	106
Table 13: Representative LC Parameters.....	107
Table 14: Tissue composition literature data. ....	130
Table 15: Plasma and blood physiological parameters. ....	131
Table 16: Drug specific parameters (Holt et al. 2019b).....	132
Table 17: Clinical data from the literature. ....	134
Table 18: BODIPY quantitation method 1. ....	137
Table 19: BODIPY quantitation method 2. ....	139
Table 20: BODIPY quantitation method 3. ....	141

## ABBREVIATIONS AND DEFINITIONS

A	Amount in the body
AAFE	Absolute average fold error
ADME	Absorption, distribution, metabolism, excretion
AP	Acidic phospholipids
AUC	Area under curve
a1-a3	Identifiers of acids, bases, and neutrals
BODIPY	4,4-Difluoro-1,3,5,7,8-Pentamethyl-4-Bora-3a,4a-Diaza- <i>s</i> -Indacene
BP	Blood to plasma ratio
c-t	Concentration-time
C <sub>1</sub> , C <sub>2</sub>	Different microsomal protein concentrations
c1-c5	Parameterized values for model
Cl	Clearance
CO <sub>2</sub>	Carbon dioxide
C <sub>p</sub>	Concentration of drug in plasma
C <sub>t</sub>	Concentration of drug in the tissue
C <sub>up</sub>	Unbound concentration in the plasma
D	Free Drug
DDI	Drug-drug interaction

DMEM	Dulbecco's Modified Eagle's Medium
DP or DT	Drug bound to protein and/or tissue components
EOC	Exposure overlap coefficient
$f_{apl}$	Fraction acidic phospholipids
FE	Fold error
FBS	Fetal Bovine Serum
$f_{ew}$	Fraction extracellular water
$f_{iw}$	Fraction intracellular water
$f_{nl}$	Fraction neutral lipids
$f_{npl}$	Fraction of neutral phospholipids
$f_{um}$	Fraction unbound in microsomes
$f_{up}$	Fraction unbound in plasma
$f_{ut}$	Fraction unbound in tissue
HCl	Hydrochloric acid
HLB	Hydrophilic-lipophilic balance
IBMX	Methylisobutylxanthine
k	Elimination rate constant
$K_p$	Tissue: plasma partition coefficients
$K_{p,dPL}$	Differential phospholipid $K_p$ prediction method
$K_{p,mem}$	Membrane-based $K_p$ prediction method

$K_{p,u}$	Tissue: plasma water partition coefficients
L	Liters
LC	Liquid chromatography
Lkl	Lipid binding constant
logP	Log of the octanol: water partition coefficient
logP <sub>vo</sub>	Log of the vegetable oil: water partition coefficient
Min	Minimum BODIPY intensity x area value
mL	Milliliters
MRT	Mean residence time
MS	Mass spectroscopy
NCA	Non-compartmental analysis
NL	Neutral lipid
NP	Neutral Phospholipids
P	Octanol: water partition coefficient
PBPK	Physiologically-based pharmacokinetic
PK	Pharmacokinetics
pK <sub>a</sub>	Ionization constant
pK <sub>a,a</sub>	Ionization constant for acids
pK <sub>a,b</sub>	Ionization constant for bases
PPB	Plasma protein binding

$P_{vo}$	Vegetable oil: water partition coefficient
R&R	Rodgers and Rowland
RLM	Rat liver microsomes
RMSE	Root mean squared error
SSE	Sum of squared error
$t_{1/2}$	Half-life
$V_c$	Volume of the central compartment
$V_d$	Volume of distribution
$V_{d,area}$	Terminal phase volume of distribution
$V_p$	Plasma volume
$V_{ss}$	Steady-state volume of distribution
$V_{ss,u}$	Unbound steady-state volume of distribution
$V_t$	Tissue volume
WAT	White adipose tissue
Wt	Weight
1C	One-compartment
2C	Two-compartment
3C	Three-compartment

## CHAPTER 1: INTRODUCTION

**'Reproduced in part' with permission from *Drug Metabolism and Disposition*, Prediction of tissue - plasma partition coefficients using microsomal partitioning: Incorporation into physiologically-based pharmacokinetic models and steady state volume of distribution predictions, 47, 12, 1050-1060. Copyright 2019 The American Society for Pharmacology and Experimental Therapeutics.**

### 1.1: Background

#### 1.1.1: Distribution

It is important to predict the clinical pharmacokinetics (PK) of a drug early in the drug discovery and development process. This helps us to better understand important properties of the compound, such as half-life and dosing regimens, and is necessary when making key program decisions. PK is the study of the time-course of a drug in the body, which is dictated by the rates and extent of drug absorption, distribution, metabolism, and excretion (ADME). Absorption describes the entrance of a drug from the site of administration to the systemic circulation or the site of measurement. Distribution is the reversible movement of drug from the systemic circulation to and from the tissues. Metabolism and excretion are both pathways to eliminate the drug from the body. Through metabolism, a drug molecule is transformed into a different chemical moiety, which is generally a more hydrophilic compound. Excretion describes the elimination of the unchanged drug from the body, for example in the urine, feces, sweat, tears, or breast milk. The disposition of a drug is determined from its elimination, and its distribution. All of the

ADME processes influence the concentration of drug in the plasma, as well as the concentration of drug at the site of action (Rowland and Tozer, 2011).

There are two primary disposition pharmacokinetic parameters: clearance (Cl) and volume of distribution ( $V_d$ ) (Rowland and Tozer, 2011). These primary parameters are dependent on the physicochemical properties of a compound and the physiological properties of the body. Cl and  $V_d$  are used to derive secondary parameters, including half-life ( $t_{1/2}$ ), mean residence time (MRT), area under the curve (AUC), and the elimination rate constant (k) (Gabrielsson and Weiner, 2010). While the Cl describes the elimination of the drug from body in units of flow, volume/time, the  $V_d$  describes the extent to which the drug distributes in the body, in units of volume (milliliters (mL) or liters (L)) (Rowland and Tozer, 2011). The  $V_d$  is defined as a proportionality constant which relates the amount of drug in the body (A) to the concentration of drug in the plasma ( $C_p$ ) or the given sampling matrix (Equation 1). It can also be defined as an “apparent volume of distribution,” and used as the mathematical volume in which the drug distributes in the body (Gabrielsson and Weiner, 2010).

$$V_d = \frac{A}{C_p}$$

Equation 1: Definition of volume of distribution.

The volume of distribution at different stages can be described using three terms: volume of distribution of the central compartment ( $V_c$ ), steady state volume of distribution ( $V_{ss}$ ), and terminal volume of distribution ( $V_{d,area}$ ). The  $V_c$  describes the volume of distribution of the drug immediately following administration and is the smallest volume. The  $V_{d,area}$  is the volume of distribution of the drug when elimination predominates. This

is the largest volume because the proportion of the concentration of drug in the plasma relative to the amount of drug in the body is the smallest. The  $V_{ss}$  describes the volume of distribution at steady state, where it is not influenced by elimination. This term is determined by protein binding, tissue binding, tissue partitioning, transporters, and permeability. The  $V_{ss}$  and  $V_{d,area}$  values are generally similar, unless elimination predominates before distribution has fully occurred (Rowland and Tozer, 2011). All three of the volume terms can be determined from clinical data, using either compartmental modeling or non-compartmental analysis (NCA). The  $V_{ss}$  and  $V_{d,area}$  can be determined using both methods. The  $V_c$ , however, requires the assumption of compartments and can only be determined by compartmental analysis (Gabrielsson and Weiner, 2010).

The distribution is determined by many factors, including physiological components and drug characteristics. Drug characteristics which can influence distribution include the molecular weight, ionization, lipophilicity, protein binding, and binding affinity. Tissue components which contribute to distribution include tissue and organelle pH, blood flow, lipids (phospholipids and neutral lipids), transporters, proteins, and water content (Figure 1) (Rowland and Tozer, 2011; Holt et al., 2019a). Distribution is characterized as perfusion-limited if the drug getting to the tissue is the rate-limitation. It is considered permeability-limited if either the membrane or the transporters are the rate-limiting step. This project focuses on perfusion-limited distribution.

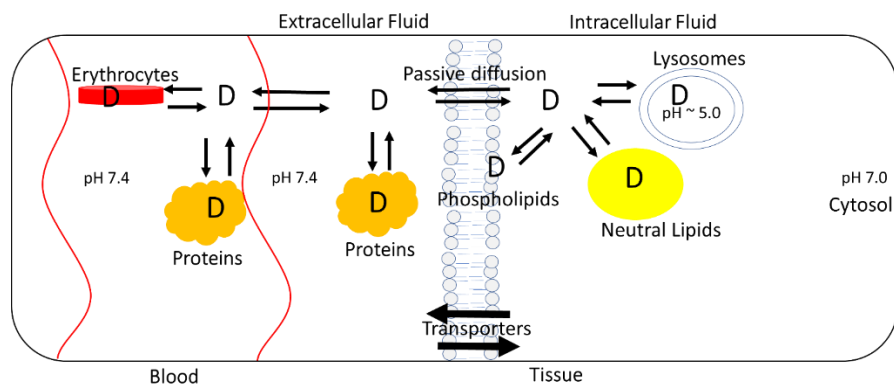


Figure 1: Tissue determinants of drug distribution (Holt et al., 2019a).

### 1.1.2: Steady-state volume of distribution prediction methods

Prediction methods have been developed to determine the  $V_{ss}$  for humans in order to understand the distribution characteristics of a compound early in drug discovery. The  $V_{ss}$  has been determined by preclinical extrapolation (Boxenbaum, 1982; Sawada et al., 1984; Obach et al., 1997; Ward and Smith, 2004), physiological equations (Oie and Tozer, 1979; Lombardo et al., 2002; Lombardo et al., 2004; Korzekwa and Nagar, 2017a), computational methods (Ghafourian et al., 2004; Lombardo et al., 2006; Zhivkova and Doytchinova, 2012a; Freitas et al., 2015; Ruiz and Gomez-Nieto, 2018), and tissue: plasma partition coefficients (Poulin and Krishnan, 1995; Poulin and Theil, 2009; Jones et al., 2011; Graham et al., 2012; Holt et al., 2019b).

Preclinical species are often used to predict the volume of distribution in humans. The  $V_{ss}$  in humans is able to be predicted from the  $V_{ss}$  of the preclinical species because tissue binding is generally conserved across species (Boxenbaum, 1982; Sawada et al., 1984; Rowland and Tozer, 2011). Allometry is a common and frequently used empirical method to compare different physiological properties of different species (Y) by relating

these parameters to the body weight (BW) (Equation 2). The coefficients a and b are determined when the given parameter from multiple species, of various sizes, are compared. Volume of distribution tends to have an exponent (b value) of 1, as there is a conservation in body composition between different mammals. Problems with allometric scaling arise when multiple processes may be occurring, and/or there are species differences in in these processes. There can also be differences in protein expression between species, therefore, plasma protein binding is often corrected for in these volume relationships (Rowland and Tozer, 2011).

$$Y = a (BW)^b$$

Equation 2: Allometric equation.

Gillette defined the  $V_{ss}$  in physiological terms, relating volume of distribution with tissue and plasma binding (Gillette, 1971; Wilkinson and Shand, 1975 ). This equation was further modified by Oie-Tozer to describe drug interactions with extracellular proteins and tissue components (Oie and Tozer, 1979). Figure 2 shows that in this model, the unbound drug (D) is able to distribute into the extracellular and intracellular fluid, where it can interact with proteins (DP) and tissue components (DT). These equations were the first physiological descriptions of  $V_d$ . They have been used to extrapolate preclinical distribution to predict the volume of distribution in humans. However, they have also been used to predict the volume of distribution from in vitro and in silico terms (Obach et al., 1997). The Oie-Tozer model has been subsequently modified to describe other tissue components that can influence the volume of distribution (Lombardo et al., 2002;

Lombardo et al., 2004; Korzekwa and Nagar, 2017a). These models use different in vitro surrogates/ and or assumptions to describe drug-tissue interactions.

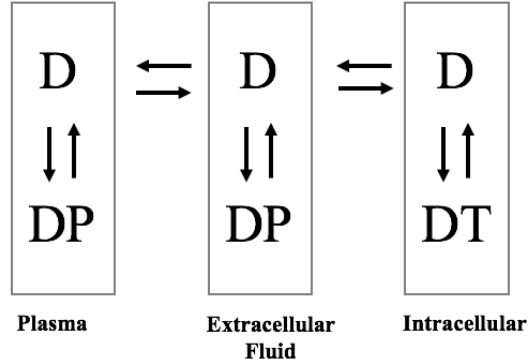


Figure 2: Schematic for Oie-Tozer equation.

$V_{ss}$  can also be predicted from tissue: plasma partition coefficients ( $K_{ps}$ ). These values are required inputs for perfusion-limited whole body PBPK models and describe the affinity of a drug for a given tissue. These values can be used to predict the  $V_{ss}$  early in drug discovery, because they can be predicted from physiological and drug-specific parameters.  $K_{ps}$  are the ratio of the concentration of drug in the tissue ( $C_t$ ) to the concentration of drug in the plasma at steady state (Equation 3). It is a way to quantitatively characterize the affinity of a drug for a given tissue. This value can be used for the prediction of the  $V_{ss}$  because  $K_{ps}$  multiplied by the tissue volumes, describe the volume of distribution of a given organ at steady state. When these values are summed, they describe the  $V_{ss}$  for a given drug (Equation 4), where  $V_p$  is the volume of the plasma and  $V_t$  is the tissue volume.

$$K_p = \frac{C_t}{C_p}$$

Equation 3: Definition of  $K_p$ .

$$V_{ss} = V_p + \sum (V_t \cdot K_p)$$

Equation 4: Definition of  $V_{ss}$ .

### 1.1.3: Tissue: plasma partition coefficient prediction methods

According to the free drug hypothesis, only the unbound, unionized drug in the plasma is capable of distributing into the tissues. In the plasma, the drug is in rapid equilibrium with plasma proteins. A certain fraction of drug is unbound in the plasma and it is possible to correct the  $K_p$  in order to reflect the concentration of drug in the tissue to the unbound concentration of drug in the plasma ( $C_{u,p}$ ). This term is the tissue: plasma water partition coefficients ( $K_{p,u}$ ) (Equation 5). It is often important to think of the  $K_p$  in these terms, as at equilibrium the unbound concentration in the tissues and the plasma is the same.

$$K_{p,u} = \frac{C_t}{C_{u,p}}$$

Equation 5: Tissue: plasma water partition coefficient definition.

$K_p$ s can be determined from *in vivo* (Arundel, 1997; Jansson et al., 2008; Poulin and Theil, 2009), *in vitro* (Clausen and Bickel, 1993; Berry et al., 2010; Berry et al., 2011), computational (Freitas et al., 2015) and composition-based models (Poulin et al., 2001; Björkman, 2002; Berezhkovskiy, 2004; Rodgers et al., 2005; Rodgers and Rowland, 2006). Most  $K_p$  prediction models have attempted to describe the interactions in a given tissue which can drive distribution. *In vitro* methods use tissue homogenates, tissue slices, or cell culture to represent tissue partitioning or determine fraction unbound in tissue. These models are frequently used to describe perfusion-limited distribution; however, often tissue

components can be disrupted which makes description of permeability-limited distribution difficult. In vivo tissue: plasma partition coefficient prediction models use vivo components to describe tissue distribution (Arundel, 1997; Björkman, 2002; Jansson et al., 2008; Poulin and Theil, 2009). These equations require either the  $K_{p,u}$  muscle or the in vivo  $V_{ss}$  in order to predict the  $K_{p,s}$  for the individual tissues. Composition-based prediction models are primarily used since they do not require an in vivo study and allow the  $K_p$  to be predicted early in drug discovery. These are reported to be bottom-up prediction models, which require in vitro and/or in silico inputs, as well as physiological parameters.

Poulin and Krishnan initially developed a composition-based model attempting to describe the interaction of a drug molecule with macromolecules in the tissues. They used three different  $K_p$  equations. The first represented drugs primarily limited to the interstitial space. The second equation represented drugs which distributed outside this space. There was a separate equation for adipose tissue. The  $K_p$  predictions for adipose tissue used the  $\log P_{vo}$  to describe partitioning into neutral lipids. They attempted to describe the make-up of the phospholipid membrane, equating phospholipids to lecithin. From this they described the phospholipid membrane as being equivalent to 30% octanol and 70% water (Poulin and Theil, 2000; Poulin et al., 2001). Berezhkovskiy modified the Poulin model to allow only the unbound drug to interact with macromolecules in the tissues (Berezhkovskiy, 2004).

Rodgers and Rowland (R&R) developed two equations for the prediction of  $K_{p,u}$ , one for acids, neutrals, and weak bases, and one for moderate to strong bases. Their prediction model for  $K_{p,u}$  used the octanol: water partition coefficient ( $\log P$ ), vegetable oil: water partition coefficient ( $\log P_{vo}$ ) and  $f_{up}$  to represent lipid and plasma protein

interactions. They used drug partitioning with erythrocytes to describe the interaction of bases with acidic phospholipids (AP) (Rodgers et al., 2005; Rodgers and Rowland, 2006).

## 1.2: Project Rationale

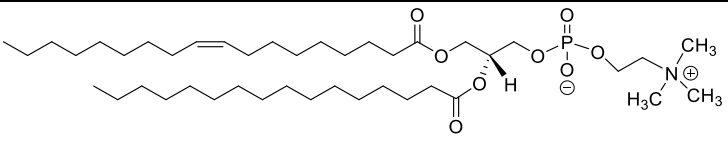
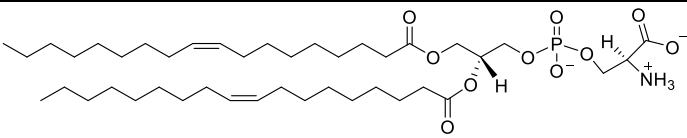
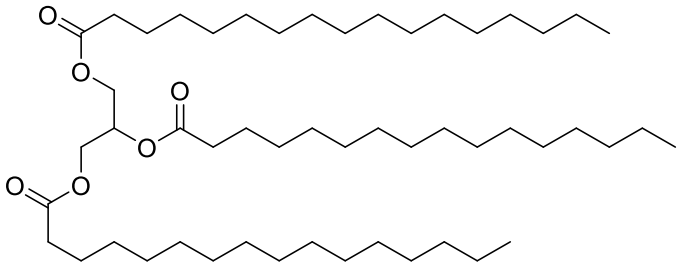
More accurate prediction of  $K_p$ s can ultimately lead to a better understanding of a drug's distribution and pharmacokinetic profile. While it is possible to experimentally determine the  $K_p$ s for a drug in vivo in preclinical species, it is time intensive and costly. If the  $K_p$  is required for a particular organ, it is usually determined experimentally. However, accurate  $K_p$  predictions are required early in drug discovery for use in perfusion limited whole-body PBPK models, as well as for  $V_{ss}$  prediction. Composition based models allow for prediction early in drug discovery and require inputs which can be determined in silico or in vitro for high-throughput predictions. These models attempt to describe the drug-tissue interactions. In the tissues, a drug interacts with different macromolecules, including countless proteins and lipids, as well as organelles within the cells. Drug sequestration into lipids ultimately decreases the unbound tissue concentration. While many models describe these interactions, they are not always completely mechanistic and rely on many assumptions. The goal of this project is to look at different experimental methods for description of lipid interactions in  $K_p$  prediction models, in order to improve the models and be ultimately more mechanistic.

### 1.2.1: Biological lipids

Lipids are a diverse set of macromolecules which are generally insoluble in water and soluble in nonpolar solvents. This broad class of macromolecules include phospholipids, neutral lipids, and steroids. Lipids have diverse biological roles and make

up membranes, store energy, and act as hormones (Nelson and Cox, 2012). Phospholipids are amphipathic and are composed of a hydrophilic head group (which can have a net charge) and hydrophobic “tails”, consisting of long chains of fatty acids (FA). Neutral lipids, which do not have a charge at physiological pH, are generally very lipophilic. Phospholipids have been characterized as being net-neutral (neutral phospholipids) or net-negative (acidic phospholipids). Additionally, functional groups on the hydrophilic head group can have both hydrogen bond acceptors and donors. Examples of these different lipids is presented in Table 1.

Table 1: Lipid or lipid surrogate characteristics.

Lipid or Lipid Surrogate	Structure	Net Charge
Phosphatidylcholine (PC)		0
Phosphatidylserine (PS)		-1
Tripalmitin		0
Octanol	$\text{H}_3\text{C}-\text{C}_7\text{H}_{15}-\text{OH}$	0

### 1.2.2: Improving description method for drug-phospholipid interactions

In all tissues (excluding adipose tissue), phospholipids are the most abundant lipid in the tissue (Nagar and Korzekwa, 2017). Poulin initially described phospholipids as being equivalent to 30% lipid and 70% water. This assumption came from the idea that lecithin (PC) has a hydrophilic-lipophilic balance (HLB) value of 14 (scaled 1-20), which gave it an approximately 70% hydrophilic nature and 30% hydrophobic (lipid) nature. However, lecithin is potentially not a good representative of the phospholipid membrane, primarily because it does not consider the charge which phospholipids have. Compounds with charges tend to have higher HLB values (Korzekwa and Nagar, 2017a).

The lipid portion is represented by the logP (octanol: water partition coefficient) (Poulin and Krishnan, 1995). Octanol is not a lipid but is a common surrogate to represent hydrophobic interactions because of structural similarities to lipids and the presence of both H bond acceptors and donors (Korzekwa et al. 2017). Octanol was traditionally used because of its relationship with lipophilicity (Poulin and Krishnan 1995). The interaction of a drug with phospholipids is difficult to represent using a single solvent system. Phospholipids are a complex system which drugs can interact preferentially with different regions (Balaz, 2009). Drugs can interact with different components of the head group and fatty acid portion (Balaz, 2009; Nagar and Korzekwa, 2017). There are many different properties, besides hydrophobicity, which are influential to phospholipid partitioning, including polar surface area (PSA), H-bond donors, and H-bond acceptors (Nagar and Korzekwa, 2017).

R&R improved descriptions of phospholipid partitioning for bases when they included an acidic phospholipid partitioning term. This term was designated to describe the

electrostatic interaction between the positively charged compounds and the negatively charged phospholipids. Assumptions are made that only the charged fractions (bases only) will interact with acidic phospholipids (AP), while the uncharged fraction will only interact with neutral phospholipids (NP). The interaction is represented by the AP association constant, which is determined from  $K_{p,u}$  for blood cells (Rodgers et al., 2005; Rodgers and Rowland, 2006). This  $K_{p,u}$  contains the blood to plasma ratio (BP), which has been shown to correlate well with the  $V_{ss,u}$  (Korzekwa and Nagar, 2017b). This term does not mechanistically describe partitioning into lipids but is an empirical term to drive phospholipid predictions. These assumptions of the characteristics of the phospholipid membrane and the interactions which drugs will have with it, lead to inaccurate assumptions and deficiencies in the  $K_p$  prediction methods.

Our laboratory published a paper on predictions of  $V_{ss}$  using a different in vitro surrogate to represent phospholipid partitioning. Instead of using the logP, microsomal partitioning was used to represent membrane partitioning. Microsomes are crude endoplasmic reticulum (ER) segments, made up of both neutral phospholipids, and acidic phospholipids. Microsomal partitioning can be predicted or determined experimentally via equilibrium dialysis. Several groups have developed prediction models to describe partitioning into microsomes (Austin et al., 2002; Hallifax and Houston, 2006; Poulin and Haddad, 2011; Nagar and Korzekwa, 2017). Using microsomal partitioning as a surrogate does not rely on as many assumptions as the phospholipid interactions described by previous  $K_p$  prediction methods. It includes interactions with both AP and NP and is therefore one phospholipid partitioning term. Both the charged and uncharged drug interact

with the microsomes. The interaction with the microsomes is represented by many different descriptors and using this term allows the predictions to be more mechanistic.

### 1.2.3: Improving description method for drug-neutral lipid interactions

Poulin and Krishnan replaced the logP with the logP<sub>vo</sub> to better describe neutral lipid partitioning in adipose tissue. The composition of adipose tissue varies greatly compared to other tissues. Vegetable oil is thought to be a good surrogate because it is composed of a mixture of simple and mixed triglycerides (Poulin et al., 2001; Nelson and Cox, 2012). However, generally the logP<sub>vo</sub> is not experimentally determined, but determined from the logP. Initially, the logP<sub>vo</sub> was determined by using the air to vegetable oil, and the water to air partition coefficient for a group of small volatile compounds. Partitioning into these immiscible phases were related to the logP. Equations relating partitioning into different immiscible phases to the logP were developed early on (Leo et al., 1971). Separate equations for hydrogen bond donors/acceptors were developed. However, the original compounds used in these relationships are not representative of drugs today for which this relationship is used. For many compounds, this relationships leads to large errors in the predicted logP<sub>vo</sub> (Korzekwa and Nagar, 2017b).

This project proposes to use experimental partitioning into adipocytes and triglycerides to represent neutral lipid (NL) partitioning. Adipocytes, also known as lipocytes or fat cells, make up adipose tissue and have a large quantity of neutral lipids in the form of triglycerides (also known as triacylglycerols). Triglycerides are defined as three fatty acid chains connected via ester linkages to one glycerol molecule. These lipids are in a low oxidation state, similar to hydrocarbons in fuel (Nelson and Cox, 2012). The triglycerides present in adipose tissue are predominantly stearic, oleic, linoleic, linolenic

palmitic, palmitoleic, and myristic acid (Dawkins and Stevens, 1966 ; Singer et al., 1977; Body, 1988; Kunesova et al., 2012). Inside the adipocytes, these triglycerides are stored in globules (also called lipid droplets or adiposomes). The globule takes up most of the cell and other organelles are pushed to the periphery.

Partitioning into adipocytes has potential as a neutral lipid partitioning surrogate, since the presence of adiposomes provides a large storage of NL. In adipose tissue, there is 40-fold more neutral lipids than in any other tissue. The average fraction of neutral lipids in adipose tissue is 0.853, while the average fraction of neutral lipid in other tissue is 0.024 (Ye et al., 2016). If the extent of partitioning can be determined in adipocytes, then it may be able to be used in the  $K_p$  predictions to represent NL, including neutral lipid partitioning in adipose tissue.

### 1.3: Hypothesis

The goal of this project is to more mechanistically and accurately describe lipid interactions in the tissues. Not only is this helpful for predicting  $K_p$ s, but can improve PBPK models, as well as  $V_{ss}$  predictions. By parameterizing phospholipid and neutral lipid partitioning differently, using microsomal and adipocyte partitioning, we can hopefully improve the  $K_p$  predictions.

#### 1.4: Introduction to specific aims

There are four specific aims for this project:

1. Experimentally determine the plasma protein binding and the tissue partitioning for the test compounds.
2. Determine how well the  $K_{p,mem}$  method is able to predict the  $V_{ss}$  and concentration-time profile for test drugs compared to the  $K_{p,dPL}$  method.
3. Partition drugs into adipocytes to represent the interaction with neutral lipids in adipose tissue.
4. Incorporate experimental adipocyte partition coefficients into workable model.

**Figure 1 used with permission from Current Pharmacology Reports, Methods to Predict Volume of Distribution, 5, 391-399. Copyright 2019 Springer Nature.**

## CHAPTER 2: PLASMA PROTEIN BINDING AND MICROSOMAL PARTITIONING

**'Reproduced in part' with permission from *Drug Metabolism and Disposition*,**

**Prediction of tissue - plasma partition coefficients using microsomal partitioning:**

**Incorporation into physiologically-based pharmacokinetic models and steady state**

**volume of distribution predictions, 47, 12, 1050-1060. Copyright 2019 The American**

**Society for Pharmacology and Experimental Therapeutics.**

### 2.1: Background/Rationale:

#### 2.1.1: Background

Both the plasma protein binding (PPB) and microsomal partitioning are important considerations in PK since they can be used to determine the unbound concentration in either plasma or a microsomal preparation. It is the unbound drug which can interact with enzymes and distribute into the tissues. Inaccurate  $f_{up}$  and  $f_{um}$  values can influence the accuracy of subsequent predictions, including the  $V_{ss}$ ,  $K_{ps}$ , drug-drug interactions (DDIs), and Cl. While the  $f_{um}$  is frequently predicted (McLure et al., 2000; Austin et al., 2002; Hallifax and Houston, 2006; Poulin and Haddad, 2011; Nagar and Korzekwa, 2017), the  $f_{up}$  is difficult to predict (Korzekwa, 2016). However, several models have been developed to predict the fraction unbound in plasma, albumin, or AAG (Hall et al., 2003; Zhivkova and Doytchinova, 2012b; Lambrinidis et al., 2015; Korzekwa, 2016; Zhivkova, 2017; Sun et al., 2018; Watanabe et al., 2018). In vitro assays are frequently used to determine these values. However, especially for highly bound drugs, there is variability associated with these values (Di et al., 2017).

For this project, a modified  $K_p$  prediction method,  $K_{p,mem}$ , is compared with the  $K_{p,dPL}$  method. The  $K_{p,dPL}$  method is fairly insensitive to changes in  $f_{up}$ , but the  $K_{p,mem}$  prediction method is influenced more dramatically by errors in the  $f_{up}$  (Ye et al., 2016; Korzekwa and Nagar, 2017a; Holt et al., 2019b). Values found in the literature can be inaccurate due to inappropriate assays or experimental error. Therefore, plasma protein and microsomal partitioning values were measured in house to ensure that accurate inputs were used for the  $K_p$  predictions.

#### 2.1.2: Techniques to determine the $f_{up}$ and $f_{um}$

Several in vitro methods exist to measure the fraction unbound in a given matrix. These include methods which physically separate the bound and unbound state, as well as techniques which are able to distinguish between the bound and unbound drug. The most common methods used are ultracentrifugation, ultrafiltration, and equilibrium dialysis. Equilibrium dialysis is the most popular method because of its ability to reduce the consequences of nonspecific binding to the apparatus (Fessey et al., 2007). In equilibrium dialysis, two cells are separated by a semi-permeable membrane with the matrix on one side and a buffer on the other side. The fraction unbound is determined after allowing the apparatus to rotate in an incubator until equilibrium is achieved, where the unbound concentration is equal on either side of the membrane. It is moderately high-throughput and important experimental considerations can be controlled, for example the pH of the system. For these reasons, equilibrium dialysis was used to determine the  $f_{up}$  and the  $f_{um}$  for our compounds.

### 2.1.3: Factors which influence measurement of the $f_{up}$ or $f_{um}$ using equilibrium dialysis

The in vitro system should model the in vivo condition as closely as possible. Therefore, the pH of the system needs to be controlled. The pH of the blood is maintained between 7.35 and 7.45 in the body due to buffering systems in place, primarily carbonic anhydrase. When conducting PPB experiments, it is necessary to keep the pH at 7.4. This includes adjusting the pH prior to the experiment, using an incubator set at 5% carbon dioxide (CO<sub>2</sub>), and using a strong buffer. Prior studies have shown that without controlling CO<sub>2</sub>, the pH of the plasma will increase and the binding to plasma proteins will change. Kochansky et al. found that from 55 compounds tested, there was an average of 2.3-fold difference between the  $f_{up}$  found with CO<sub>2</sub> and the  $f_{up}$  found without CO<sub>2</sub> (Kochansky et al., 2008). Curran et al determined that using 5% CO<sub>2</sub> and a strong buffer was required to keep the plasma at pH 7.4, and that deviations from pH 7.4 led to changes in the measured fraction unbound in plasma (Curran et al., 2011).

Other experimental details need to be considered. To avoid volume shifts, the appropriate volume, as well as a buffer with appropriate strength needs to be used. The stability of the drug in the medium are crucial as well and this can often determine the incubation time used. Other factors, including nonspecific binding to the apparatus and solubility in the medium need to be considered, as this can influence the movement of the drug across the membrane and the unbound concentration. Low drug concentrations are generally used (approximately 2  $\mu$ M), and saturation of protein binding and membrane partitioning is not expected. However, assays can be done both at a low drug concentration, as well as at therapeutic concentration (Kwon, 2002). Lastly, the plasma quality and

preparation needs to be considered. While fresh plasma would be preferred, frozen plasma is usually used because of convenience.

The microsomal partitioning depends on the microsomal protein concentration used. Assays done at a higher microsomal protein concentration will have more partitioning (and therefore a lower  $f_{um}$ ). Often lower microsomal protein concentrations are used to create a scenario with less drug partitioning, and therefore a higher unbound fraction. This can allow for easier and more accurate measurements. The partitioning at different microsomal concentrations can be determined using an equation from Austin et al 2002 (Austin et al., 2002).

Human plasma was used because of species differences in protein binding. For 10% of current drugs, there is as high as a 5-fold difference in the  $f_{up}$  between species with the greatest being a 16-fold difference (Fessey et al., 2007). While plasma proteins, including albumin, share structural and functional homology, as well as similar concentrations in the blood across species, differences in the amino acid sequences in the binding sites can lead to differences in the extent of protein binding. Tissue partitioning, however, is considered to be similar across species. For these reasons, human plasma is used for determination of the  $f_{up}$  in humans. Rat liver microsomes (RLM) are used instead of human liver microsomes for membrane partitioning because of similarities between tissue partitioning.

## 2.2: Materials

A Harvard Apparatus 96-well equilibrium dialyzer and single-plate Harvard Apparatus (Holliston, MA) plate rotator were used for equilibrium dialysis experiments. Human plasma was obtained from U.S. Biological (Salem, MA) and Innovative Research

Inc (Novi, MI). Rat liver microsomes (RLM) were obtained from BD Biosciences (San Jose, CA) and Corning Life Sciences (Tewksbury, MA). Warfarin, fluconazole, glyburide (glybenclamide), ketoprofen, fenofibrate, +/- cis diltiazem hydrochloride, +/- verapamil hydrochloride, caffeine, betaxolol hydrochloride, dimethyl sulfoxide (DMSO), nicardipine hydrochloride, metoprolol tartrate, felodipine, and nafcillin sodium were obtained from Sigma Aldrich (St. Louis, MO). Quinidine gluconate, formic acid, acetonitrile, and diphenhydramine hydrochloride were obtained from Fisher Scientific (Norristown, PA). Mibefradil hydrochloride was obtained from Cayman Chemical Company (Ann Arbor, MI). Diclofenac sodium was obtained from Calbiochem (Burlington, MA). Fenofibric acid was obtained from Kano Laboratories (Nashville, TN). One mg/mL solutions of phenytoin, diazepam, and midazolam in methanol were obtained from Cerilliant (a Sigma Aldrich company). The 100 mM PBS and 0.3 mM MgCl<sub>2</sub> dialysis buffer was composed of magnesium hydrochloride hexahydrate (Fisher Scientific), potassium phosphate monobasic (Sigma), and potassium phosphate dibasic (Fisher Scientific). An Agilent 1100 HPLC and API 4000 mass spectrometer and Agilent 1100 HPLC and API 4000 Q-Trap mass spectrometer were used to determine the concentrations for equilibrium dialysis.

## 2.3: Methods

### 2.3.1: Development of quantification methods of probe drugs

LC and MS parameters were determined for all test compounds using an Agilent 1100 HPLC and AB SCIEX API 4000 mass spectrometer, and an Agilent 1100 HPLC and AB SCIEX API 4000 Q-trap mass spectrometer. A 100 ng/mL drug solution in 50:50 acetonitrile (ACN)/water solution was infused into the MS at a rate of 10  $\mu$ L/min using a

Harvard Apparatus syringe pump and a one mL syringe. Some drugs were initially optimized using Compound Optimization mode, which gives an initial declustering potential (DP), collision energy (CE), and collision cell exit potential (CXP). Following compound optimization, manual tuning was used to further optimize these parameters. In Q1 MS mode, the parent ion conditions were optimized. The temperature of the source was set to 400 degrees Celsius (C). The optimal DP, or the DP which gave the highest intensity for the parent ion, was determined by ramping the parameter from 0 to 150 in increments of three.

Following optimization of the DP, the daughter ion was optimized in Product Ion Mode (MS2). The CE was determined by ramping the parameter from 5 to 130 volts in increments of 3. The CXP was optimized by ramping the parameter from 0 to 55 volts in increments of 1. The CE and CXP which gives the highest daughter ion signal was chosen. Another parameter which can be optimized was the collision gas (CAD), which can vary from 4 to 12 volts. Generally, the higher the CAD, the higher the signal. The parent and daughter ion were monitored together in multiple reaction monitoring mode (MRM).

An LC-MS/MS method was then developed in order to get chromatographic separation of the drug. An optimal method was selected in which the drug is retained on the column and has an appropriate peak height (based on desired sensitivity). An internal standard was selected which had similar physiochemical characteristics (will come out in same method) and could be run on the same method as the analyzed drug. A Luna 3  $\mu\text{m}$  C18 (2) 100A, 30 x 2 mm column was used for all compounds.

Stock solutions of the test compounds were made in DMSO to make 10 mg/mL solutions. These solutions were diluted to 1 mg/mL (in DMSO) and then further into 10

$\mu\text{g/mL}$  in 50:50 acetonitrile and water. For equilibrium dialysis experiments, the standard curve was created in the matrix of interest (either human plasma or RLM (0.5 mg/mL solutions) which encompassed both the buffer and matrix concentrations (ranging from 4000 ng/mL to 1.9 ng/mL). For partitioning assays, the standard curves were made in blank buffer. For drugs with a fraction unbound close to one, a more condensed standard curve was used in order to differentiate between concentrations in the buffer/matrix side. Standard curve samples, from equilibrium dialysis experiments, were prepared for LC-MS/MS analysis by addition of 25  $\mu\text{L}$  of standard in matrix, 25  $\mu\text{L}$  of the buffer, and 100  $\mu\text{L}$  of internal standard in ACN. For the partitioning assay, 20  $\mu\text{L}$  of the buffer, and 40  $\mu\text{L}$  of internal standard in ACN were prepared for LC-MS/MS. Standard curves were tested to determine if the LC-MS/MS method had appropriate sensitivity, accuracy, and was linear throughout the concentration-range required.

### 2.3.2: Equilibrium dialysis

Equilibrium dialysis was used to determine the fraction unbound in plasma ( $f_{\text{up}}$ ) and microsomes ( $f_{\text{um}}$ ) for the probe drugs using a protocol modified from prior studies (Kochansky et al., 2008; Curran et al., 2011; Di et al., 2017). Human plasma was adjusted to pH 7.4 by adding 1 M HCl. For  $f_{\text{um}}$  determination, a 0.5 mg/mL rat liver microsomal solution was prepared from a 20 mg/mL pooled rat liver microsome stock solution. For highly bound compounds, a dilution method was used. Plasma was diluted using a 100 mM phosphate buffer and 3 mM  $\text{MgCl}_2$  solution to either 50% or 10% plasma. A 50% dilution of plasma was used for warfarin, while a 10% dilution was used for ketoprofen, nicardipine, glyburide, diclofenac, felodipine, and mibefradil. Drug solutions (2  $\mu\text{M}$ ) in either plasma or microsomes were added to wells on one side of the dialyzer, and blank 100 mM

phosphate buffer with 3 mM of MgCl<sub>2</sub> was added to the other side. The dialyzer plate was placed in the plate rotator, set to a speed of approximately 22 rotations per minute, and incubated for 22 hours at 37 degrees Celsius and 5% CO<sub>2</sub>. LC-MS/MS was used for the determination of the concentration of drug in the buffer and the matrix.

### 2.3.3: Determination of the $f_{up}$ and $f_{um}$

The fraction unbound in a given matrix was determined by dividing the concentration of drug on the buffer side by the concentration of drug on the matrix side. For protein binding experiments using the dilution method, the  $f_{up}$  is calculated by Equation 6, where  $D$  is the dilution factor,  $f_{u,d}$  is the fraction unbound in plasma measured in the diluted matrix, and  $f_{up}$  is the fraction unbound in plasma.

$$f_{up} = \frac{1/D}{\left(\left(\frac{1}{f_{u,d}}\right) - 1\right) + 1/D}$$

Equation 6: Correction used to account for use of dilutions in assay.

Experimental  $f_{um}$  values were measured at microsomal concentrations between 0.5 mg/mL and 2 mg/mL, and converted to values for 1 mg/mL (Equation 7) (Austin et al., 2002), where  $f_{u2}$  is the corrected unbound fraction,  $C_2$  is the 1 mg/mL microsomal protein concentration,  $C_1$  is the microsomal protein concentration used in assay, and  $f_{u1}$  is the fraction unbound in matrix measured during the assay. The average fraction unbound, standard deviation (SD), and the coefficient of variation (CV) were determined for each assay.

$$f_{u2} = \frac{1}{\frac{C_2}{C_1} \left( \frac{1 - f_{u1}}{f_{u1}} \right) + 1}$$

Equation 7: Correcting for different microsomal protein concentration.

## 2.4: Results

### 2.4.1: Quantitation methods

LC-MS/MS methods were developed for all 19 compounds. An LC-MS/MS method was developed for caffeine in microsomes, but a method for drug in plasma was not developed because of the contamination of caffeine in the commercially available plasma source. Appendix B contains the MS Operating Parameters for the probe drugs and internal standards. Appendix C displays the LC conditions. Representative standard curves and chromatograms can be found in Appendix D.

### 2.4.2: Microsomal partitioning and plasma protein binding

Microsomal partitioning and PPB were determined for the probe compounds. The results are shown in Table 2. For caffeine, no protein binding value was able to be determined because of the contamination in commercially bought human plasma. Protein binding has been measured for many of the compounds, under different conditions. Originally, 10% CO<sub>2</sub> was used in the incubation, but in order to best buffer the plasma, 5% CO<sub>2</sub> is currently used. For some drugs, the change in CO<sub>2</sub> has no effect (ex. metoprolol), however, for other drugs, there is a change in the measured  $f_{up}$  when the CO<sub>2</sub> is increased (Table 2). Microsomal partitioning was run at either 5% and/or 10% CO<sub>2</sub>. The CO<sub>2</sub> did not influence the fraction unbound in microsomes, and therefore, values were not rerun at 5% CO<sub>2</sub>.

Table 2: Experimental  $f_{up}$  and  $f_{um}$ .

Compound	$F_{up}$ , 0%*	$F_{up}$ , 10%	$F_{up}$ , 5%	$F_{um}$ , 10%	$F_{um}$ , 5%	Predicted $F_{um}$ ***
Betaxolol	0.436-0.439	0.59 (3%)	0.50 (12%)	0.77 (3%)	x	0.65
Diphenhydramine	0.26-0.28	0.32 (9%)	0.43 (4%)	0.71 (4%)	0.83 (4%)	0.7
Metoprolol	0.83-0.87	0.87 (12%)	0.83 (11%)	0.8 (3%)	x	0.84
Nicardipine	0.0013-0.0017	0.0023 (17%)	0.0024 (7%)	0.039 (12%)	x	0.063
Caffeine	0.55-0.67	x	x	x	0.98** (4%)	0.98
Midazolam	0.027-0.030	0.036 (4%)	0.026 (17.1%)	0.71 (4%)	0.68 (6%)	0.65
Glyburide	0.0015-0.0017	0.0052 (17%)	0.0012 (16%)	0.9 (17%)	0.72 (9%)	0.91
Ketoprofen	x	0.0297 (15%)	0.0041 (9%)	0.90 (4%)	x	0.85
Warfarin	x	x	0.0076 (13%)	x	0.98 (16%)	0.85
Nafcillin	x	x	0.123 (6%)	x	0.94 (14%)	0.84
Diclofenac	x	x	0.0014 (18%)	x	0.78 (4%)	0.910
Diazepam	x	x	0.012 (9%)	x	0.74 (4%)	0.63
Felodipine	x	x	0.0017 (12%)	x	0.023 (27%)	0.110
Fluconazole	x	x	0.93 (14%)	x	0.94 (14%)	0.97
Phenytoin	x	x	0.18 (7%)	x	0.83 (3%)	0.9
Quinidine	x	x	0.15 (8%)	x	0.815 (10%)	0.55
Verapamil	x	x	0.088 (20%)	x	.37 (19%)	0.4
Diltiazem	x	x	0.76 (8%)	x	0.48 (2%)	0.75
Mibefradil	x	x	0.031 (11%)	x	0.034 (15%)	0.010

\*n=2, range of values shown, \*\*x: not determined, \*\*\*F<sub>um</sub> values were predicted using method from Nagar et al 2017.

## 2.5: Discussion and conclusions

LC-MS/MS methods were developed for all compounds and had acceptable sensitivity for plasma protein binding and microsomal partitioning. The fraction unbound in plasma and microsomes were determined for the probe drugs to be utilized in the K<sub>p</sub> predictions and PBPK modelling. Plasma protein binding was originally conducted with and without CO<sub>2</sub> for eight compounds. This was done to reiterate that the pH of the equilibrium dialysis system was important in the determination of the f<sub>up</sub> and f<sub>um</sub>. PPB protocols were ultimately optimized according to new recommended protocols (Curran et al. 2011, Di et al 2017).



Figure 3: Bicarbonate buffer system

The pH in the plasma is controlled by the bicarbonate buffer system (Figure 3). In the body, the plasma pH is maintained by the presence of carbonic anhydrase in blood cells, plasma proteins, and other endogenous molecules (Lehninger, 2012). The equilibrium dialysis system loses CO<sub>2</sub> to the environment, when CO<sub>2</sub> is not present during the incubation. This leads to the pH of the solution to increase. When 10% CO<sub>2</sub> is used, the pH of the system will decrease (pH of blank plasma was measured to be ~7) (Curran et al. 2011). 5% CO<sub>2</sub> has been recommended in order to keep the pH at 7.4 (Di et al. 2017, Curran et al 2011). Because there is a change in the pH, there is a drug-specific change in the f<sub>up</sub> measured (Kochansky et al., 2008; Curran et al., 2011). For some compounds, changes in CO<sub>2</sub> concentrations do not lead to a significant change in the protein binding measured, for example metoprolol. For more highly bound compounds, for example glyburide and

nicardipine, changes in the pH can dramatically change the experimental  $f_{up}$ . Plasma protein values for highly bound compounds can have a lot of variability (Di et al., 2017) and other methods, for example the dilution method, are recommended to mitigate variability. For these compounds, the dilution method was done in order to get more accurate values.

Microsomal partitioning values are very similar to the values predicted using model developed in Nagar et al. 2017. Microsomal partitioning is not significantly influenced by differing CO<sub>2</sub> concentrations, as they do not have the bicarbonate-buffer system present. Therefore, either 5% or 10% CO<sub>2</sub> levels are acceptable.

Modifications to this current equilibrium dialysis protocol could be done to ensure that the  $f_{up}$  and  $f_{um}$  values are representative of drug binding in the body. Determination of the  $f_{up}$  and  $f_{um}$  values at different time points (for example, at 6 hours, 12 hours, and 22 hours), could ensure that equilibrium has been met. Also, different drug concentrations could be used, for example one at sub-saturation levels, and the therapeutic concentration found in plasma. This would determine whether there are any nonlinearities in binding.

CHAPTER 3: PREDICTION OF TISSUE - PLASMA PARTITION COEFFICIENTS  
USING MICROSOMAL PARTITIONING

**'Reproduced in part' with permission from *Drug Metabolism and Disposition*,  
Prediction of tissue - plasma partition coefficients using microsomal partitioning:  
Incorporation into physiologically-based pharmacokinetic models and steady state  
volume of distribution predictions, 47, 12, 1050-1060. Copyright 2019 The American  
Society for Pharmacology and Experimental Therapeutics.**

3.1: Background/Rationale:

3.1.1: Differential phospholipid  $K_p$  prediction method

In most currently used composition-based models,  $\log P$  is used to model the phospholipid partitioning (0.3 P). A shortcoming of using  $\log P$  to represent phospholipid partitioning is the lack of orientation-specific interactions with phospholipid membranes (Balaz, 2009; Nagar and Korzekwa, 2012; Nagar and Korzekwa, 2017). Additionally, both neutral and ionized bases are known to interact with all phospholipids, and not just net-neutral and net-acidic phospholipids, respectively. Therefore, current methods to calculate  $K_p$  appear to be based on mechanistically unsound assumptions. Previously, we used microsomal partitioning ( $f_{um}$ ) instead of  $\log P$  to parameterize phospholipid partitioning in  $V_{ss}$  model (Korzekwa and Nagar, 2017a). Partitioning into microsomes (unsorted phospholipid vesicles) is used extensively in clearance predictions, can be determined experimentally, or can be predicted (Austin et al., 2002; Halifax and Houston, 2006; Poulin and Haddad, 2011; Nagar and Korzekwa, 2017). A benefit of using  $f_{um}$  to represent

phospholipid partitioning is that it measures interactions with all phospholipids for both charged and uncharged species.

Previous studies have compared different  $K_p$  prediction methods and their ability to predict both tissue  $K_p$  and/or  $V_{ss}$  (De Buck et al., 2007; Poulin and Theil, 2009; Jones et al., 2011; Graham et al., 2012; Zou et al., 2012; Chan et al., 2018). These studies came to different conclusions on the most accurate  $K_p$  model, primarily dependent on the drug dataset used (De Buck et al., 2007; Graham et al., 2012). Graham et al. showed that the R&R method was able to better predict  $K_p$  and  $V_{ss}$  for different classes of drugs than other composition-based models. The Poulin and Theil method led to good  $V_{ss}$  predictions, but required in vivo data (ex.  $K_{p,u}$  muscle) (Poulin and Theil, 2009; Graham et al., 2012). More recently, the ability of composition-based  $K_p$  models and preclinical extrapolation methods to predict the  $V_{ss}$  were compared (Chan et al., 2018). Composition-based models predicted  $V_{ss}$  with accuracy similar to preclinical extrapolation. They noted that the Rodgers method was able to predict  $V_{ss}$  well for drugs with logP values less than 3, and that many drugs with large errors in  $V_{ss}$  for composition-based models, also had errors in preclinical extrapolation (Chan et al., 2018). Since the R&R method is considered the gold standard for  $K_{p,u}$  predictions, our  $K_{p,u}$  prediction model is compared to this method for its ability to predict the  $V_{ss}$  and simulate the concentration time profile for a set of 19 drugs. This method is referred to as the  $K_{p,dPL}$  method throughout this paper, as the phospholipid interactions for neutrals and ionized bases are described using two distinct terms.

### 3.1.2: Simulations

In PK several different types of models are used, including physiologically based pharmacokinetic models (PBPK), compartmental models, hybrid models, and

mathematical models. PBPK models can be used to predict drug disposition early in drug discovery. PBPK models are a type of physiological model which considers physiological parameters, like flow rates and tissue volumes, in order to describe the concentration-time profile. The different organs of the body are represented as different compartments which are connected together via the arterial and venous blood compartments (Figure 4). Differential equations are used to describe the change in concentration with time in these tissue compartments. These models require both physiological and drug-specific inputs.

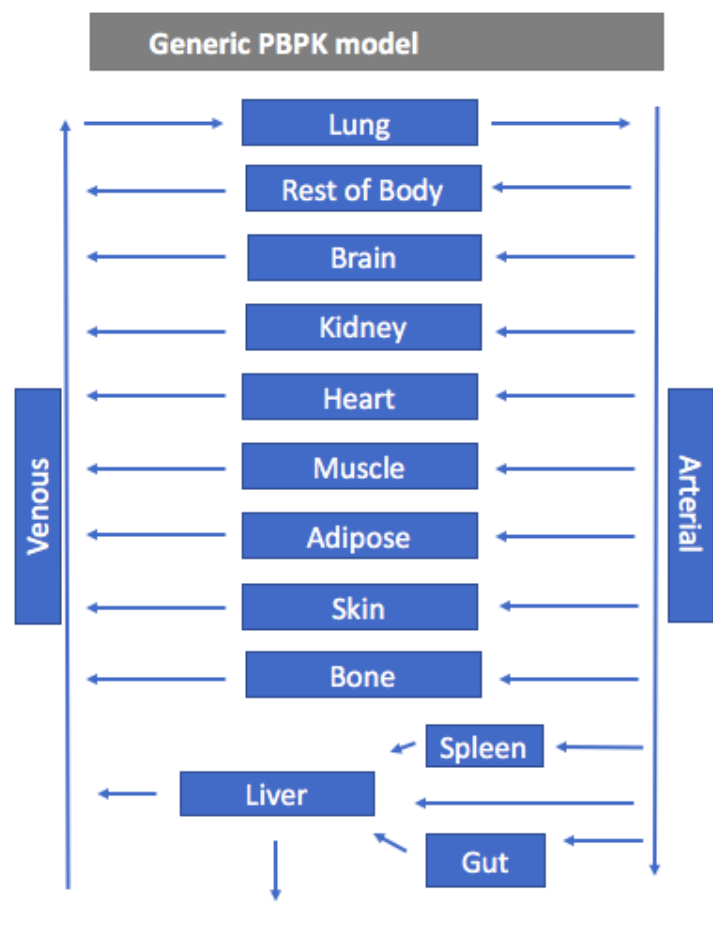


Figure 4: Generic perfusion-limited whole body PBPK model.

Models which are built from in silico or in vitro derived inputs, and do not require clinical data are considered to be bottom-up models. Top-down models can be developed or incorporated with bottom-up models later in drug discovery when clinical data is known. In these models, distribution is often described as being perfusion-limited or permeability-limited. With perfusion-limited distribution, the only limitation to drug distribution to a given tissue is the blood flow and tissues are considered to be well-stirred compartments. With permeability-limited distribution, barriers exist which acts as the rate-limiting step to distribution. These barriers are often the membrane, efflux transporters, or tight junctions between cells (ex. blood brain barrier). Additionally, PBPK models can be described as whole-body models (where all the tissues are broken up into compartments, with negligible tissues lumped), or lumped models (where tissues are lumped based on perfusion, size, composition, etc.) (Peters, 2012). In this project, a whole-body, perfusion limited PBPK model is used. Distribution to the tissues is driven by the interaction the drug has with the tissue components.

### 3.1.3: Data analysis

Exposure overlap coefficients, in some disciplines referred to as the overlapping coefficients, describes the similarity of two curves. They are often used in economics, statistics, and biology, for example in probability models and cost analysis. They are calculated by determining the overlapping portion of two curves and dividing that area by the observed/actual area. The closer the value to 1, the better the similarity between the data (more overlap). To be used to describe how well the predicted  $K_p$ s can predict the shape of the concentration-time profiles, the AUC needs to be equal for the two profiles being considered. For this study, since the clearance is kept constant and the dose is not

changed, there is no difference in the AUC between the observed and predicted c-t profiles and the EOC method can be used. Historically, this measurement has been done using the root mean squared error (RMSE). However, errors early on in the concentration-time profile can lead to big differences in the RMSE. For this reason, we use EOCs, which if the AUCs are equal can describe the similarity between two curves.

### 3.2: Materials

Mathematica v 11.0. (Wolfram, Champaign, IL) was used for all compartmental modeling and simulations. Literature data from plots were digitized using Engauge Plot Digitizer v 10.4.

### 3.3: Methods

#### 3.3.1: Probe drug selection and data collection

A diverse set of drugs, made up of acids, bases, and neutrals, was selected to compare prediction methods. Originally, the goal was to select drugs which had protein binding data already available in the literature (Kochansky et al., 2008); however, in order to get more accurate values the  $f_{up}$  values were determined experimentally. Drugs were considered neutral when primarily uncharged at physiological pH (7.4). Unless noted otherwise, the acidic and basic  $pK_a$  values ( $pK_{a,a}$  and  $pK_{a,b}$ ) for neutrals was set at 14 and 1 respectively. Any significant ionized and neutral fraction is considered by both methods. The probe drugs were selected based on the availability of literature IV PK data, as well as drug specific parameters. The structures for these compounds are shown in Appendix A.

Average experimental IV bolus and/or infusion C-t profiles for 19 drugs studies were collected from the literature. If the data was represented as graphical concentration-time profiles, the plots were digitized. When average subject weight was available, simulations were conducted to reproduce the observed  $V_{ss}$  for that average weight. The observed clearance and the steady state volume of distribution were determined by compartmental analysis using standard equations with Mathematica. One-compartment (1C), two-compartment (2C), and three-compartment (3C) models were fit to the observed data (Appendix E). The model which resulted in the lowest AICc value was chosen.

Literature physiological data were used for  $K_p$  predictions and PBPK modeling (Appendix F) (Brown et al., 1997; Poulin and Theil, 2002; Fenneteau et al., 2010; Ye et al., 2016). For drug specific parameters ( $\log P$ ,  $pK_a$ , and BP), experimental values from the literature were preferred over calculated/predicted values, and if more than one experimental value was found, then the experimental values were averaged.

The  $\log P_{vo}$  (log of the vegetable oil: buffer partition coefficient) was calculated from  $\log P$  using equation 8 (Leo et al., 1971). This term is used to represent neutral lipid partitioning in adipose tissue in the  $K_{p,dPL}$  method; however, it is not used in the  $K_{p,mem}$  prediction method.

$$\log P_{vo} = 1.115 \cdot \log P - 1.35$$

Equation 8: Determination of the  $\log P_{vo}$  from the  $\log P$ .

### 3.3.2: Simulations

A generic PBPK model was used, with the tissues represented by 10 compartments (adipose, bone, brain, gut, kidney, liver, lungs, muscle, skin, spleen), representing the

major tissues in the body (Figure 4). The differential equations for this model are presented in Appendix I. These compartments are linked via arterial and venous blood flows. All elimination is assumed to be hepatic and the extraction ratio is determined from the observed clearance using equation 9.

$$ER = \frac{Cl}{60 \cdot Q_{liver} \cdot BP}$$

Equation 9: Determination of the extraction ratio (ER).

$K_p$  values were predicted for each of the tissues using both methods ( $K_{p,dPL}$  and  $K_{p,mem}$ ). The original  $K_{p,dPL}$  method uses two separate equations, one for acids, weak bases, and neutrals, and another for moderate-to-strong bases (Equations 10 and 11) (Rodgers et al., 2005; Rodgers and Rowland, 2006).

Equation 10 shows the  $K_{p,dPL}$  equation for moderate to strong bases, where  $f_{ew}$  is the fractional volume of extracellular water,  $f_{iw}$  is the fractional volume of intracellular water,  $P$  is the octanol: water partition coefficient,  $[AP]$  is the concentration of acidic phospholipids in the tissue,  $K_{ap}$  is the association constant for acidic phospholipids in the tissue,  $f_{nl}$  is the fractional volume of neutral lipids,  $f_{npl}$  is the fractional volume of neutral phospholipids,  $pK_{a,b}$  is the basic ionization constant,  $pK_{a,a}$  is the acidic ionization constant.

Equation 11 shows the  $K_{p,dPL}$  equation for acids, weak bases, and neutrals, where  $[PR]_T/[PR]_P$  is the plasma protein tissue (extracellular fluid) to plasma ratio.

$$K_{pu,tissue} = f_{ew} + \frac{1 + 10^{pKab-pHiw}}{1 + 10^{pKab-pHp}} \cdot f_{iw} + \frac{K_{AP} \cdot [AP] \cdot 10^{pKab-pHiw}}{1 + 10^{pKab-pHiw}} + P \cdot f_{nl} + \frac{(0.3P + 0.7) \cdot f_{npl}}{1 + 10^{pKab-pHp}}$$

Equation 10:  $K_{p,dPL}$  equation for moderate to strong bases.

The first two terms of the equation describe the drug which is in the extracellular and intracellular water. Both the ionized and unionized drug is present in aqueous components. The third term describes the interaction between ionized bases and acidic phospholipids. The fourth term is the neutral lipid partitioning term, with the fraction of neutral lipids multiplied by the octanol: water partition coefficient. The last term describes the interaction between neutral bases and neutral phospholipids, where again, the octanol: water partition coefficient is used to represent drug-lipid interactions.

$$K_{pu,tissue} = f_{ew} + \frac{1 + 10^{pHiw-pKaa}}{1 + 10^{pHp-pKaa}} \cdot f_{iw} + \frac{P \cdot f_{nl} + (0.3P + 0.7) \cdot f_{NP}}{1 + 10^{pHp-pKaa}} + \left( \frac{1}{f_{up}} - 1 - \left( \frac{P \cdot f_{nl} + (0.3P + 0.7) \cdot f_{NP}}{1 + 10^{pHp-pKaa}} \right) \right) \cdot \frac{[PR]_T}{[PR]_P}$$

Equation 11: The  $K_{p,dPL}$  equation for acids, weak bases, and neutrals.

In Equation 11, the first two terms represent the drug in the aqueous phase, while the third term again describes the interaction with neutral phospholipids and neutral lipids (with only the unionized drugs being able to interact with the lipids). The last term

describes the drug-protein interaction in the tissue, with  $[PR]_T/[PR]_P$  representing the protein ratio (or the proteins in the tissue compared to those in the plasma).

For Equation 10, the association constant for blood cells (used to represent acidic phospholipid association constant) is defined in Equation 12, and the tissue: plasma water partition coefficient ( $K_{p,u}$ ) for the blood cells is defined in Equation 13.

$$K_{a,BC} = \left( Kp_{u,BC} - \frac{1 + 10^{pka-pHBC}}{1 + 10^{pKa-pHp}} F_{iw,BC} - \frac{P_{ow} \cdot f_{nl,BC} + (0.3P_{ow} + 0.7)f_{np,BC}}{1 + 10^{pka-pHp}} \right) \cdot \left( \frac{1 + 10^{pKa-pHp}}{[AP^-]_{BC} 10^{pKa-pHBC}} \right)$$

Equation 12: Association constant for red blood cells.

$$Kp_{u,BC} = \frac{BP + H - 1}{H \cdot f_{up}}$$

Equation 13:  $K_{p,u}$  for red blood cells.

The tissue: plasma partition coefficient ( $K_p$ ) can be determined from  $K_{p,u}$  by equation 14:

$$Kp = Kp_u \cdot f_{up}$$

Equation 14: Relationship between the  $K_p$  and  $K_{p,u}$ .

For the  $K_{p,mem}$  method we use the previously reported equation (Korzekwa and Nagar, 2017a) that considers both phospholipid membrane partitioning with  $f_{um}$  and neutral lipid partitioning with  $P$  (Equation 15). The first term describes the drug-tissue protein interaction, where  $r$  is the protein ratio between the tissue and plasma. As described

previously for  $V_{ss}$  predictions (Korzekwa and Nagar, 2017a), the tissue-specific  $r$  values for bases were decreased by 2.23 fold due to the lower amount of  $\alpha$ -acid glycoprotein in the extracellular fluid relative to albumin (Rowland and Tozer, 2011). The second two terms describe the drug in the aqueous parts of the tissue (intracellular and extracellular water). The fourth term describes the phospholipid interaction, where  $f_{pl}$  is fractional volume of phospholipid,  $LKl$  is the lipid binding constant,  $P$  is the octanol water partition coefficient, and  $a$  is the parameterized coefficient. The last term is the neutral lipid partitioning term, where again only the neutral drug is assumed to interact with the triglycerides and the  $b$  term is the parameterized coefficient. For all pH partitioning, plasma and tissue pH values were assumed to be 7.4 and 7.0, respectively.

$$\begin{aligned}
 Kp_{tissue} = & r(1 - f_{up}) + f_{iw} \cdot f_{up} \cdot \frac{10^{pKab-7.0} + 10^{7.0-pKaa} + 1}{10^{pKab-7.4} + 10^{7.4-pKaa} + 1} + f_{ew} \cdot f_{up} + f_{pl} \\
 & \cdot \frac{10^{pKab-7.0} + 10^{7.0-pKaa} + 1}{10^{pKab-7.4} + 10^{7.4-pKaa} + 1} \cdot f_{up} \cdot a \cdot LKL \\
 & + \frac{f_{nl} \cdot f_{up} \cdot b \cdot P}{10^{pKab-7.0} + 10^{7.0-pKaa} + 1}
 \end{aligned}$$

Equation 15:  $K_{p,mem}$  equation.

In the  $K_{p,mem}$  prediction method  $\log P$  is used directly. The  $a$  and  $b$  terms in Equation 15 were parameterized using the tissue  $K_p$  values and tissue composition data from Rodgers (Rodgers et al., 2005; Rodgers and Rowland, 2006). This dataset contained 381 drugs. Most of the  $f_{um}$  values for this large dataset were calculated with our previously reported model (Nagar and Korzekwa, 2017) since in house experimental values were not available for this dataset.  $\log K_{p,u}$  values and the  $\log$  of Eq. 15 were used to fit  $a$  and  $b$ , with no additional weighting (log transformation results in  $1/Y$  weighting). Outliers were identified

using the BoxWhisker function in Mathematica with outliers defined as > 1.5 times the interquartile range. Another model, which included an additional parameter for partitioning into adipose, was evaluated but did not improve predictions. The lipid concentrations multiplied by the lipid binding constant, L times K<sub>L</sub>, (LKL), was calculated from f<sub>um</sub> with Equation 16, using f<sub>um</sub> values normalized to 1 mg/mL microsomal protein.

$$LKL = L \times K_L = \frac{1 - f_{um}}{f_{um}}$$

Equation 16: Determination of LKL.

Exposure Overlap Coefficients (EOCs) were used to quantify the ability to predict the shape of the concentration-time profile (Equation 17). They are calculated by determining the overlapping portion of the experimental and predicted c-t profile curves and dividing that area by the experimental area under the curve (AUC). Since the experimental clearance values were used for all predictions, both experimental and predicted c-t profiles will have the same AUC (Nagar et al., 2017). This allows the EOC to be used as a direct comparison of curve shapes. Differences in the average EOCs were determined using the t-test.

$$EOC = \frac{\text{Overlapping Area}}{AUC}$$

Equation 17: EOC determination.

### 3.3.3: V<sub>ss</sub> predictions

V<sub>ss</sub> was determined from the predicted K<sub>p</sub> values and physiologic volumes using Equation 18, where V<sub>p</sub> is the plasma volume, and V<sub>t</sub> represents the tissue volume.

$$V_{ss} = Vp + \sum Vt \cdot Kp$$

Equation 18: Equation for  $V_{ss}$  predictions.

Predicted  $V_{ss}$  values were compared to observed values determined by compartmental modeling. To evaluate the predictive precision of the two methods, the fold error (FE), and the average absolute fold error (AAFE) values were determined for all compounds, and for different subsets. The FE is determined by dividing the predicted over the observed (Equation 19). Equation 20 determines the AAFE, or the geometric mean of the absolute fold error, where n is the number of drugs. The AAFE is a measure of how precisely the two methods predict  $V_{ss}$ .

$$Fold\ Error = \frac{Predicted\ V_{ss}}{Observed\ V_{ss}}$$

Equation 19: Determination of the fold error.

$$AAFE = 10^{\frac{1}{n} \sum |\log FE|}$$

Equation 20: AAFE determination.

### 3.4: Results

#### 3.4.1: Data collection

All the clinical IV bolus and/or IV infusion data was collected for the nineteen probe drugs (Appendix H). One of the initial probe drugs, piroxicam, was dropped because IV data could not be found for this drug. Plasma protein binding and microsomal

partitioning were determined experimentally as described in chapter two, with the exception of plasma protein binding for caffeine due to caffeine contamination in all plasma samples. A caffeine  $f_{up}$  value of 0.72 was determined by averaging values found in the literature. The other drug specific parameters were collected from the literature (Appendix G). Human BP values could not be found for betaxolol and nafcillin. For betaxolol, the  $f_{up}$  values are similar for rat and human, and therefore the rat BP value of 2.0 was used. For nafcillin, a value of 0.55 (1-hematocrit) was used, which is the BP ratio of similar compounds in humans (Greene et al., 1978). Also, this will not affect  $V_{ss}$  predictions since BP is not included in the  $K_p$  equations for acids.

#### 3.4.2: Parameterization of a and b terms

The parameters a and b in Equation 15 were fit to the experimental tissue reported  $K_{p,u}$  values for the rat (Rodgers et al., 2005; Rodgers and Rowland, 2006). The a and b coefficients are used in the lipid descriptor terms, a for phospholipids and b for neutral lipids. After sequential removal of twenty outliers (out of 401), optimized parameters were  $a = 1383 \pm 85$  and  $b = 0.096 \pm 0.029$ . A b1 term, used on for neutral lipids in adipose tissue, was attempted to be incorporated but did not improve the overall fit.

The predicted versus observed  $K_{p,u}$  values for 381 drugs are shown in Figure 5. The different colors represent different tissues (blue - adipose, red - bone, green - brain, purple - gut, light blue - heart, orange - kidney, magenta - liver, yellow - lung, light green - muscle, brown - skin, black – spleen). The  $R^2$  value for the fit was 0.80. There was no consistent characteristic for the removed outliers with the exception of the over-prediction of phencyclidine in four tissues, and the under-prediction of basic compounds in the lung (five drugs).

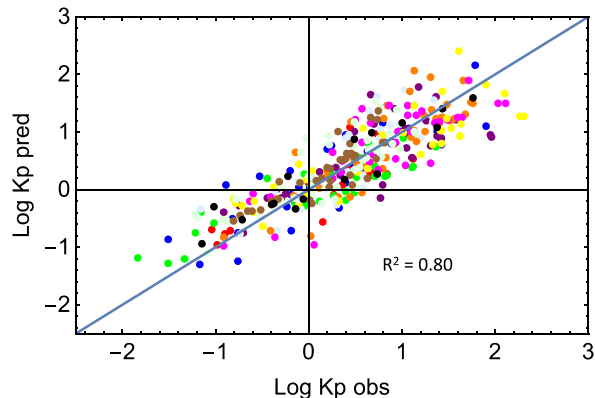


Figure 5: Observed versus predicted rat  $K_{p,u}$  values from Equation 15.

### 3.4.3: Steady-state volume of distribution

Figure 6 and Table 6 show the observed versus predicted  $V_{ss}$  values using either the  $K_{p,dPL}$  prediction method or the  $K_{p,mem}$  prediction method. The red dots represented the  $V_{ss}$  prediction using  $K_{p,dPL}$  method, while the blue dots represented the  $V_{ss}$  predictions using  $K_{p,mem}$  method. The accuracy of the  $V_{ss}$  predictions was analyzed by determining the percent of predictions within a range of absolute fold errors (Table 4) and AAFE (Table 3). For the total dataset of 19 drugs, the  $K_{p,mem}$  and  $K_{p,dPL}$  methods had comparable AAFE values (2.12 and 2.27, respectively). The  $K_{p,mem}$  and  $K_{p,dPL}$  methods had one (mibefradil) and two (diphenhydramine, felodipine) outliers, respectively. When these were excluded, the AAFE were again comparable.

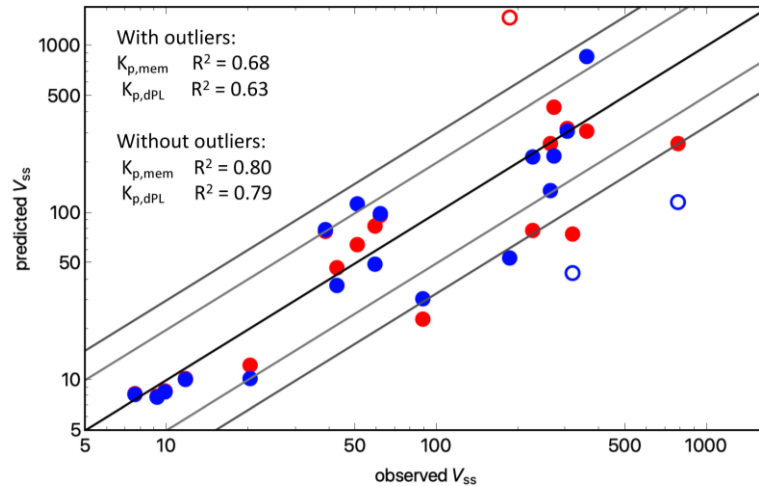


Figure 6: Observed  $V_{ss}$  versus the Predicted  $V_{ss}$ .

Ten different categories were compared in Tables 3 and 4. For predictions less than 1.5-fold error,  $K_{p,mem}$  scored higher in 5 categories, lower in 2 categories, and the same in 3 categories as  $K_{p,dPL}$  (Table 4). For predictions less than 3-fold error,  $K_{p,mem}$  scored lower in 5 categories and the same in 5 categories as  $K_{p,dPL}$ . When comparing all 19 drugs, the AAFE with  $K_{p,mem}$  versus  $K_{p,dPL}$  was 2.12 versus 2.27, respectively (Table 3). Across the 10 categories, the AAFE was lower for  $K_{p,mem}$  than  $K_{p,dPL}$  in 8 categories. When outliers were excluded in each method, the AAFE was lower for  $K_{p,mem}$  than  $K_{p,dPL}$  in 5 categories. For all categories in Table 3, there were no statistically significant differences in average fold error between  $K_{p,mem}$  and  $K_{p,dPL}$ .

Table 3: Absolute average fold error for  $V_{ss}$  predictions using both  $K_{p,mem}$  and  $K_{p,dPL}$  prediction methods.

Category	AAFE		AAFE (excluding outliers)	
	$K_{p,mem}$	$K_{p,dPL}$	$K_{p,mem}$	$K_{p,dPL}$
All Compounds	2.12	2.27	1.80	1.70
Acids	1.24	1.32	1.24	1.32
Bases	2.52	2.45	1.76	1.82
Neutrals	2.32	2.82	2.32	1.91
$\log P < 3$	1.66	1.68	1.66	1.68
$\log P > 3$	2.54	2.81	1.95	1.73
$f_{um} < 80\%$	2.36	2.41	1.81	1.92
$f_{um} > 80\%$	1.79	2.07	1.79	1.39
$f_{up} < 10\%$	2.45	2.42	1.84	1.86
$f_{up} > 10\%$	1.76	2.11	1.76	1.56

Table 4: Fraction of drugs whose predictions were less than 1.5-, 2-, and 3-fold error.

	< 1.5-fold error		< 2-fold error		< 3-fold error	
	$K_{p,mem}$	$K_{p,dPL}$	$K_{p,mem}$	$K_{p,dPL}$	$K_{p,mem}$	$K_{p,dPL}$
All Compounds	10/19	9/19	14/19	11/19	15/19	16/19
Acids	4/5	4/5	5/5	4/5	5/5	5/5
Bases	3/8	3/8	5/8	5/8	6/8	6/8
Neutrals	3/6	2/6	4/6	2/6	4/6	5/6
$\log P < 3$	5/9	5/9	8/9	5/9	8/9	9/9
$\log P > 3$	5/10	4/10	6/10	6/10	7/10	7/10
$f_{um} < 0.8$	6/11	4/11	8/11	6/11	8/11	9/11
$f_{um} > 0.8$	4/8	5/8	6/8	5/8	7/8	7/8
$f_{up} < 0.1$	6/10	4/10	7/10	6/10	7/10	8/10
$f_{up} > 0.1$	4/9	5/9	7/9	8/9	8/9	8/9

As discussed previously (Korzekwa and Nagar, 2017b), Equations 10, 12 and 13 indicate that  $K_{p,u,tissue}$  and ultimately  $V_{ss,u}$  should be proportional to  $K_{p,u,BC}$  (Equation 13), first experimentally observed by Hinderling (Hinderling, 1997). Also,  $f_{up}$  in the denominator of Eq. 7 is ultimately multiplied by  $f_{up}$  in the PBPK framework (Equation 14). Therefore, predicted  $V_{ss}$  values for bases should be relatively insensitive to  $f_{up}$  when using Equation 10. The impact on predicted  $V_{ss}$  after a 2-fold decrease in  $f_{up}$  is shown in Table 5. As expected, changing  $f_{up}$  for acids has little effect, since plasma protein binding is high and  $V_{ss}$  is low. For neutrals, a 2-fold decrease in  $f_{up}$  results in an average 1.7-fold increase

in  $V_{ss}$  for both methods. For bases, a 2-fold decrease in  $f_{up}$  results in an average 2-fold decrease in  $V_{ss}$  for  $K_{p,mem}$ , but an average 1.05-fold increase with  $K_{p,dPL}$ .

Table 5: Fold decrease in  $V_{ss}$  upon a 2-fold decrease in the  $f_{up}$

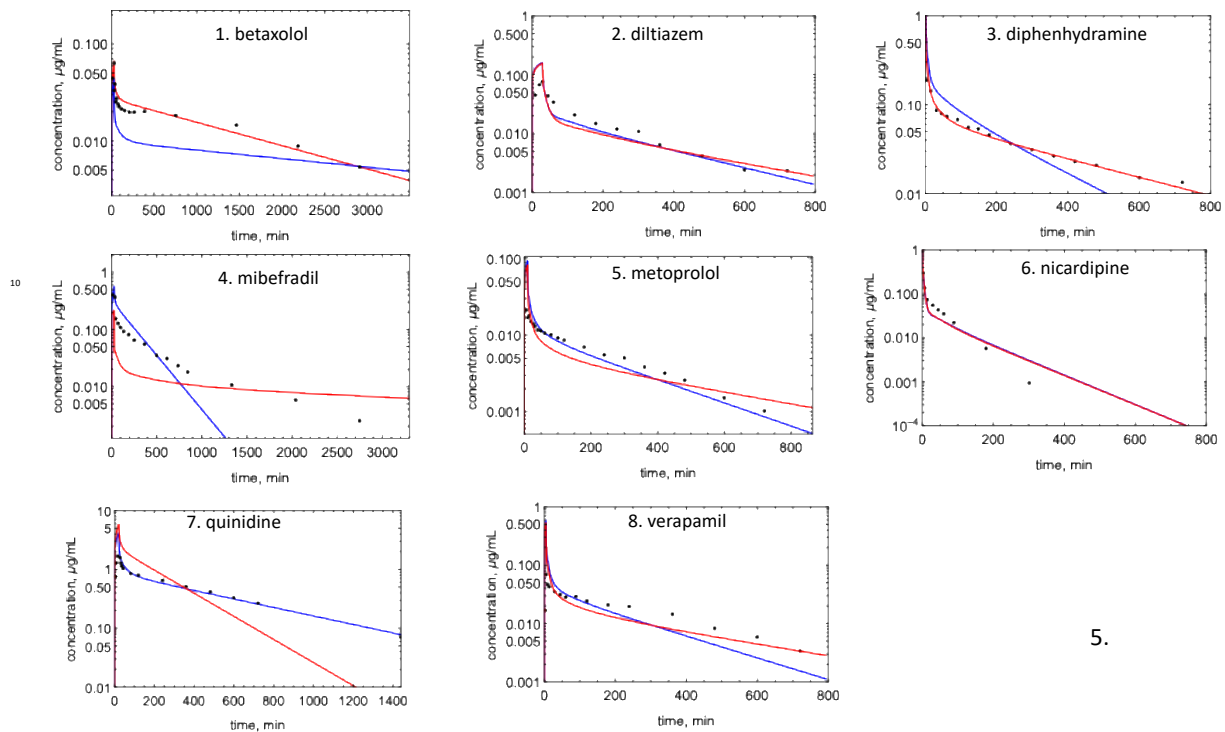
	Fold decrease in $V_{ss}$ upon a 2-fold decrease in $f_{up}$			
Compound	$K_{p,mem}$		$K_{p,dPL}$	
Betaxolol	1.97		0.95	
Diltiazem	1.98		1.05	
Diphenhydramine	1.94		0.82	
Metoprolol	1.98		0.75	
Mibefradil	2.00		0.95	
Nicardipine	1.90		1.01	
Quinidine	1.89		1.00	
Verapamil	1.95	average (bases)	1.06	average (bases)
		$1.95 \pm 0.04$		$0.95 \pm 0.11$
Caffeine	1.66		1.59	
Diazepam	1.41		1.53	
Felodipine	1.79		1.66	
Fluconazole	1.82		1.70	
Midazolam	1.78		1.86	
Phenytoin	1.78	average (neutrals)	1.79	average (neutrals)
		$1.71 \pm 0.15$		$1.69 \pm 0.12$

Table 5 continued

	Fold decrease in $V_{ss}$ upon a 2-fold decrease in $f_{up}$			
Compound	$K_{p,mem}$		$K_{p,dPL}$	
Diclofenac	1.01		1.01	
Glyburide	1.05		1.03	
Ketoprofen	1.01		1.00	
Nafcillin	1.19		1.09	
Warfarin	1.01	average (acids)	1.01	average (acids)
		$1.05 \pm 0.08$		$1.03 \pm 0.04$

#### 3.4.4: Simulations

Concentration-time profiles were simulated using both  $K_p$  prediction methods for nineteen drugs (Figure 7-9). An example of EOC calculation is shown in Figure 10 for verapamil. EOCs were determined for all nineteen drugs (Table 6). Overall, there is no significant difference in the average EOC values for the  $K_{p,mem}$  or  $K_{p,dPL}$  method. However, there were some interesting deviations between the methods. C-t profiles were poorly predicted by both methods for five drugs: mibefradil, diazepam, felodipine, diclofenac, and nafcillin. In addition, the  $K_{p,dPL}$  method poorly predicted the profiles for betaxolol and diphenhydramine. Some possible explanations for these discrepancies are discussed below.



5.

Figure 7: Simulated concentration-time profiles for basic drugs.

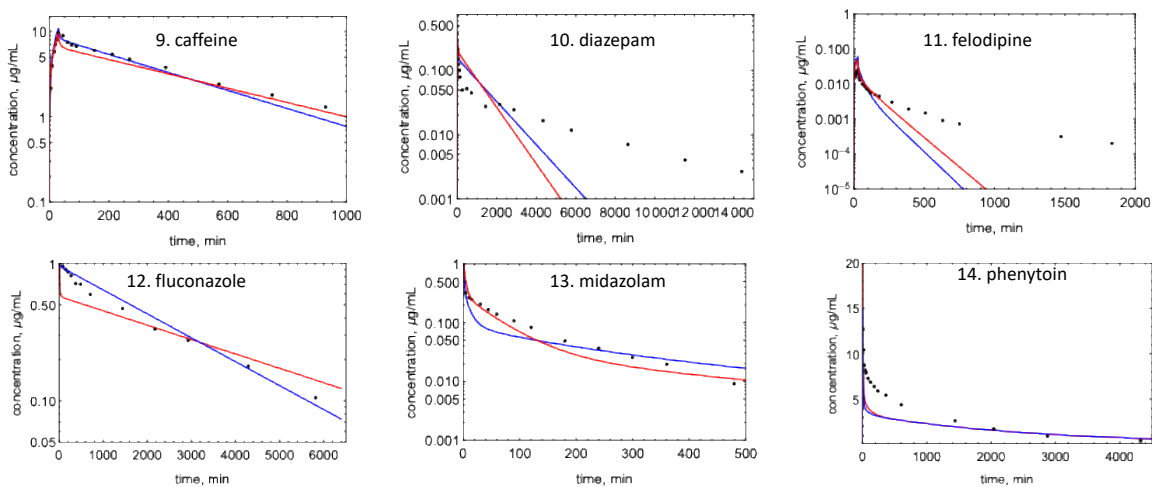


Figure 8: Simulated concentration-time profiles for neutral drugs.

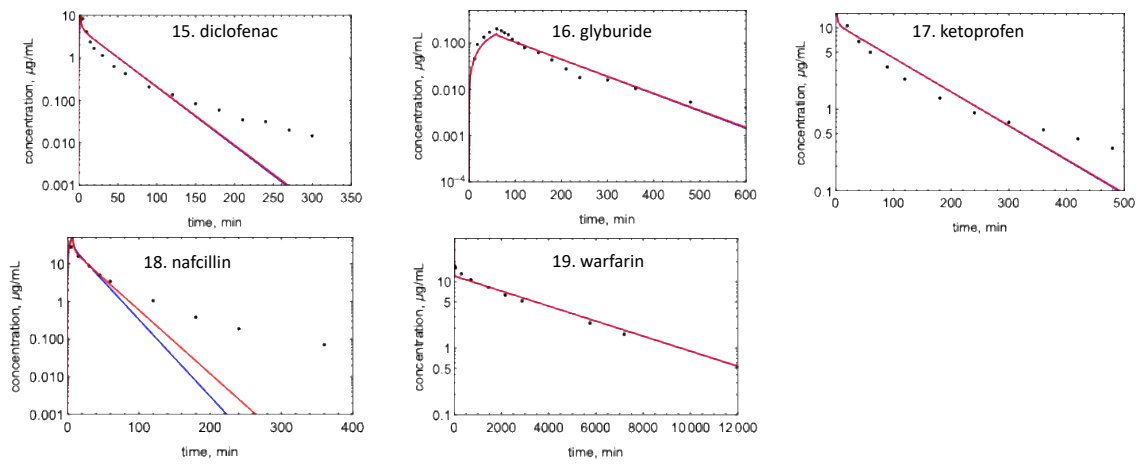


Figure 9: Simulated concentration-time profiles for acidic drugs.

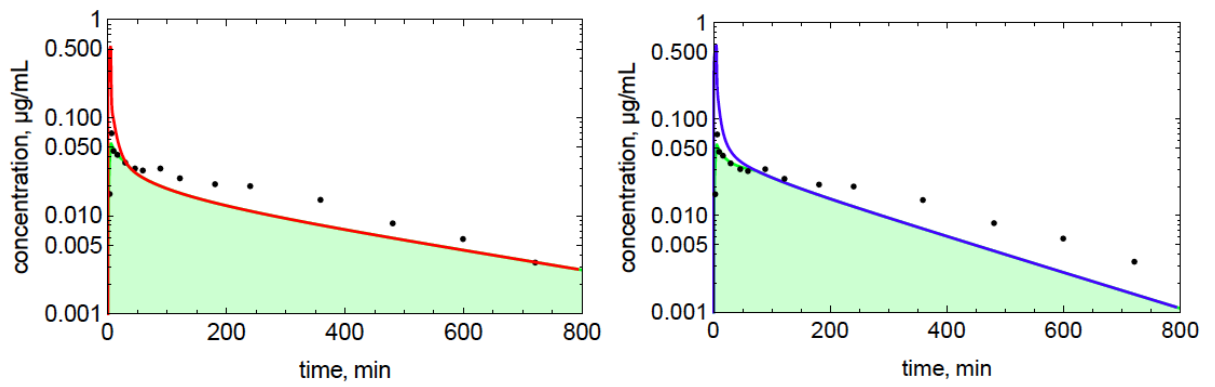


Figure 10: EOC determination for verapamil.

Table 6: Observed and predicted  $V_{ss}$  and EOC values for both methods

	Observed $V_{ss}$ (L)	Predicted $V_{ss}$ $K_{p,mem}$ method (L)	Predicted $V_{ss}$ $K_{p,dPL}$ method (L)	EOC $K_{p,mem}$ method	EOC $K_{p,dPL}$ method
Betaxolol	360	307	856	0.97	0.61
Diltiazem	306	320	309	0.76	0.80
Diphenhydramine	788	260	115	0.97	0.87
Metoprolol	274	429	217	0.76	0.87
Mibefradil	187	1470	53.2	0.81	0.82
Nicardipine	62	96.4	98.5	0.79	0.78
Quinidine	227	78.3	215	0.96	0.73
Verapamil	266	258	136	0.73	0.76
Caffeine	42.8	47.0	36.7	0.87	0.93
Diazepam	89.5	22.9	30.5	0.55	0.61
Felodipine	320	74.3	43.4	0.68	0.56
Fluconazole	59.3	83.4	49.1	0.85	0.99
Midazolam	51.2	64.1	113	0.82	0.71
Phenytoin	38.8	77.0	79.1	0.78	0.77
Diclofenac	9.23	7.98	7.89	0.84	0.84
Glyburide	11.78	10.2	10.0	0.86	0.87
Ketoprofen	9.9	8.54	8.47	0.89	0.89
Nafcillin	20.4	12.2	10.1	0.86	0.81
Warfarin	7.66	8.20	8.15	0.96	0.97
			Average	0.82 +/- 0.11	0.80 +/- 0.12

### 3.5: Discussion and conclusions

Tissue partition coefficients, and ultimately  $V_{ss}$  are determined primarily by competition between plasma protein binding and lipid partitioning. The  $K_{p,dPL}$  method considers binding to neutral lipids such as triglycerides and neutral phospholipids in membranes, with acidic phospholipids considered separately (Rodgers et al., 2005; Rodgers and Rowland, 2006). The method assumes that neutral molecules only interact with neutral phospholipids, and only ionized bases interact with acidic phospholipids, an assumption questioned previously (Korzekwa and Nagar, 2017b). The major acidic phospholipid is phosphatidylserine and major neutral phospholipid is phosphatidylcholine. Although phosphatidylcholine is net neutral and phosphatidylserine is net acidic, both molecules are zwitterions. Interactions between charged species in the polar head group region are dynamic processes with conformational changes occurring in a picosecond time-frame (Tieleman et al., 1997). Balaz compiled experimental data evaluating the orientation of exogenous molecules in membranes (Balaz, 2009). Hydrophilic molecules accumulate in the polar head group region, amphiphilic molecules at the interface, and hydrophobic molecules in the hydrophobic core. Our lab has used this concept to develop quantitative models for membrane partitioning (Nagar and Korzekwa, 2017).

The  $K_{p,mem}$  model is based on previously reported  $V_{ss}$  models (Korzekwa and Nagar, 2017a). The  $K_p$  model described here uses the phospholipid component of tissues and  $f_{um}$  to model membrane partitioning, and  $\log P$  for neutral lipid interactions. Equation 15 was parameterized using reported tissue composition data and tissue  $K_p$  values (Rodgers et al., 2005; Rodgers and Rowland, 2006). Only two constants were parameterized:  $a$ , the

scaling factor for membranes, and  $b$  for neutral lipids. Although the two methods use different mechanistic assumptions, the resulting fit for  $K_{p,mem}$  (Figure 5) is similar to that reported by Rodgers for  $K_{p,u}$  parameterization (Rodgers et al., 2005).

The volume of distribution is generally low for acids due to high plasma protein binding and low partitioning into membranes and neutral lipids. At physiologic pH, most acids are negatively charged, and membranes have few hydrogen bond donors. Therefore, microsomal partitioning is low for acids, with  $f_{um}$  values ranging from 0.72-0.98 (Table 2). Both the  $K_{p,mem}$  and  $K_{p,dPL}$  assume that only the neutral acids partition into tissues, and both methods predict  $V_{ss}$  with similar accuracy (AAFE 2.12 and 2.27 for  $K_{p,mem}$  and  $K_{p,dPL}$ , respectively, Table 3). This is expected since any model that restricts a compound with low  $f_{up}$  to the plasma and extracellular space will predict a  $V_{ss}$  approximately equal to that of plasma proteins (~7.5 L) (Rowland and Tozer, 2011). Under-prediction of acids with  $V_{ss}$  values  $> 9$ , e.g. nafcillin, is frequently observed (Chan et al., 2018). Transporter activity (e.g. OATPs) could be one reason for the under-prediction.

When two outliers for the  $K_{p,dPL}$  analysis (diphenhydramine, felodipine) are excluded,  $V_{ss}$  predictions for neutrals using  $K_{p,dPL}$  improved from an AAFE of 2.82 to 1.91 (Table 3). For diphenhydramine, the  $K_{p,dPL}$  method resulted in a 6.9 -fold under prediction and  $K_{p,mem}$  gave a 3-fold under-prediction (not an outlier). For felodipine,  $K_{p,dPL}$  resulted in a 7.4-fold under prediction and  $K_{p,mem}$  gave a 4.3-fold under-prediction (not an outlier). The reason for these poor predictions is unknown but it may be difficult to predict  $V_{ss}$  of a highly protein bound and highly partitioned neutral compound (felodipine).

$K_{p,mem}$  uses a single equation for bases, neutrals, and acids and predicts  $V_{ss}$  for bases with similar accuracy to  $K_{p,dPL}$  which uses different equations for bases.  $K_{p,dPL}$  assumes that ionized bases only interact with acidic phospholipids. This interaction is parameterized with BP, using the erythrocyte partition coefficient to parameterize binding of the ionized base to acidic phospholipids. Mechanistically, the assumption that bases bind only to acidic phospholipids is questionable. Hydrophobic bases bind to neutral phospholipid as well, with key interactions between the cation and negatively charged phosphate, and the hydrophobic region with the hydrophobic membrane core. From Equation 10, it is clear that for moderate to strong bases with  $V_{ss} >$  total body water,  $K_p$  values are dominated by the acidic phospholipid binding terms. Therefore, although binding to only acidic phospholipids was assumed, a similar relationship is possible, assuming that ionized bases bind to all phospholipids. The ratio of neutral to acidic phospholipids is relatively constant across tissues (CV = 15%) (Rodgers et al., 2005), and total phospholipids can be substituted for neutral phospholipids. The  $K_{BC}$  term in Equation 10 would be smaller, but the relevant phospholipid term in Equation 15 would be larger.

Another implication of using BP to predict  $K_{p,u}$  for bases is the insensitivity of  $V_{ss}$  to measured  $f_{up}$ . For acids,  $V_{ss}$  is insensitive to  $f_{up}$  since tissue partitioning is minimal.  $V_{ss}$  values for bases are expected to be proportional to  $f_{up}$  since they partition heavily into tissues from the unbound concentration in cytosol (assumed to be equal to the unbound concentration in plasma). This is observed for  $K_{p,mem}$  but not for  $K_{p,dPL}$  (Table 5). This is a consequence of using BP (which is determined by both  $f_{up}$  and erythrocyte partitioning) to calculate  $K_{p,u}$ .  $V_{ss}$  predictions can be relatively accurate when BP is used to predict  $K_p$

for bases, since errors in  $f_{up}$  are not manifest and unbound  $V_{ss}$  for bases is proportional to erythrocyte partitioning (Hinderling, 1997). However, errors in  $f_{up}$  can still result in many other inaccuracies, including in predictions of clearance and target activity.

Overall, the  $K_{p,mem}$  and  $K_{p,dPL}$  models give similarly accurate predictions, explaining 68 and 63 percent of the variance in  $V_{ss}$  (80 and 79 percent without outliers), respectively. Several factors may explain the remaining variance. First, there can be significant variability in the  $V_{ss}$  measured across clinical studies. Not all pharmacokinetic datasets provide body weights, and often a body weight of 70 kg was assumed. Also, experimental data from multiple sources are used, e.g. BP values. Graham et al. observed a 7% decrease in accuracy when predicted instead of experimental logP values were used (Graham et al., 2012). For  $f_{up}$ , differences between laboratories can be very large. Several recent publications discuss assay conditions for protein binding, including dilution and use of CO<sub>2</sub> (Kochansky et al., 2008; Curran et al., 2011; Di et al., 2017). In this study, we measured a  $f_{up}$  of 0.03 for mibefradil, whereas a value of <0.005 was reported previously (Clozel et al.1991). Use of a smaller  $f_{up}$  would result in a better prediction with  $K_{p,mem}$ , but exclusion of our data is not justified.

Since AUC is determined by experimental clearance and dose for both methods, the AUC values for the simulations are normalized, and the EOC captures differences in the shape of the c-t profile (Figure 10). Several c-t profiles in Figures 7-9 are not well-predicted by either method. Although there are differences in the EOC for some drugs, the average EOC for the  $K_{p,mem}$  and  $K_{p,dPL}$  prediction methods were not significantly different. Since clearance is constant, when  $V_{ss}$  is over predicted (e.g. betaxolol using  $K_{p,dPL}$ , and

mibefradil using  $K_{p,mem}$ , Figure 7), the terminal half-life is over predicted. When  $V_{ss}$  is under predicted (e.g. diphenhydramine using  $K_{p,dPL}$ , Figure 7), the terminal half-life is under predicted. Perhaps the most significant deficiency of the reported modeling approaches is the assumption of perfusion-limited distribution. As seen with diazepam, felodipine, diclofenac and nafcillin, accurate c-t profiles are not predicted even when  $V_{ss}$  is well-predicted. For verapamil (Figures 7) the distribution phase is not well predicted, presumably due to a combination of using a perfusion-limited model and an experimental clearance. Clearly, multi-compartmental distribution is not accurately modeled with perfusion-limited distribution.

In conclusion,  $K_{p,mem}$  can be used to predict  $K_{p,u}$  with accuracy similar to  $K_{p,dPL}$ . An advantage of using  $f_{um}$  to parameterize membrane partitioning is that  $f_{um}$  is used for clearance prediction and is generated early in the discovery/development process. Also, differentiating between acidic and neutral phospholipids for bases and using 0.3 P for neutral compounds is not mechanistically justified. Finally, since both the extent and rate of membrane partitioning and permeability are important, a mechanistically sound basis for membrane interactions is necessary for improved physiologic PK models.

## CHAPTER 4: REPRESENTING NEUTRAL LIPID PARTITIONING

### 4.1: Background/Rationale

#### 4.1.1: Background

Lipid partitioning has been traditionally represented using the logP (Poulin and Theil, 2000; Rodgers et al., 2005; Rodgers and Rowland, 2006; Graham et al., 2012). For adipose tissue, this term has not been sufficient to describe the neutral lipid partitioning. To this end, Poulin et al introduced the logP<sub>vo</sub> as a replacement term for the logP as an in vitro surrogate for adipose tissue. Inclusion of this term for neutral lipids improved K<sub>p</sub> predictions for adipose tissue (Poulin et al., 2001). However, the logP<sub>vo</sub> coefficient is often not experimentally determined but predicted from the logP. This relationship was originally determined from a set of volatile compounds, where the partitioning of a drug between water: air and oil: air was used to derived a linear relationship between oil: water and octanol: water partition coefficients (Leo and Hansch, 1971). Several equations exist to describe this relationship, differing for different types of compounds, including hydrogen bond acceptors and hydrogen bond donors (Leo and Hansch, 1971; Poulin and Krishnan, 1996).

A potential alternative surrogate for neutral lipid partitioning is partitioning into adipocytes. Adipocytes, also known as fat cells, are cells that contain a large fraction of adiposomes. Adiposomes are membrane bound vesicles which are filled primarily with triglycerides (Body, 1988). Triglycerides are a type of neutral lipid, which does not have a charge, is not soluble in water, and has no hydrogen bond donors. The goal of this specific

aim is to design partitioning assays in order to determine the partition coefficient for a drug into adipocytes.

#### 4.1.2: Cell source

Two methods can be used to obtain mature adipocytes. The first method is to isolate mature adipocytes or pre-adipocytes from rats or mice (Bjorntorp et al., 1978; Ruiz-Ojeda et al., 2016). The second method is to purchase a pre-adipocyte cell-line and differentiate them into mature adipocytes (Ruiz-Ojeda et al., 2016).

Primary adipocytes can be isolated from either rats or mice and grown in cell culture. Ependymal fat pads can be removed, and mature adipocytes can be isolated following a collagenase digestion. Mature adipocytes are not the only cell within the adipose tissue, and additionally all the cells would need to additionally undergo mesh separation, and centrifugation, all of which can reduce the integrity of the adipocytes (Parlee et al., 2014). The isolated adipocytes can be diverse in size, and therefore triglyceride level. Also, despite the prevalence of adipose tissue in rats, isolation from rats can result in low yields of viable mature adipocytes (Rotondo et al., 2016).

Pre-adipocyte cell-lines have been used frequently in studies of adipose tissue function. They can be maintained and cultured greater than 12 passages. These cells are generally restricted in the number of passages which they can undergo without loss of function/viability because they are not a continuous cell line. Differentiation from pre-adipocytes, when using optimized methods, can lead to increased yields.

For differentiating pre-adipocytes, different cell lines can be used (Ruiz-Ojeda et al., 2016). There are several mouse pre-adipocyte lines, including 3T3-L1, 3T3-F442A, C3H10T1/2, MEFs, and OP9 (Ruiz-Ojeda et al., 2016). Different cell lines can be used,

based on the type of assay needed. Primary pre-adipocytes, including subcutaneous or visceral pre-adipocytes, from rats/mice can also be obtained and differentiated, but the yield is generally low. For the number of cells needed for this project, this option is not viable.

3T3-L1 is a mouse-derived pre-adipocyte cell line which can be converted into adipocytes. 3T3-L1 cells were originally developed from murine-swiss 3T3 cells and can be used as a pre-adipocyte cell line (Green and Kehinde, 1974). After the 3T3-L1 cells are in growth arrest, the cells are treated with pro-differentiative agents and in approximately 2-3 weeks, the cells will be fully differentiated into adipocytes.

#### 4.1.3: Differentiation

Many factors influence the differentiation potential of the 3T3-L1 cells. Mehra et al showed that the dish type and culture dish provider could impact the differentiation efficiency. Using optimal dishes, they were able to get a differentiation efficiency of approximately 80% (Mehra et al., 2007). Zebisch et al showed that the use of rosiglitazone (in addition to insulin, IBMX, and dexamethasone), could yield almost complete differentiation of the 3T3-L1 cells. When the protocol suggested by ATCC was used (without rosiglitazone), full differentiation was not achieved. Furthermore, they did not see a significant difference when collagen coated plates were used (Zebisch et al., 2012). For this study, 96-well clear bottom plates were used for cell culture, in order to use confocal microscopy to characterize the cells.

Passage number has also been shown to influence the overall differentiation of 3T3-L1 cells. Cells with lower passage numbers should be used, as the differentiation efficiency decreases with higher passage numbers (Mehra et al., 2007; Zebisch et al., 2012). A lower

medium height resulted in more neutral lipid accumulation (Sheng et al., 2014). As fibroblasts are differentiated, they can be easily displaced from the bottom of the well. Peeling of the differentiated cells can also occur when the medium is added too forcefully, or the cells spend too long without medium. Caution was taken throughout the differentiation process in the handling and aspirating out of the medium. The original fibroblasts from ATCC have an unknown original passage number, so all subsequent passages from purchase were noted. Cells were originally cultured and sub-cultured to ensure that all cells used in these studies were between passage numbers +7 to +9.

#### 4.1.4: Methods of characterization/quantification

For this study, it was necessary to characterize and quantitate the neutral lipid content in the differentiated 3T3-L1 cells. For partitioning, differences in neutral lipid content can be significant. In many experiments with adipocytes, not only is the triglyceride amount important but also the function of the adipocyte. However, in this case, since we are investigating partitioning into the tissue components, these tests were not necessary. Several dyes can be used to preferentially interact with the lipid droplets in adipocytes, including Oil Red O, Nile Red, and BODIPY (Zebisch et al., 2012; Storms et al., 2014). The BODIPY dye was used in this study as it could be used on live cells and did not require the cells to be fixed or disrupted in order to quantitate.

#### 4.1.5: Partitioning assay

In order to show that there is a difference in the partitioning into the adipocytes (compared with undifferentiated fibroblasts), both cell types were used in the partitioning assay. Confocal microscopy was used to characterize both of these cells at different time points following differentiation, as well as for each well in the partitioning assay. A recent

paper (Treyer et al., 2018), determined the importance of neutral lipid partitioning and its impact of intracellular bioavailability. They determined the time for different drugs to reach equilibrium and found that 45 minutes was sufficient. For this reason, in this study a 1-hour incubation time is used for both the BODIPY dye and the drug.

## 4.2: Materials

### 4.2.1: Cell culture and differentiation

Cell culture work was done in a horizontal laminar flow cell culture hood and a water-jacketed incubator set at 37 degrees Celsius and 5% CO<sub>2</sub>. 3T3-L1 Mouse Embryonic Fibroblasts were obtained from ATCC. Trypsin 0.25% (w/v)-0.53 mM EDTA, fetal bovine serum (FBS), and Penicillin/Streptomycin-100x (P/S) were obtained from Gibco. FBS was heat inactivated by heating at 56 degrees Celsius for 30 minutes and then filtered. Rosiglitazone was obtained from Cayman Chemicals. Methylisobutylxanthine (IBMX) and bovine insulin were obtained from Sigma Aldrich. Dulbecco's modified eagle's medium (DMEM) with high glucose, L-glutamine, and sodium pyruvate from Genesee Scientific. 25 cm<sup>2</sup> and 75 cm<sup>2</sup> flasks were obtained from Corning. 70% isopropyl alcohol was purchased from VWR Chemicals All other cell culture supplies were available in lab, including water-soluble dexamethasone, pipettes, 100% isopropyl alcohol, ethanol, wide-bore pipette tips, Dimethyl sulfoxide (DMSO), and a light microscope.

### 4.2.2: Confocal imaging

BODIPY 493/503 (4,4-Difluoro-1,3,5,7,8-Pentamethyl-4-Bora-3a,4a-Diaza-s-Indacene) and Hoechst 33342 were obtained from Invitrogen. Phosphate buffered saline (PBS) was obtained from SAFC. A PerkinElmer-High Content Analysis

System Operetta CLS was used for all confocal microscopy work. CellCarrier and ViewPlate 96-well plates were obtained from PerkinElmer.

#### 4.2.3: Partitioning

Caffeine, +/-cis diltiazem hydrochloride, dimethyl sulfoxide (DMSO), and felodipine were obtained from Sigma Aldrich (St. Louis, MO). Formic acid and acetonitrile were obtained from Fisher Scientific (Norristown, PA). Diclofenac sodium was obtained from Calbiochem (Burlington, MA). Fenofibric acid was obtained from Kano Laboratories (Nashville, TN). One mg/mL solution of midazolam in methanol was obtained from Cerilliant (a Sigma Aldrich company). An Agilent 1100 HPLC and API 4000 mass spectrometer and Agilent 1100 HPLC and API 4000 Q-Trap mass spectrometer were used to determine the drug buffer concentrations.

### 4.3: Methods

#### 4.3.1: Cell culture and passaging

Aseptic conditions were used in order to prevent contamination (Bykowski and Stevenson, 2008). The horizontal laminar flow hood and incubator were thoroughly cleaned, with 10% bleach solution and 70% isopropyl alcohol, before initial use. To determine if the hood was thoroughly cleaned, a dish with medium was prepared in the hood and incubated overnight. The dish can be checked for turbidity and growth. Before and after using the hood, the surface was sprayed with 70% isopropyl alcohol. All objects brought into the cell culture hood were sprayed with 70% isopropyl alcohol. Penicillin and streptomycin were used in the cell culture medium to prevent bacterial growth.

Cells were previously purchased from ATCC and cell culture protocols were modified from the ATCC product sheet for the 3T3-L1 cells (ATCC, 2018). Previously frozen cells (passage +4 and +5) were removed from cell-tank and thawed quickly (by swirling cryotubes in a water bath warmed to 37 degrees, taking care not to get water over cryotube lid). These cells were suspended in ~ 5 mL complete growth medium (composed of 90% DMEM, 10% FBS, 1X P/S) in a 15 mL centrifuge tube and centrifuged at ~200 x g for five minutes. The supernatant was removed by vacuum aspiration and the cells were re-suspended and dispersed in 5 mL of complete growth medium by pipetting the suspension up and down to mix. 15 mL of complete growth medium and the 5 mL suspension were added to a 75 cm<sup>2</sup> cell culture flask. The cells were incubated in an incubator set at 37 degrees and 5% CO<sub>2</sub>. After 48 hours, the medium was changed or if the cells were between 60-90% confluence, they were sub-cultured.

To subculture the cells, the medium was aspirated and 1x trypsin was added to the cells (3 mL for a 25 cm<sup>2</sup> flask or 5 mL for a 75 cm<sup>2</sup> flask). The trypsin was allowed to incubate with the cells for no more than five minutes or when about 95% of the cells were displaced (appeared round and floating) The solution was pipetted into a centrifuge tube and rinsed with ~5 mL of complete growth medium. This suspension was centrifuged at 200 x g for five minutes and subsequently re-suspended in ~ 5 mL complete growth medium. The cells were generally passaged (1:5) via the suspension method. 4 mL of complete growth medium was placed in five 25 cm<sup>2</sup> flasks. 1 mL of the cell suspension was added to each flask. The cells were allowed to grow until they reached 60-90% confluence, where they were either passaged or frozen. These cells were sub-cultured into

25 cm<sup>2</sup> flasks (for passaging) or placed into the 96 well plate for the partitioning assay and confocal imaging.

Cells were frozen by using the complete growth medium, supplemented with 5% DMSO (a cryoprotective substance) (Phelan and May, 2017). Cells were suspended (following centrifugation) in the freezing medium and aliquoted in 0.5 to 1 mL volumes into cryopreservation tubes (2 mL). The tubes were labelled with the passage number and cell type. These tubes were moved to the -80-degree Celsius freezer for at least 24 hours and then transferred to the liquid nitrogen cell tank.

#### 4.3.2: Differentiation of pre-adipocytes to adipocytes

The protocol to differentiate the 3T3-L1 cells into adipocyte-like cells was modified from protocols from ATCC and Zebisch et al (ATCC, 2011; Zebisch et al., 2012). To make differentiation medium, the complete growth medium was supplemented with differentiating agents, water-soluble dexamethasone, IBMX, bovine insulin, and rosiglitazone. Stock solutions of these differentiating agents were created and stored at -20 degrees Celsius. Fresh differentiating medium was created each time, by adding the differentiating factors to complete growth medium warmed to 37 degrees Celsius. Table 7 shows the stock concentrations, desired final concentrations of differentiating agents, and the volume added to 50 mL of complete growth medium.

Table 7: Differentiating agents.

	Storage Conditions	Stock Concentration	Desired final concentration of differentiating agents	Volume ( $\mu\text{L}$ ) added to 50 mL	Notes
Water-soluble dexamethasone	Stored at -20 degrees Celsius for 6 months	10 mM in water	0.25 $\mu\text{M}$	5	**water-soluble dexamethasone needs to be used, as dexamethasone lacks suitable solubility in water/buffer
IBMX	Stored at -20 degrees Celsius for 6 months	200 mM in DMSO	0.5 mM	31.3	
Bovine insulin	Stored at 4 degrees Celsius	10 mg/mL in HEPES	1.0 $\mu\text{g/mL}$	5	
Rosiglitazone	Stored at -20 degrees Celsius	20 mM in DMSO	2 $\mu\text{M}$	5	

The cells were allowed to reach 100% confluence and were maintained at confluence for 48 hours, at which point, an equal volume of differentiation medium was added to each well. After 48 hours, maintenance medium was added and every 48 hours afterward the maintenance medium was replaced. After 7-14 days the cells were fully differentiated. At various points before and following differentiation, confocal microscopy was used to monitor the development of lipid droplets and compare the neutral lipid content to that of undifferentiated fibroblasts.

#### 4.3.3: Cell characterization/neutral lipid quantification

A 5 mM BODIPY solution in DMSO was prepared and further aliquoted at 0.010 mM concentration in 600  $\mu$ L amber centrifuge tubes. This was done in order to limit the number of freeze-thaw cycles. Freezing and thawing BODIPY will decrease the integrity of the dye. The vials were stored at -20 degrees Celsius until use and care was taken to prevent exposure of samples/BODIPY dye to direct light.

The initial assay was performed to determine the appropriate concentration of BODIPY dye to use with the cells. BODIPY concentrations ranging from 1  $\mu$ M to 0.1 nM were incubated for 1.5 hours with the cells and DAPI was added before imaging. Each of these concentrations were also imaged with one of the test drugs (2  $\mu$ M midazolam) to see if there was an interference or effect with the drug on board. This assay also provided a starting point to optimize the confocal parameters for imaging in the future.

Subsequent optimization assays were done in order to confirm optimal test conditions. For example, differences included sources of dyes, age cells, washing of cells, and also the use of medium versus buffer for the 1-hour incubation step. After the test drugs were selected, these drugs were tested to see if there were any differences in the BODIPY fluorescence in the presence of drug and without. Further examination was done to optimize the method, including determining whether the presence of drug influenced the BODIPY exposure, whether medium or buffer was optimal, and whether a washing step was needed to reduce background. Also, different aliquots of dye were used, as well as fresh dye to determine if differences in imaging could be explained by the loss of integrity of the dye.

The optimized partition assay was conducted as follows: A buffer solution containing 15 nM BODIPY and 5  $\mu$ M drug was allowed to incubate with the cells (both differentiated and undifferentiated) in buffer (to decrease the overall time drug needed to spend in buffer). Two wells (one for differentiated and one for undifferentiated cells) only received BODIPY and no drug to serve as a control. After 45 minutes, Hoechst 33342 was added directly to the wells. After 60 minutes, 40  $\mu$ L of buffer was removed for LC-MS/MS analysis and the cells were washed with blank buffer. Eleven cells were selected throughout the plate in order to obtain a representative sample of the neutral lipid content in the well (Figure 11). The plate was scanned via confocal microscopy and the overall fluorescence was determined for both cell types.

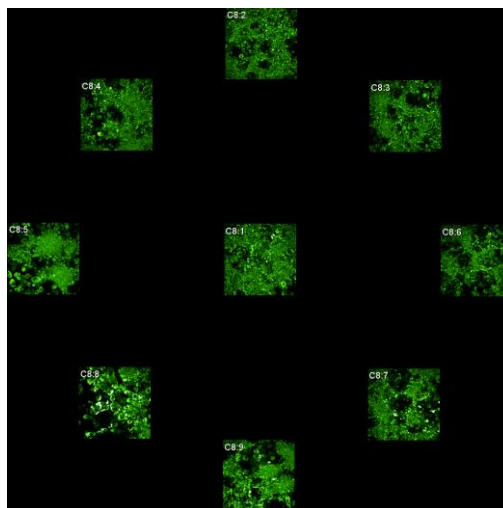


Figure 11: Analyzed fields in each well.

The samples were quantified using the software Harmony 4.8. The different height images were stacked (using maximum projection). This merges all the images into one, which helps eliminate bias if there is focus height difference across the plate. Using the BODIPY signal, the neutral lipids are quantified. In order to eliminate background, the

signal restricted to the cytoplasm is examined. The threshold is adjusted for sensitivity of detection (based on brightness of background compared to the lipid droplets). The same settings were used for the differentiated and undifferentiated cells. The outputs included the BODIPY intensity, as well as the average neutral lipid area.

#### 4.3.4: Partitioning assay

1 mg/mL drug solutions were made in DMSO. These drugs were chosen based on their characteristics including ionization and lipophilicity. Diclofenac, an acid, and quinidine, a base was used. Additionally, midazolam, caffeine, and felodipine were used to represent neutrals. Caffeine, a neutral hydrophilic drug, was included as a negative control as it was not expected to partition into cells.

The partitioning assays were performed in a 96 well format. Partitioning experiments were done on day fifteen post-differentiation. Undifferentiated fibroblasts were plated on the 96-well plate, the week of the experiment. The final concentration of all substances used in assay include 15 nM BODIPY, 1/10000 Hoechst, and 5  $\mu$ M drug in buffer. The medium was aspirated off and the buffer (with BODIPY and drug) was added the wells. Four replicates of each drug were used for partitioning into both differentiated and undifferentiated cells. The drugs were allowed to partition into cells for 1 hour, at which point 40  $\mu$ L of buffer was removed. The remaining buffer was removed, and equal volume of blank buffer was added to the wells. The cells were imaged via confocal microscopy. The concentration of drug in the buffer was determined via LC-MS/MS. The samples were prepared for LC-MS/MS by add 20  $\mu$ L of the drug in buffer and 40  $\mu$ L of internal standard spiked in acetonitrile. The partitioning in the differentiated versus undifferentiated cells were compared using the t-test.

#### 4.3.5: Data analysis and model development

The adipocyte partition coefficient was determined by dividing the amount of drug in adipocytes by the drug in the buffer (Equation 21). The amount of drug in the adipocytes was estimated by subtracting the amount of drug in the buffer, by the total drug introduced to the well. Ideally, it would be preferable to experimentally determine the drug concentration in the adipocytes. However, the assumption was made that the drug is either in the buffer or in the adipocytes and none is lost. A t-test was used to determine whether there was a significant difference in the adipocyte: buffer partition coefficient in differentiated versus undifferentiated cells.

*Adipocyte: buffer partition coefficient*

$$= \frac{\text{Total amount of drug} - \text{Drug in buffer}}{\text{Drug in buffer}}$$

Equation 21: Determination of the adipocyte: buffer partition coefficient

The adipocyte partition coefficient values were plotted against neutral lipid fluorescence. This provided insight into how the partitioning is related to the neutral lipid content. The log of the adipocyte: buffer partition coefficient was plotted against the logP, and logLkl.

With partitioning data, along with the confocal imaging, initial modeling efforts were attempted in order to determine whether the adipocyte partition coefficients were able to demonstrate partitioning into neutral lipids. The BODIPY intensity, logP, and pK<sub>a</sub> were used as inputs, and ultimately six terms were parameterized from the model.

## 4.4: Results

### 4.4.1: Confocal microscopy method optimization

The ideal BODIPY concentration was determined using different concentration (1  $\mu\text{M}$  to 0.1 nM) in order to see which concentration gave good contrast between the background and the desired BODIPY signal. Too high of a concentration leads to overexposure. Figure 12 shows the confocal images at 1 nM BODIPY in medium, with blue DAPI staining used. Ultimately this concentration was optimized again, with a new stock of BODIPY. In partitioning assays, a 15 nM BODIPY concentration was used. The influence of the drug on the BODIPY signal was tested with all of the probe drugs (felodipine, midazolam, caffeine, diclofenac, and quinidine). There were no differences between the wells or in the BODIPY signal.

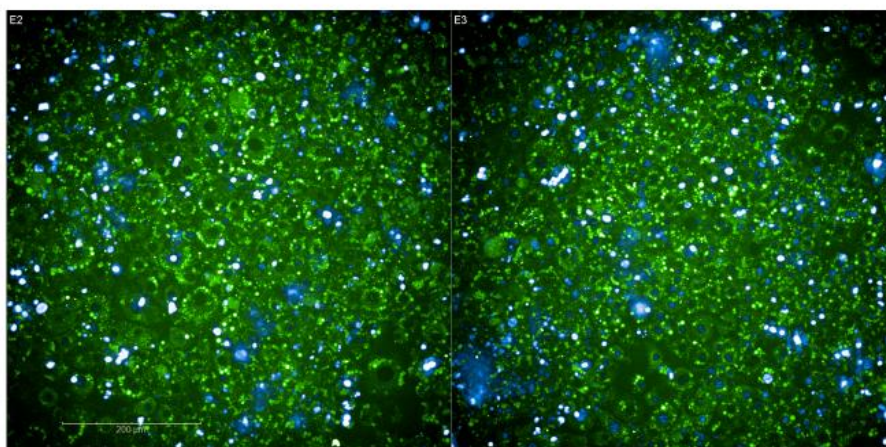


Figure 12: Optimization of BODIPY concentration. Images are at 1 nM BODIPY using 20x magnification. Image on left is BODIPY alone, while image on right is with 2  $\mu\text{M}$  midazolam.

Throughout the course of optimization, different sources of BODIPY were used. If the vial was thawed and refrozen and exposed to light, there was a decrease in the integrity

of the dye and the ability of the dye to target the lipid droplets. Figure 13 shows an image used from an older vial of BODIPY, where many of the large lipid droplets are not stained. A new BODIPY solution was ultimately made (as discussed in the methods) and aliquoted into smaller volumes.

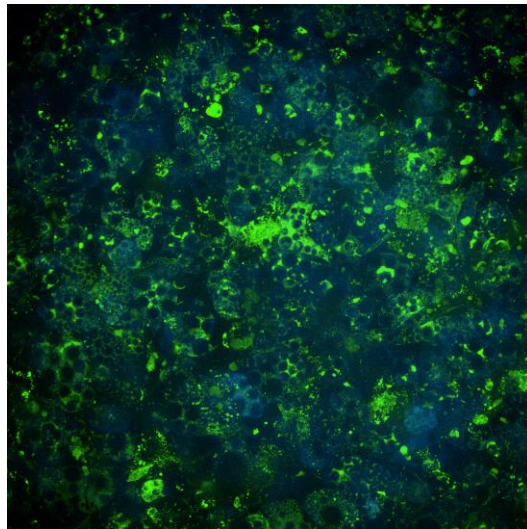


Figure 13: Attempt on using BODIPY to identify lipid droplets (20x magnification and 1 nM BODIPY concentration was used).

The length of time that the cells could be exposed to buffer was also investigated. Figure 14 shows cells where the BODIPY was incubated in buffer and then washed with blank buffer prior to use. The longer the cells spent in buffer, the more likely they were to detach or peel from the bottom of the plate. In order to reduce the amount of time the cells spent in buffer, the drug and BODIPY were co-incubated for an hour prior to imaging.

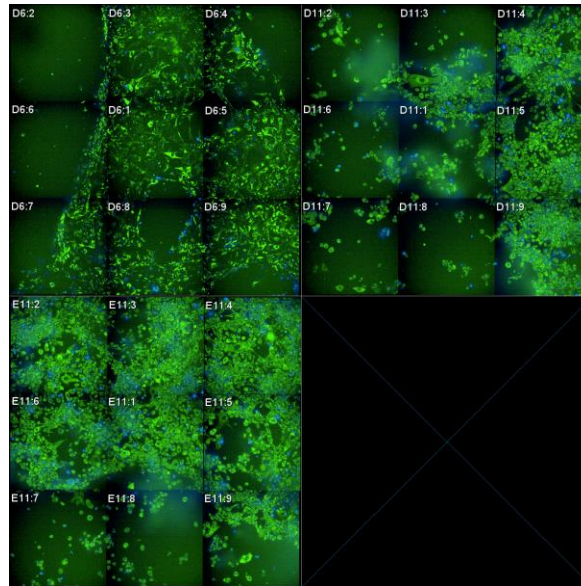


Figure 14: Effect of incubation and wash with buffer on attachment of cells (1 nM BODIPY and 20x magnification was used).

#### 4.4.2: Cell characterization/neutral lipid quantification

The cells were imaged for at both 20x and 40x magnification. Figure 15 shows both cell types at 40x magnification. While the Hoechst was able to accurately dye the nucleus in the undifferentiated cells, the dye was not able to accurately stain the differentiated cells. For this reason, the Hoechst could not be used for quantification. The quantification was done on both the fibroblasts and the differentiated fibroblast, ultimately using three different methods (Appendix J). Quantitation method one and two, utilized a threshold of 0.4 and 0.7 respectively, while quantitation method three used two different thresholds for the different cell types. Quantitation method two was ultimately used for the quantitation of the BODIPY intensity and BODIPY intensity area because it had the best contrast between the background and the lipid droplets. Figure 16 shows the difference in BODIPY intensity between the fibroblasts and the differentiated cells. The two images have the same settings used to examine them and the brighter the green, the more intense the BODIPY

signal. The purple and pink outlines in Figure 16 show the area being considered for BODIPY intensity.

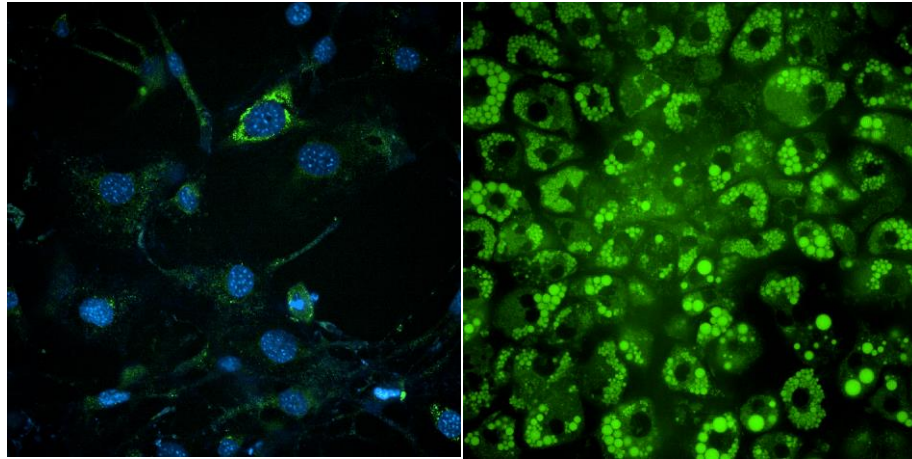


Figure 15: 40x magnification of undifferentiated 3T3-L1 cells (left) and differentiated 3T3-L1 cells (right) (15 nM BODIPY was used).

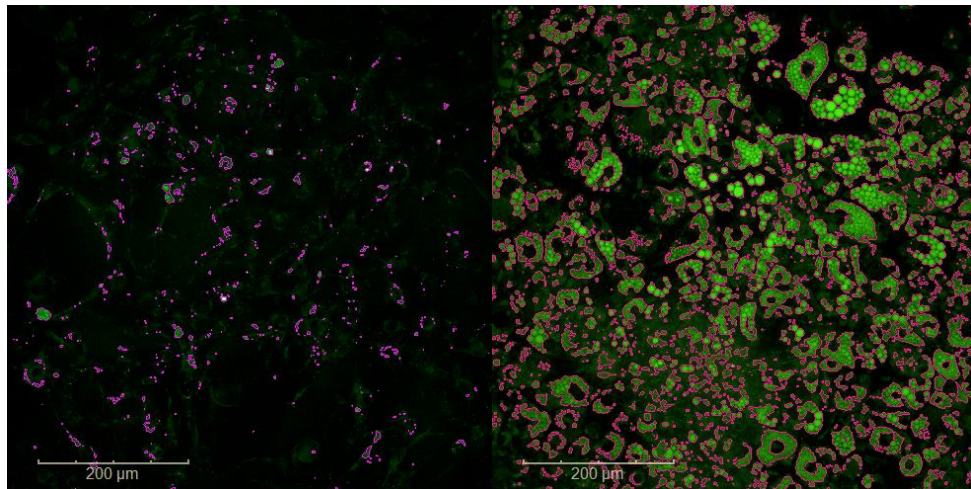


Figure 16: Quantification of BODIPY intensity in undifferentiated cells (left) and differentiated cells (right) (15 nM BODIPY and 20x magnification was used).

A comparison of the overall intensity of the BODIPY signal can be seen in Figure 17. Wells B7-B10, C7-C10, D7-D10, E7-E10, F7-F10, and G6 were the differentiated cells. While the rest were undifferentiated 3T3-L1 cells. The darker the color seen on the heat map, the higher the intensity. The lowest value detected was 1471 and the maximum value was 5203.

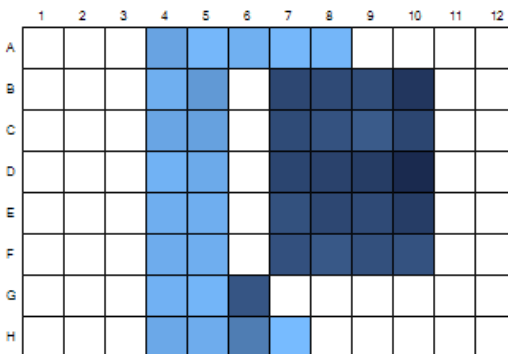


Figure 17: Heat map of the BODIPY signal in wells used for assay.

Overall, both the undifferentiated and differentiated cells were fairly uniform in their lipid composition, based on the intensity of the signal (Figure 18 and 19). The differentiated cells had a significantly greater BODIPY intensity than the undifferentiated cells, and when the average intensity for the different cells was examined for each compound, there was no significant difference between them.

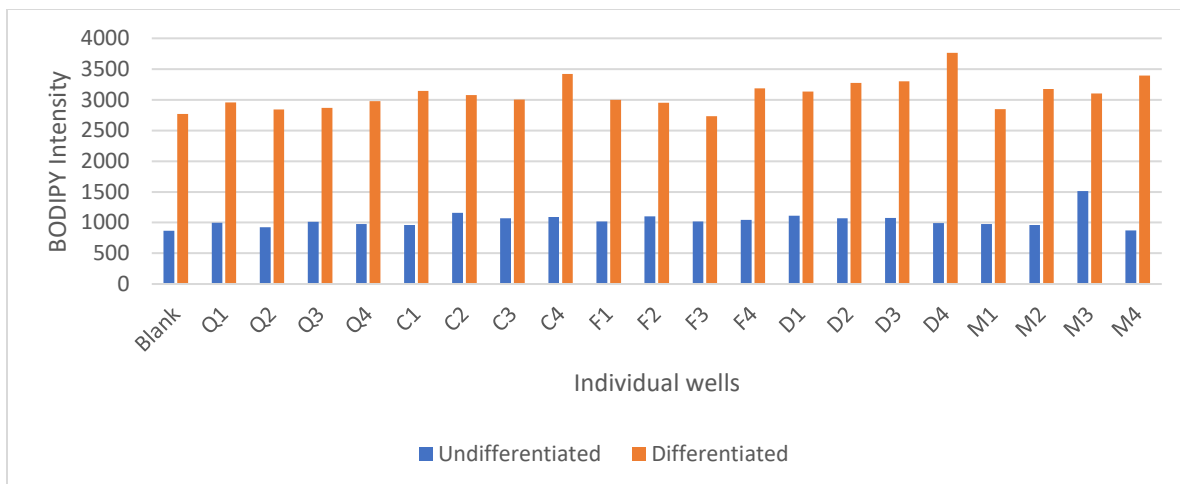


Figure 18: Comparison of BODIPY intensity for each well. Q: quinidine, C: caffeine, F: felodipine, D: diclofenac, M: midazolam.

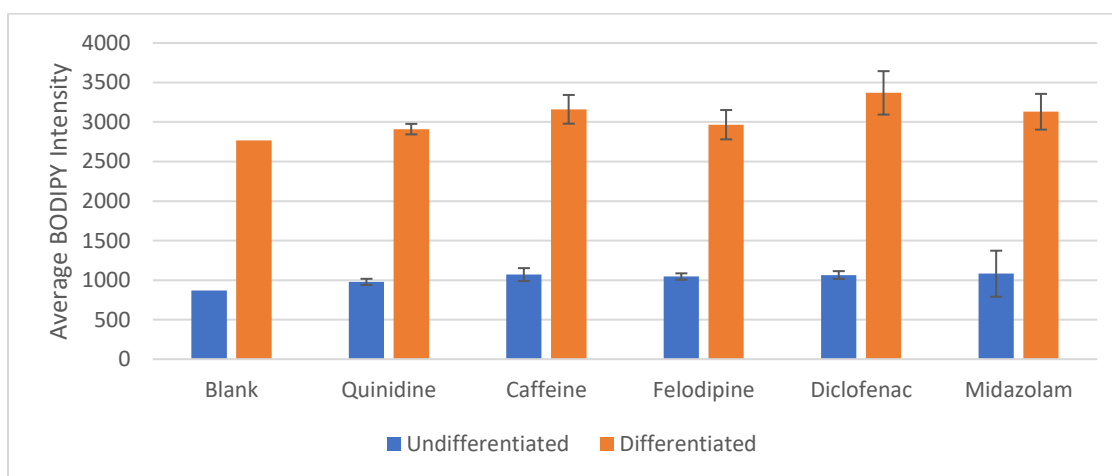


Figure 19: Comparison of average BODIPY intensity for different compounds.

Another output is the BODIPY lipid area comparison. Figure 20 shows this area for the different wells. As the differentiated cells are bigger, with more lipid droplets, the area is significantly greater. However, it can also be seen that for different wells the area fluctuated throughout the plate, whether it was from the imaging or from the plating of the cells.

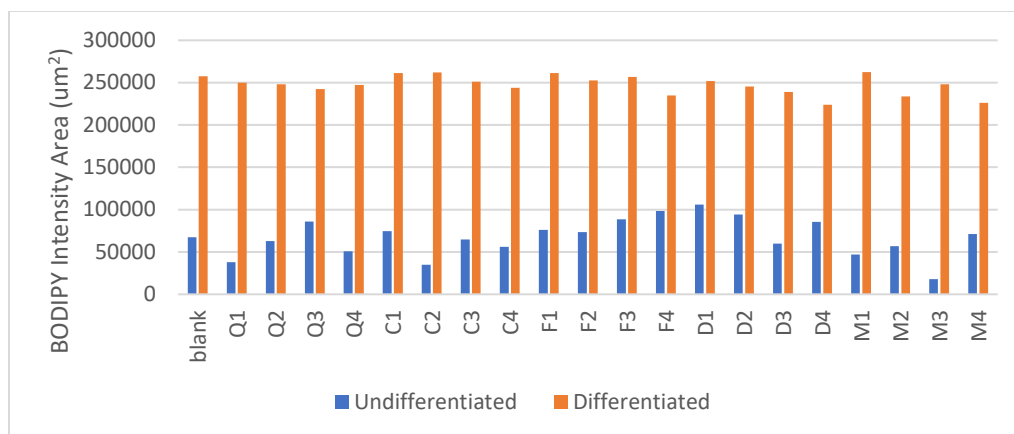


Figure 20: Neutral lipid area comparison for different wells.

#### 4.4.3: Partitioning

Overall, felodipine had the highest measured partition coefficient, followed by diclofenac, and midazolam. Felodipine showed the greatest difference in partitioning between the differentiated and undifferentiated cells (Figure 21 and Table 8). Caffeine, the negative control, had no significant difference between the partition coefficients for differentiated versus undifferentiated cells.

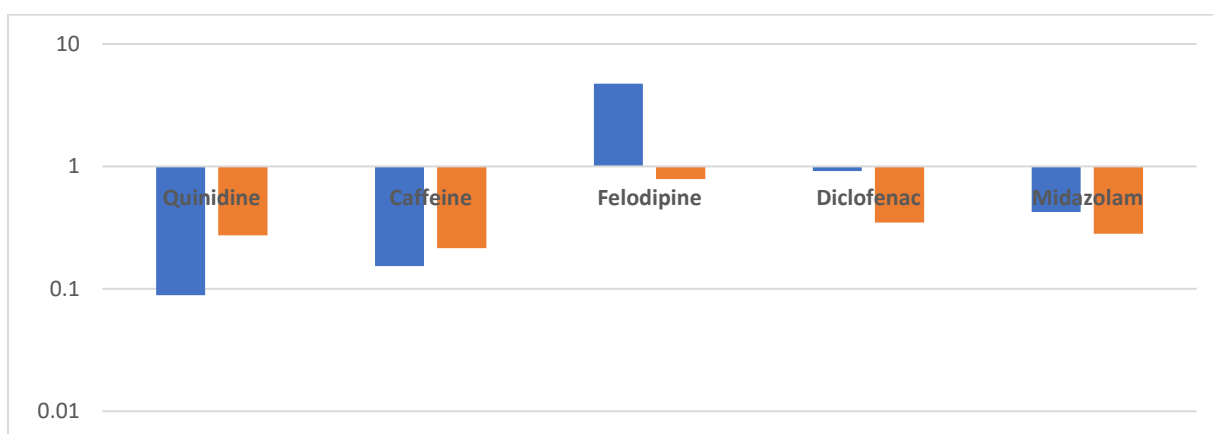


Figure 21: Comparison of average partition coefficient between differentiated and undifferentiated cells.

Table 8: Comparison of partition coefficients.

Drug	Differentiated*	Undifferentiated*	Significance**
Diclofenac	0.92 (14%)	0.35 (22%)	p=0.000242; yes
Caffeine	0.15 (38%)	0.22 (28%)	p=0.19; no
Midazolam	0.42 (19%)	0.28 (44%)	p=0.17; no
Felodipine	4.75 (8%)	0.79 (39%)	p=0.00001; yes
Quinidine	0.089 (75%)	0.27 (56%)	p=0.07; no

\*Average partition coefficient (CV), \*\*t test was used, and significance was determined with p value < 0.05

The partitioning results were compared with the fold difference in BODIPY intensity between the differentiated versus undifferentiated cells. Despite differences in lipid content (based on BODIPY intensity), there does not seem to be an increase in the adipocyte partitioning term (Figure 22). For many of the drugs there is a decreasing trend in the adipocyte partitioning, as the intensity increases.

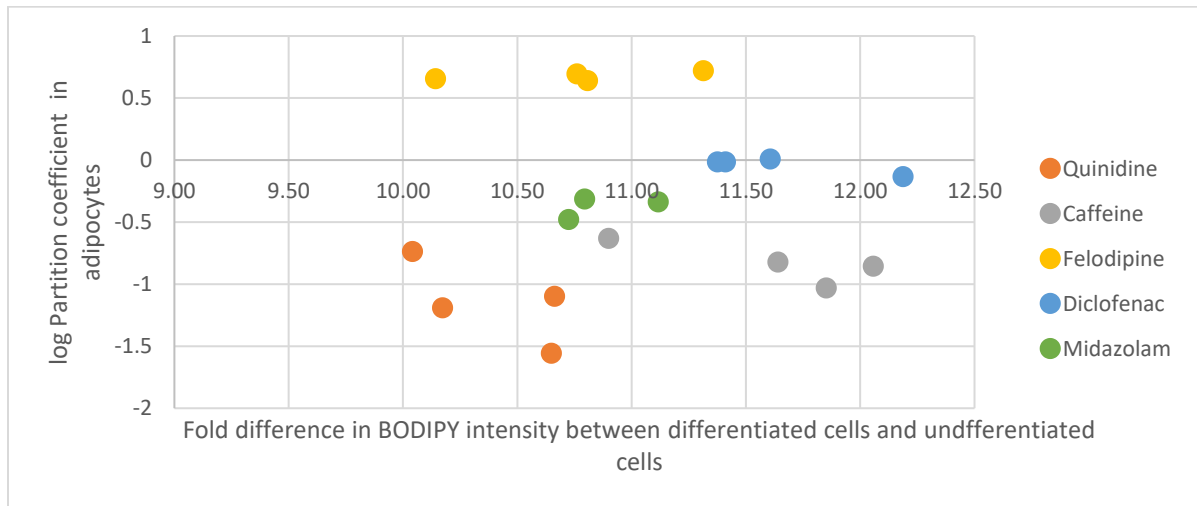


Figure 22: The fold difference in BODIPY intensity plotted against log of the adipocyte: buffer coefficient from differentiated cells.

The log of the adipocyte partitioning term was plotted against the different surrogates. In Figure 23, the logP is plotted against the adipocyte partition coefficient ( $R^2=0.2455$ ). In Figure 24, a plot of the logLkI versus the log of the ratio of the partition coefficients showed a decent relationship ( $R^2= 0.8592$ ). As the phospholipid partitioning surrogate increases, there is also an increase in the ratio of the adipocyte partition coefficient to the fibroblasts.

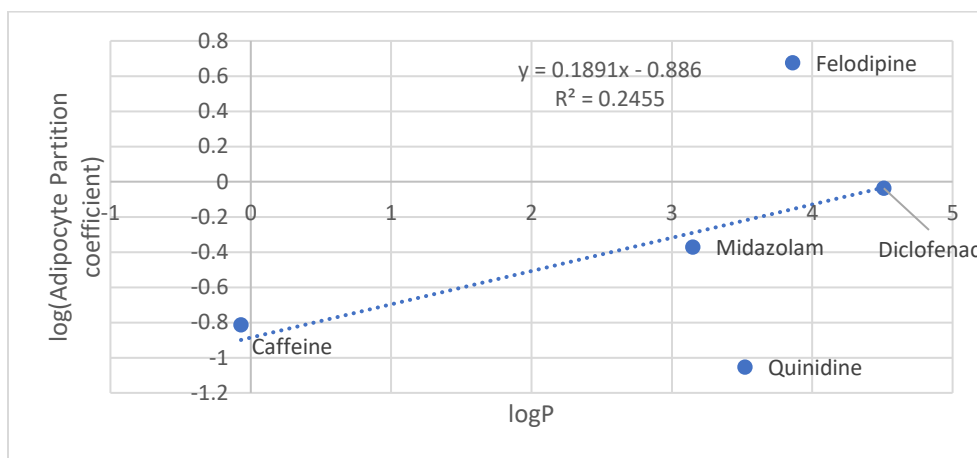


Figure 23: Comparison of the logP and the log of the adipocyte partition coefficient.

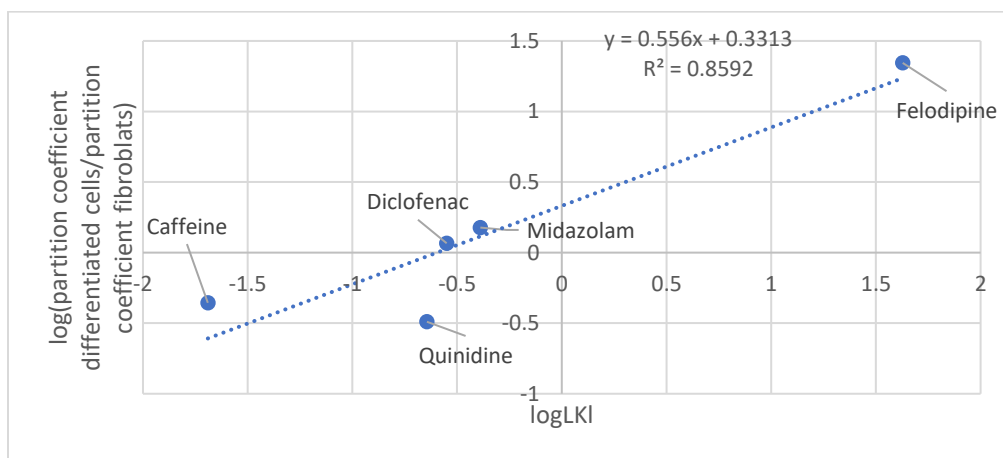


Figure 24: Comparison of the logLkI and log of the adipocyte partition coefficient ratio.

#### 4.4.4: Initial model development

Initial modeling efforts were undertaken in order to determine whether the adipocyte partition coefficient could be used to represent neutral lipid partitioning. The first step was to identify which fraction of the drug would interact with either phospholipids or neutral lipids. Ionized and unionized bases can interact with the phospholipid component, while only the neutral fraction of the neutral and acidic compounds will interact with that the neutral lipid component. For all classes, only unionized drug will interact with neutral lipids. The neutral fraction for interaction neutral lipids was not modified, but the neutral fraction which would interact with phospholipids was scaled (Nagar et al., 2017).

Equation 22 was the model developed, where intensity is the BODIPY intensity multiplied by the intensity area, min is the minimum value from the model, c1-c5 were coefficients which were determined from fitting the data, a1-a3 were set to 0 or 1 and used to identify acid, bases, and neutrals (a1: acids, a2: neutrals, and a3: bases), P is the octanol: water partition coefficient, and  $pK_{a,a}$  and  $Pk_{a,b}$  represent the acidic and basic ionization constants. C5 was an additional term to represent nonspecific binding. 1/Y weighting was used.

$$K_p = \left( \frac{\text{intensity}}{\text{min}} \right) \cdot |c1| \cdot \frac{1}{10^{(pkab-7.2)} + 10^{(7.2-pkaa)} + 1} \cdot P + (a1 \cdot |c2| + a2|c3|) \cdot \frac{1}{10^{0.4(pka,b-7.2)} + 10^{0.4(7.2-pka,a)} + 1} \cdot P + a3 \cdot |c4| \cdot P + c5$$

Equation 22: Initial model developed to describe lipid interactions

The correlation matrix is presented in table 10, and the c1-c5 values predicted from the model are shown in table 9. The experimental partition values were plotted against the predicted values, with a line representing the line of unity (Figure 25). The R<sup>2</sup> value was 0.954755. The neutral lipid term (c1) was found to be significant, while the correlation matrix did not show any significant correlation between the different terms.

Table 9: Parameter estimates.

	Estimate	Standard Error	t-statistic	P-value
c1	0.0000298479	1.69 x10 <sup>-6</sup>	17.5955	5.84625 x 10 <sup>-19</sup>
c2	0.000179036	0.0000684984	2.61372	0.013116
c3	0.0000391356	0.0000232107	1.6861	0.100672
c4	0.0000168886	0.0000401207	0.420944	0.67637
c5	0.155549	0.0835406	1.86195	0.071023

Table 10: Correlation matrix.

	C1	C2	C3	C4	C5
C1	1	0.0367624	-0.518221	0.00513855	-0.0596087
C2	0.0367624	1	0.356174	0.501818	-0.663134
C3	-0.518221	0.356174	1	0.426676	-0.534803
C4	0.00513855	0.501818	0.426676	1	-0.756569
C5	-0.0596087	-0.663134	-0.534803	-0.756569	1

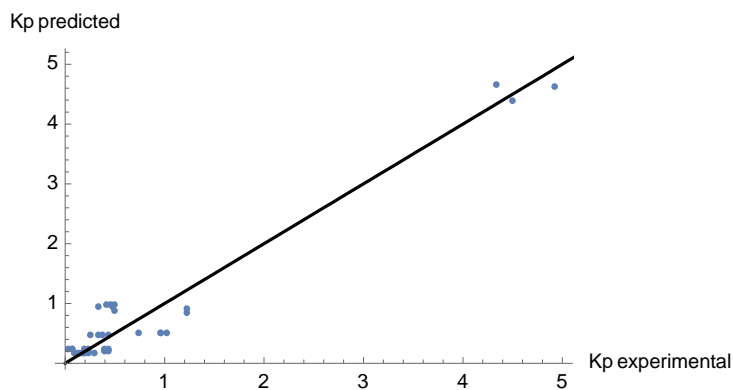


Figure 25: Experimental Kp plotted against the predicted Kp.

#### 4.5: Discussion and conclusions

By differentiating 3T3-L1 fibroblasts, adipocyte-like cells can be obtained. These cells have a large number of adiposomes, which are filled with neutral lipids. These cells were chosen as a potential surrogate for neutral lipid partitioning in adipose tissue because of the difference in the lipid composition in the tissue. Neutral lipids are 40x more abundant in adipose tissue, as opposed to phospholipids.

Throughout the course of this study, the cells were grown and characterized using confocal microscopy. Drugs were partitioned into these cells, as well as undifferentiated fibroblasts (as a means of comparison). Drugs were selected from the previous data set used to examine the use of microsomal partitioning to represent phospholipid partitioning in Specific Aim 2. The drugs chosen for this assay, included, an acid, base, as well as different neutrals, caffeine, midazolam, and felodipine. These drugs differ in their ionization at pH 7.4, as well as their lipophilicity.

The five drugs were partitioned into the two cell types and were imaged via confocal microscopy. For two of the drugs, felodipine and diclofenac, there was a significant difference in the partition coefficient determined from the two cell types. This

difference was the largest for felodipine (a neutral, highly bound compound). Both drugs have high logP values. Felodipine has a logP of 3.86, while diclofenac has a logP of 4.51. However, as the fold difference in BODIPY intensity increased, there was not an observed increase in the partitioning for these compounds (Figure 22). One reason for this, could be that the fold difference in BODIPY intensity between the two cells did not differ drastically between the wells. Partitioning the drug into the lipids, at different times after differentiation may show some bigger differences.

Adipocytes, while having a large number of triglycerides, also have a phospholipid component. Drugs will need to be able to cross the membrane in order to interact with the triglycerides. This increase in phospholipid content, could have led to an increase in the partition coefficient measured. In order to determine whether the adipocyte partitioning terms were able to describe the neutral lipid partitioning, an initial model was developed.

The model developed required five terms to be parameterized. Unfortunately, due to the number of drugs which were used in the partitioning assay (and the number of replicates) there was insufficient data available to parameterize the model. However, initial modeling work indicated that neutral lipid partitioning contributed to the partitioning into the adipocytes. As only five of the nineteen drugs were used, doing partitioning for the rest (and at different neutral lipid levels) may provide sufficient data to build a useful model.

The quantification method could be improved with the use of a nuclear dye to target the nucleus. This would allow quantitation to be normalized to cell number, which may provide a better comparison of intensity. Also, if different concentrations of neutral lipids were used, a better relationship could be determined between the BODIPY intensity and neutral lipid content.

## CHAPTER 5: SUMMARY AND FUTURE DIRECTIONS

**'Reproduced in part' with permission from *Drug Metabolism and Disposition*, Prediction of tissue - plasma partition coefficients using microsomal partitioning: Incorporation into physiologically-based pharmacokinetic models and steady state volume of distribution predictions, 47, 12, 1050-1060. Copyright 2019 The American Society for Pharmacology and Experimental Therapeutics.**

### 5.1: Summary

Composition-based  $K_p$  prediction equations attempt to determine drug distribution into the tissues by describing the interactions a drug can have in the tissues. Plasma protein interactions are described using a protein ratio and the fraction unbound in plasma, while lipid partitioning has traditionally been described using the  $\log P$  and  $\log P_{vo}$ . However, the  $\log P$  does not fully represent all the interactions a drug can have with lipids, while the  $\log P_{vo}$  is calculated from the  $\log P$ . The phospholipid interaction is important because not only are phospholipids the predominant lipid in most tissues, but a drug can interact with different regions of the phospholipid membrane. Neutral lipid partitioning is most important in adipose tissue, where the neutral lipid fraction is greatest. The overall goal of the project was to see if the lipid partitioning could be parameterized in different ways, to more mechanistically describe the interactions in the tissues.

Four specific aims were proposed. The first specific aim was to experimentally determine the plasma protein binding and the microsomal partitioning for the 19 probe drugs. The second specific aim was to compare two different  $K_p$  prediction equations,

$K_{p,mem}$  and  $K_{p,dPL}$ , which described phospholipid partitioning in different ways. The third specific aim was to determine drug partitioning in adipocytes. The fourth specific aim was to incorporate this term into a  $K_p$  prediction model.

Specific Aim 1 focused on experimentally determining the plasma protein binding and microsomal partitioning. In order to do this, LC-MS/MS methods were developed for the nineteen drugs. Equilibrium dialysis was used to determine the  $f_{up}$  and  $f_{um}$  for the probe compounds. All plasma protein binding values were determined at 5%  $CO_2$ , because of the influence of pH on the protein binding measurements.

Specific Aim 2 examined if the use of microsomal partitioning could be used to represent phospholipid partitioning in  $K_p$  prediction models. Two  $K_p$  prediction models were used, one which used microsomal partitioning to represent total phospholipid partitioning ( $K_{p,mem}$ ), and one which used two terms to represent partitioning into phospholipids ( $K_{p,dPL}$ ). The ability of the methods to predict the  $V_{ss}$  and the concentration-time profile were compared by examining the AAFE and EOC values. Overall, both methods were able to predict the  $V_{ss}$  and the shape of the concentration-time profile with comparable accuracy.

Specific Aim 3 attempted to determine an adipocyte partition coefficient which could be used to describe the drug interaction with neutral lipids in adipose tissue. In order to do this, adipocytes were differentiated from 3T3-L1 cells, a mouse embryonic cell line. The cells were imaged by confocal microscopy and the lipophilic dye, BODIPY, was used to identify lipid droplets in the cells. The differentiated cells resulted in 12.5x more BODIPY intensity than the undifferentiated cells. Five test drugs (from the nineteen-drug dataset) were partitioned into differentiated and undifferentiated 3T3-L1 cells. For only

two of the drugs (felodipine and diclofenac) was there a significant difference in the partitioning into differentiated versus undifferentiated cells. Partitioning of the drug into neutral lipids did not increase, when the fold intensity in BODIPY (between differentiated and undifferentiated cells) increased. An initial model was developed describing the lipid interactions in adipocytes and using the BODIPY intensity to relate the neutral lipid differences. In this model, neutral lipid partitioning did contribute to the overall partitioning into the adipocytes.

## 5.2: Future directions

Improved predictions of the tissue  $K_{ps}$  can ultimately help improve pharmacokinetic predictions early in drug discovery. Current  $K_p$  prediction models make assumptions of how a drug will interact with different tissue components. One of the goals of this project was to provide a more mechanistic description of drug-tissue interactions.

As previously discussed, the logP has traditionally been used to describe lipid partitioning, because of its relationship to hydrophobicity. The more hydrophobic a compound, the higher the logP (as the compound prefers the octanol phase). This term had not been able to fully describe the tissue partitioning in adipose tissue. This is because, while for most tissues, phospholipid partitioning is the predominant lipid term, in adipose tissue, neutral lipid partitioning is the term that dominates (with almost 40x the neutral lipids, compared to phospholipids). This difference in composition makes it difficult to describe the distribution.

Poulin et al. introduced the  $\log P_{vo}$  to describe neutral lipid partitioning in adipose tissue (Poulin et al., 2001). The problem with these values is that they are difficult to measure. Relationships between the logP and  $\log P_{vo}$  have been developed for a small data

set, in order to predict the vegetable oil: water partition coefficient (Leo and Hansch, 1971). It is this value which is used in most  $K_p$  prediction models.

This project was designed to look at two different in vitro surrogates which could provide a more mechanistic description of lipid partitioning. Microsomal partitioning allows for a drug to interact with all phospholipids and does not rely on inaccurate assumptions of how neutral/ionized drugs will interact with the membrane. The use of adipocyte partitioning was drawn from the idea that the partitioning into the triglyceride-rich adipocytes could be used to describe a drug's interaction with neutral lipids in the body.

By using different lipid partitioning terms, we did not expect to see an improvement for the  $V_{ss}$  prediction for acids (as these drugs do not really partition into lipids). Acids are generally ionized at physiological pH and it is most favorable for the uncharged fraction to interact with neutral lipids. Neutral compounds are completely unionized at physiological pH and partitioning into phospholipids, and neutral lipids in adipose tissue, is expected to occur. For bases, neutral lipid partitioning may not have as significant of a role as phospholipid partitioning and/or lysosomal partitioning.

One problem moving forward, however, is the degree to which predictions can be improved by altering how neutral lipid partitioning in adipose tissue is described. Microsomal partitioning was originally used in a physiological  $V_{ss}$  prediction equation (Korzekwa and Nagar, 2017a). The inclusion of neutral lipid partitioning did not significantly improve the predictions of  $V_{ss}$ . When parameterizing the terms, a and b, for the  $K_{p,mem}$  equation with rat data, the b coefficient for neutral lipid partitioning for the tissues was low. A separate b1 value for neutral lipid partitioning in adipose tissue, did not improve the fit.

The results from this study are similar to a previous study to determine factors which influenced the intracellular bioavailability (Treyer et al., 2018). They looked at the role of neutral lipid partitioning and phospholipid partitioning in a cell assay (also using 3T3-L1 cells), where they determined that the driving force for tissue interactions in these cells is the interaction with the phospholipids. They found that the increase in neutral lipids did not translate into an increase in the partition coefficient. In chapter four, experimental partition coefficients were determined in fibroblasts and adipocytes. While a significant difference in the partition coefficients was only seen with two of the drugs (diclofenac and felodipine), initial modeling attempts have shown that neutral lipid partitioning contributed to the overall distribution into the cells. As only five of the nineteen drugs were used in the partitioning experiments, more data could lead to a better model and neutral lipid partitioning surrogate.

Different surrogates to represent neutral lipids could be used moving forward. Some potential options include using triglycerides or lipid nanoparticles. The vegetable oil: water partitioning term is an example of a triglyceride partitioning terms; however, this term is not experimentally determined. One of the reasons this term is not determined experimentally is because of the difficulty in measuring the concentration of drug in the different phases accurately. Potentially, improving methods to determine the amount/concentration of drug in the different phases would allow triglyceride partitioning to be used. The phases would need to be successfully separated and the drug would need to be quantitated in both phases accurately. For lipid nanoparticles, different dialysis methods are used in order to determine the unbound concentration. Potentially the fraction of drug that is interacting with the lipid core could be determined.

Also, as discussed in chapter four, confocal microscopy is an excellent tool to determine how a drug is interacting with the adipocytes. Other dyes can be used to describe the lipids inside the cell. Also, fluorescent drugs could be partitioned into the cells, which may help us understand the overall fraction which interacts with the neutral lipid core.

For many of the drugs, using either the  $K_{p,mem}$  or  $K_{p,dPL}$  method, the terminal phase distribution was not predicted well. One reason for this, may be because of the assumption of perfusion-limited distribution. In this model, it is assumed that the drug getting into the tissues/cells is not the rate-limiting step and a well-stirred model is assumed. The development of permeability-limited PBPK models, could potentially help describe the concentration of drug in the tissues more accurately.

Another future direction is to look at the role transporters and permeability play on the prediction of tissue distribution. Transporter-mediated distribution can result in inaccurate predictions of  $K_p$  and  $V_{ss}$ , particularly for some acids. OATP transporters can alter hepatic intracellular concentrations by two orders of magnitude (Kulkarni et al., 2016). Therefore, uptake into this organ alone can result in a 2-fold increase in  $V_{ss}$ . Efflux transporters (e.g. P-gp and BCRP) will have a smaller impact. The decrease in  $V_{ss}$  due to P-gp and BCRP at the blood-brain barrier would result in a 2% decrease in  $V_{ss}$ . The impact from the liver would be even smaller since efflux transporters in the apical membrane would only decrease liver concentrations by 50% (Korzekwa and Nagar, 2014).

Also, assumptions are made concerning the interactions drugs will have in the tissues/cells. In most models, lysosomal partitioning is excluded, even though lysosomal partitioning will affect the tissue distribution for bases. For strong bases, partitioning into lysosomes due to pH differences results in lysosomal concentrations >200 times cytosolic

concentrations. Assuming 5% lysosomes and 60% intracellular water in cells, partitioning of a strong base into lysosomes can increase the  $K_{p,u}$  six-fold. As discussed previously, whereas lysosomal partitioning certainly occurs, it is likely to be highly correlated with phospholipid partitioning of bases (Korzekwa and Nagar, 2017a).

This study showed that a different surrogate, microsomal partitioning, can be used to represent phospholipid partitioning. The  $K_{p,mem}$  method was able to predict the  $V_{ss}$  and shape of the concentration-time profile with comparable accuracy to the  $K_{p,dPL}$  method. Additionally, drugs were partitioned into adipocytes and fibroblasts, in order to represent neutral lipid partitioning in adipose tissue. This project suggests that lipid partitioning can be parameterized in different ways, in order to more mechanistically describe drug distribution.

## REFERENCES CITED

- Agarwal SK, Kriel RL, Brundage RC, Ivaturi VD, and Cloyd JC (2013) A pilot study assessing the bioavailability and pharmacokinetics of diazepam after intranasal and intravenous administration in healthy volunteers. *Epilepsy Res* **105**:362-367.
- Albert KS, Hallmark MR, Sakmar E, Weidler DJ, and Wagner JG (1975) Pharmacokinetics of diphenhydramine in man. *Journal of Pharmacokinetics and Biopharmaceutics* **3**:159-170.
- Arundel P (1997) A multi-compartmental model generally applicable to physiologically-based pharmacokinetics., in: *IFAC Symposium*, University of Warwick, UK.
- ATCC (2011) Chemically-Induced Differentiation of ATCC CL-173 (3T3-L1) using Single-component Commercially-available Reagents, American Type Culture Collection, Manassas, VA.
- ATCC (2018) 3T3-L1 (ATCC CL-173), American Type Culture Collection, Manassas, VA.
- Austin RP, Barton P, Cockroft SL, Wenlock MC, and Riley RJ (2002) The influence of nonspecific microsomal binding on apparent intrinsic clearance, and its prediction from physicochemical properties. *Drug Metabolism and Disposition* **30**:1497-1503.
- Avdeef A (2003) *Absorption and Drug Development: Solubility, Permeability, and Charge State*. Wiley.
- Balaz S (2009) Modeling Kinetics of Subcellular Disposition of Chemicals. *Chem Rev* **109**:1793-1899.
- Berezhkovskiy LM (2004) Volume of distribution at steady state for a linear pharmacokinetic system with peripheral elimination. *Journal of Pharmaceutical Sciences* **93**:1628-1640.
- Berry LM, Li C, and Zhao ZY (2011) Species Differences in Distribution and Prediction of Human V-ss from Preclinical Data. *Drug Metabolism and Disposition* **39**:2103-2116.

- Berry LM, Roberts J, Be XH, Zhao ZY, and Lin MHJ (2010) Prediction of V<sub>ss</sub> from In Vitro Tissue-Binding Studies. *Drug Metabolism and Disposition* **38**:115-121.
- Bjorntorp P, Karlsson M, Pertoft H, Pettersson P, Sjoström L, and Smith U (1978) Isolation and characterization of cells from rat adipose-tissue developing into adipocytes. *Journal of Lipid Research* **19**:316-324.
- Björkman S (2002) Prediction of the volume of distribution of a drug: Which tissue-plasma partition coefficients are needed? *Journal of Pharmacy and Pharmacology* **54**:1237-1245.
- Blanchard J and Sawers SJA (1983) The absolute bioavailability of caffeine in man. *Eur J Clin Pharmacol* **24**:93-98.
- Body DR (1988) The lipid composition of adipose tissue. *Progress in Lipid Research* **27**:39-60.
- Boxenbaum H (1982) Interspecies scaling, allometry, physiological time, and the ground plan of pharmacokinetics. *Journal of Pharmacokinetics and Biopharmaceutics* **10**:201-227.
- Brittain He (2007) *Profiles of Drug Substances, excipients, and related methodology*. Academic Press.
- Brown RP, Delp MD, Lindstedt SL, Rhomberg LR, and Beliles RP (1997) Physiological parameter values for physiologically based pharmacokinetic models. *Toxicol Ind Health* **13**:407-484.
- Bykowski T and Stevenson B (2008) Aseptic Technique. *Current Protocols in Microbiology* **11**:A.4D.1-A.4D.11.
- Campbell BC, Kelman AW, and Hillis WS (1985) Noninvasive assessment of the hemodynamic-effects of Nicardipine in normotensive subjects. *Br J Clin Pharmacol* **20**:S55-S61.
- Chan R, De Bruyn T, Wright M, and Broccatelli F (2018) Comparing Mechanistic and Preclinical Predictions of Volume of Distribution on a Large Set of Drugs. *Pharm Res* **35**:11.

- Clausen J and Bickel MH (1993) Prediction of drug distribution in distribution dialysis and in vivo from binding to tissues and blood. *Journal of Pharmaceutical Sciences* **82**:345-349.
- Clozel JP, Osterrieder W, Kleinbloesem CH, Welker HA, Schlappi B, Tudor R, Hefti F, Schmitt R, and Eggers H (1991) RO 40-5967 - A new nonhydropyridine calcium-antagonist. *Cardiovasc Drug Rev* **9**:4-17.
- Curran RE, Claxton CRJ, Hutchison L, Harradine PJ, Martin IJ, and Littlewood P (2011) Control and Measurement of Plasma pH in Equilibrium Dialysis: Influence on Drug Plasma Protein Binding. *Drug Metabolism and Disposition* **39**:551.
- Dawkins MJR and Stevens JF (1966 ) Fatty Acid Composition of Triglycerides from Adipose Tissue. *Nature* **209**:1145-1146.
- De Buck SS, Sinha VK, Fenu LA, Gilissen RA, Mackie CE, and Nijssen MJ (2007) The prediction of drug metabolism, tissue distribution, and bioavailability of 50 structurally diverse compounds in rat using mechanism-based absorption, distribution, and metabolism prediction tools. *Drug Metab Dispos* **35**:649-659.
- Debruyne D (1997) Clinical pharmacokinetics of fluconazole in superficial and systemic mycoses. *Clin Pharmacokinet* **33**:52-77.
- Debruyne D, Hurault de Ligny B, P Ryckelynck J, Albessard F, and Moulin M (1987) *Clinical Pharmacokinetics of Ketoprofen After Single Intravenous Administration as a Bolus or Infusion.*
- Di L, Breen C, Chambers R, Eckley ST, Fricke R, Ghosh A, Harradine P, Kalvass JC, Ho S, Lee CA, Marathe P, Perkins EJ, Qian M, Tse S, Yan ZY, and Zamek-Gliszczyński MJ (2017) Industry Perspective on Contemporary Protein-Binding Methodologies: Considerations for Regulatory Drug-Drug Interaction and Related Guidelines on Highly Bound Drugs. *J Pharm Sci* **106**:3442-3452.
- Diez I, Colom H, Moreno J, Obach R, Peraire C, and Domenech J (1991) A Comparative in-vitro study of transdermal absorption of a series of calcium-channel antagonists. *J Pharm Sci* **80**:931-934.
- Edgar B, Regardh CG, Johnsson G, Johansson L, Lundborg P, Lofberg I, and Ronn O (1985) Felodipine Kinetics in Healthy-Men. *Clin Pharmacol Ther* **38**:205-211.

- Fenneteau F, Poulin P, and Nekka F (2010) Physiologically Based Predictions of the Impact of Inhibition of intestinal and Hepatic Metabolism on Human Pharmacokinetics of CYP3A Substrates. *J Pharm Sci* **99**:486-514.
- Fessey RE, Austin RP, Barton P, Davis AM, and Wenlock MC (2007) The Role of Plasma Protein Binding in Drug Discovery. *Pharmacokinetic Profiling in Drug Research*.
- Freitas AA, Limbu K, and Ghafourian T (2015) Predicting volume of distribution with decision tree-based regression methods using predicted tissue:plasma partition coefficients. *Journal of Cheminformatics* **7**:17.
- Gabrielsson J and Weiner D (2010) *Pharmacokinetic and Pharmacodynamic Data Analysis: Concepts and Applications*.
- Ghafourian T, Barzegar-Jalali M, Hakimiha N, and Cronin MTD (2004) Quantitative structure-pharmacokinetic relationship modelling: apparent volume of distribution. *Journal of Pharmacy and Pharmacology* **56**:339-350.
- Gillette JR (1971) Factors affecting drug metabolism. *Annals of the New York Academy of Sciences* **179**:43-66.
- Graham H, Walker M, Jones O, Yates J, Galetin A, and Aarons L (2012) Comparison of in-vivo and in-silico methods used for prediction of tissue: plasma partition coefficients in rat. *Journal of Pharmacy and Pharmacology* **64**:383-396.
- Green H and Kehinde O (1974) Sublines of mouse 3T3 cells that accumulated lipid. *Cell* **1**:113-116.
- Greene DS, Quintiliani R, and Nightingale CH (1978) Physiological perfusion model for cephalosporin antibiotics I: Model selection based on blood drug concentrations. *J Pharm Sci* **67**:191-196.
- Gugler R, Manion CV, and Azarnoff DL (1976) Phenytoin- Pharmacokinetics and Bioavailability. *Clin Pharmacol Ther* **19**:135-142.
- Hall LM, Hall LH, and Kier LB (2003) QSAR modeling of beta-lactam binding to human serum proteins. *Journal of Computer-Aided Molecular Design* **17**:103-118.

- Hallifax D and Houston JB (2006) Binding of drugs to hepatic microsomes: Comment and assessment of current prediction methodology with recommendation for improvement. *Drug Metabolism and Disposition* **34**:724-726.
- Hansch C, A. L, and DH. H (1995) Exploring QSAR: Hydrophobic, Electronic, and Steric Constraints, ACS Publications
- Heizmann P, Eckert M, and Ziegler WH (1983) Pharmacokinetics and Bioavailability of Midazolam in Man. *Br J Clin Pharmacol* **16**:S43-S49.
- Hermann P, Rodger SD, Remones G, Thenot JP, London DR, and Morselli PL (1983) Pharmacokinetics of Diltiazem After Intravenous and Oral-Administration. *Eur J Clin Pharmacol* **24**:349-352.
- Hinderling PH (1997) Red blood cells: a neglected compartment in pharmacokinetics and pharmacodynamics. *Pharmacol Rev* **49**:279-295.
- Hiskey CF, Whitman G, and Bullock E (1962) Spectrophotometric study of aqueous solution of Warfarin Sodium. *Journal of Pharmaceutical Sciences* **51**:43-46.
- Holt K, Nagar S, and Korzekwa K (2019a) Methods to Predict Volume of Distribution. *Current Pharmacology Reports* **5**:391-399.
- Holt K, Ye M, Nagar S, and Korzekwa K (2019b) Prediction of Tissue-Plasma Partition Coefficients Using Microsomal Partitioning: Incorporation into Physiologically based Pharmacokinetic Models and Steady-State Volume of Distribution Predictions. *Drug Metabolism and Disposition* **47**:1050-1060.
- Ishihama Y, Nakamura M, Miwa T, Kajima T, and Asakawa N (2002) A rapid method for pK(a) determination of drugs using pressure-assisted capillary electrophoresis with photodiode array detection in drug discovery. *J Pharm Sci* **91**:933-942.
- Jansson R, Bredberg U, and Ashton M (2008) Prediction of drug tissue to plasma concentration ratios using a measured volume of distribution in combination with lipophilicity. *Journal of Pharmaceutical Sciences* **97**:2324-2339.
- Jones R, Jones HM, Rowland M, Gibson CR, Yates JWT, Chien JY, Ring BJ, Adkison KK, Ku MS, He HD, Vuppugalla R, Marathe P, Fischer V, Dutta S, Sinha VK, Bjornsson T, Lave T, and Poulin P (2011) PhRMA CPCDC Initiative on

Predictive Models of Human Pharmacokinetics, Part 2: Comparative Assessment of Prediction Methods of Human Volume of Distribution. *J Pharm Sci* **100**:4074-4089.

Kochansky CJ, McMasters DR, Lu P, Koeplinger KA, Kerr HH, Shou M, and Korzekwa KR (2008) Impact of pH on plasma protein binding in equilibrium dialysis. *Mol Pharm* **5**:438-448.

Korzekwa K (2016) Models for Nonspecific Binding and Partitioning, in: *New Horizons in Predictive Drug Metabolism and Pharmacokinetics* (Wilson AGE ed), pp 53-65, Royal Soc Chemistry, Cambridge.

Korzekwa K and Nagar S (2014) Compartmental Models for Apical Efflux by P-glycoprotein: Part 2-A Theoretical Study on Transporter Kinetic Parameters. *Pharm Res* **31**:335-346.

Korzekwa K and Nagar S (2017a) Drug Distribution Part 2. Predicting Volume of Distribution from Plasma Protein Binding and Membrane Partitioning. *Pharmaceutical Research* **34**:544-551.

Korzekwa K and Nagar S (2017b) On the Nature of Physiologically-Based Pharmacokinetic Models -A Priori or A Posteriori? Mechanistic or Empirical? *Pharm Res* **34**:529-534.

Kulkarni P, Korzekwa K, and Nagar S (2016) Intracellular Unbound Atorvastatin Concentrations in the Presence of Metabolism and Transport. *J Pharmacol Exp Ther* **359**:26-36.

Kunesova M, Hlavaty P, Tvrzicka E, Stankova B, Kalouskova P, Viguerie N, Larsen TM, Van Baak MA, Jebb SA, Martinez JA, Pfeiffer AFH, Kafatos A, Handjieva-Darlenska T, Hill M, Langin D, Zak A, Astrup A, and Saris WHM (2012) Fatty Acid Composition of Adipose Tissue Triglycerides After Weight Loss and Weight Maintenance: the DIOGENES Study. *Physiological Research* **61**:597-607.

Kwon Y (2002) Handbook of Essential Pharmacokinetics and Pharmacodynamics and Drug Metabolism for Industrial Scientists Kluwer Academic Publishers.

- Lambrinidis G, Vallianatou T, and Tsantili-Kakoulidou A (2015) In vitro, in silico and integrated strategies for the estimation of plasma protein binding. A review. *Advanced Drug Delivery Reviews* **86**:27-45.
- Leo A and Hansch C (1971) Linear free-energy relationships between partitioning solvent systems. *Journal of Organic Chemistry* **36**:1539-1544.
- Leo A, Hansch C, and Elkins D (1971) Partition coefficients and their uses. *Chem Rev* **71**:525-616.
- Li R, Bi YA, Vildhede A, Scialis RJ, Mathialagan S, Yang X, Marroquin LD, Lin J, and Varma MVS (2017) Transporter-Mediated Disposition, Clinical Pharmacokinetics and Cholestatic Potential of Glyburide and Its Primary Active Metabolites. *Drug Metab Dispos* **45**:737-747.
- Lombardo F, Obach RS, DiCapua FM, Bakken GA, Lu J, Potter DM, Gao F, Miller MD, and Zhang Y (2006) Hybrid mixture discriminant analysis-random forest computational model for the prediction of volume of distribution of drugs in human. *Journal of Medicinal Chemistry* **49**:2262-2267.
- Lombardo F, Obach RS, Shalaeva MY, and Gao F (2002) Prediction of volume of distribution values in humans for neutral and basic drugs using physicochemical measurements and plasma protein binding data. *Journal of Medicinal Chemistry* **45**:2867-2876.
- Lombardo F, Obach RS, Shalaeva MY, and Gao F (2004) Prediction of human volume of distribution values for neutral and basic drugs. 2. Extended data set and leave-class-out statistics. *Journal of Medicinal Chemistry* **47**:1242-1250.
- Ludden TM, Boyle DA, Giesecker D, Kennedy GT, Crawford MH, Ludden LK, and Clementi WA (1988) Absolute Bioavailability and Dose Proportionality of Betaxolol in Normal Healthy-Subjects. *J Pharm Sci* **77**:779-783.
- Maguire KP, Burrows GD, Norman TR, and Scoggins BA (1980) Blood-Plasma Distribution Ratios of Psychotropic-Drugs. *Clin Chem* **26**:1624-1625.
- McAllister RG and Kirsten EB (1982) The Pharmacology of Verapamil. IV. Kinetics and Dynamic Effects After Single Intravenous and Oral Doses. *Clin Pharmacol Ther* **31**:418-426.

- McLure JA, Miners JO, and Birkett DJ (2000) Nonspecific binding of drugs to human liver microsomes. *British Journal of Clinical Pharmacology* **49**:453-461.
- Mehra A, Macdonald I, and Pillay TS (2007) Variability in 3T3-L1 adipocyte differentiation depending on cell culture dish. *Analytical Biochemistry* **362**:281-283.
- Nagar S and Korzekwa K (2012) Commentary: Nonspecific Protein Binding versus Membrane Partitioning: It Is Not Just Semantics. *Drug Metab Dispos* **40**:1649-1652.
- Nagar S and Korzekwa K (2017) Drug Distribution. Part 1. Models to Predict Membrane Partitioning. *Pharm Res* **34**:535-543.
- Nagar S, Korzekwa RC, and Korzekwa K (2017) Continuous Intestinal Absorption Model Based on the Convection-Diffusion Equation. *Mol Pharm* **14**:3069-3086.
- Nelson D and Cox M (2012) *Lehninger Principles of Biochemistry*. W.H.Freeman.
- O'Neil M (2006) *The Merck Index- An Encyclopedia of Chemicals, Drugs, and Biologicals*. Merck and Co, Inc., Whitehouse Station, NJ.
- O'Reilly RA, Welling PG, and Wagner JG (1971) Pharmacokinetics of Warfarin following intravenous administration to man. *Thrombosis Et Diathesis Haemorrhagica* **25**:178-186.
- Obach RS (1999) Prediction of human clearance of twenty-nine drugs from hepatic microsomal intrinsic clearance data: An examination of in vitro half-life approach and nonspecific binding to microsomes. *Drug Metab Dispos* **27**:1350-1359.
- Obach RS, Baxter JG, Liston TE, Silber BM, Jones BC, MacIntyre F, Rance DJ, and Wastall P (1997) The prediction of human pharmacokinetic parameters from preclinical and in vitro metabolism data. *Journal of Pharmacology and Experimental Therapeutics* **283**:46-58.
- Oie S and Tozer TN (1979) Effect of altered plasma-protein binding on apparent volume of distribution. *Journal of Pharmaceutical Sciences* **68**:1203-1205.

- Pandey M, Arikotla J, Kumar A, Malik R, and Charde SY (2013) *Determination of pKa of felodipine using UV-Visible spectroscopy.*
- Parlee SD, Lentz SI, Mori H, and MacDougald OA (2014) Quantifying size and number of adipocytes in adipose tissue. *Methods in enzymology* **537**:93-122.
- Peters S (2012) *Physiologically-Based Pharmacokinetic (PBPK) Modeling and Simulations: Principles, Methods, and Applications in the Pharmaceutical Industry.*
- Phelan K and May KM (2017) Mammalian Cell Tissue Culture Techniques. *Current Protocols in Molecular Biology* **117**:A.3F.1-A.3F.23.
- Poulin P and Haddad S (2011) Microsome Composition-Based Model as a Mechanistic Tool to Predict Nonspecific Binding of Drugs in Liver Microsomes. *J Pharm Sci* **100**:4501-4517.
- Poulin P and Krishnan K (1995) A biologically-based algorithm for predicting human tissue-blood partition coefficients of organic chemicals. *Human & Experimental Toxicology* **14**:273-280.
- Poulin P and Krishnan K (1996) Molecular structure-based prediction of the partition coefficients of organic chemicals for physiological pharmacokinetic models. *Toxicology Methods* **6**:117-137.
- Poulin P, Schoenlein K, and Theil FP (2001) Prediction of adipose tissue : plasma partition coefficients for structurally unrelated drugs. *Journal of Pharmaceutical Sciences* **90**:436-447.
- Poulin P and Theil FP (2000) A Priori prediction of tissue : plasma partition coefficients of drugs to facilitate the use of physiologically-based pharmacokinetic models in drug discovery. *Journal of Pharmaceutical Sciences* **89**:16-35.
- Poulin P and Theil FP (2002) Prediction of pharmacokinetics prior to in vivo studies. 1. Mechanism-based prediction of volume of distribution. *J Pharm Sci* **91**:129-156.
- Poulin P and Theil FP (2009) Development of a Novel Method for Predicting Human Volume of Distribution at Steady-State of Basic Drugs and Comparative Assessment With Existing Methods. *J Pharm Sci* **98**:4941-4961.

- Recanatini M (1992) Partition and Distribution Coefficients of Aryloxypropranolamine Beta-Adrenoceptor Antagonists. *J Pharm Pharmacol* **44**:68-70.
- Regårdh C, Borg K, Johansson R, Johnsson G, and Palmer L (1974) Pharmacokinetic studies on the selective beta1-receptor antagonist metoprolol in man. *Journal of Pharmacokinetics and Biopharmaceutics* **2**:347-364.
- Rekker R and Mannhold R (1992) *Calculation of drug lipophilicity: the hydrophobic fragmental constant approach*. VCH.
- Riddell JG, Harron DWG, and Shanks RG (1987) Clinical pharmacokinetics of beta-adrenoceptor antagonists- An Update. *Clin Pharmacokinet* **12**:305-320.
- Ripa S, Ferrante L, and Prenna M (1993) Pharmacokinetics of Fluconazole in Normal Volunteers. *Chemotherapy* **39**:6-12.
- Robinson MA and Mehvar R (1996) Enantioselective distribution of verapamil and norverapamil into human and rat erythrocytes: The role of plasma protein binding. *Biopharm Drug Dispos* **17**:577-587.
- Rodgers T, Leahy D, and Rowland M (2005) Physiologically based pharmacokinetic modeling 1: Predicting the tissue distribution of moderate-to-strong bases. *J Pharm Sci* **94**:1259-1276.
- Rodgers T and Rowland M (2006) Physiologically based pharmacokinetic modelling 2: Predicting the tissue distribution of acids, very weak bases, neutrals and zwitterions. *J Pharm Sci* **95**:1238-1257.
- Rodgers T and Rowland M (2007) Mechanistic approaches to volume of distribution predictions: Understanding the processes. *Pharm Res* **24**:918-933.
- Rotondo F, Romero MD, Ho-Palma AC, Remesar X, Fernandez-Lopez JA, and Alemany M (2016) Quantitative analysis of rat adipose tissue cell recovery, and non-fat cell volume, in primary cell cultures. *PeerJ* **4**:24.
- Rowland M and Tozer T (2011) *Clinical Pharmacokinetics and Pharmacodynamics: Concepts and Applications*. Williams and Wilkins.

- Ruiz IL and Gomez-Nieto MA (2018) Robust QSAR prediction models for volume of distribution at steady state in humans using relative distance measurements. *Sar and Qsar in Environmental Research* **29**:529-550.
- Ruiz-Ojeda FJ, Ruperez AI, Gomez-Llorente C, Gil A, and Aguilera CM (2016) Cell Models and Their Application for Studying Adipogenic Differentiation in Relation to Obesity: A Review. *International Journal of Molecular Sciences* **17**:26.
- Sangster J (1993) LOGKOW- a DataBank of evaluated octanol-water partition coefficients. Laboratories SR ed, Montreal.
- Sangster J (1994) *Octanol-Water Partition-Coefficients: Fundamentals and Physical Chemistry*. Wiley, New York.
- Sawada Y, Hanano M, Sugiyama Y, Harashima H, and Iga T (1984) Prediction of the volumes of distribution of basic drugs in humans based on data from animals. *Journal of Pharmacokinetics and Biopharmaceutics* **12**:587-596.
- Scavone JM, Luna BG, Harmatz JS, Von Moltke L, and Greenblatt DJ (1990) Diphenhydramine kinetics following intravenous, oral, and sublingual dimenhydrinate administration. **11**:185-189.
- Sheng X, Tucci J, Malvar J, and Mittelman SD (2014) Adipocyte differentiation is affected by media height above the cell layer. *International Journal of Obesity* **38**:315-320.
- Singer P, Gnauck G, Honigmann G, Schliack V, and Laeuter J (1977) The Fatty Acid Composition of Triglycerides in Arteries, Depot Fat and Serum of Amputated Diabetics. *Atherosclerosis* **28**:87-92.
- Stella VJ, Martodihardjo S, Terada K, and M. Rao V (1998) Some relationships between the physical properties of various 3-acyloxymethyl prodrugs of phenytoin to structure: Potential in vivo performance implications. *J Pharm Sci* **87**:1235-1241.
- Storms ZJ, Cameron E, Siegler HD, and McCaffrey WC (2014) A Simple and Rapid Protocol for Measuring Neutral Lipids in Algal Cells Using Fluorescence. *Jove-Journal of Visualized Experiments* **87**.

- Sun LX, Yang HB, Li J, Wang TDY, Li WH, Liu GX, and Tang Y (2018) In Silico Prediction of Compounds Binding to Human Plasma Proteins by QSAR Models. *Chemmedchem* **13**:572-581.
- Tieleman DP, Marrink SJ, and Berendsen HJC (1997) A computer perspective of membranes: molecular dynamics studies of lipid bilayer systems. *Biochimica et Biophysica Acta (BBA) - Reviews on Biomembranes* **1331**:235-270.
- Treyer A, Mateus A, Wisniewski JR, Boriss H, Matsson P, and Artursson P (2018) Intracellular Drug Bioavailability: Effect of Neutral Lipids and Phospholipids. *Molecular Pharmaceutics* **15**:2224-2233.
- Uchimura T, Kato M, Saito T, and Kinoshita H (2010) Prediction of Human Blood-to-Plasma Drug Concentration Ratio. *Biopharm Drug Dispos* **31**:286-297.
- Ueda CT, Hirschfeld DS, Scheinman MM, Rowland M, Williamson BJ, and Dzindzio BS (1976) Disposition Kinetics of Quinidine. *Clin Pharmacol Ther* **19**:30-36.
- Waller ES, Sharanevych MA, and Yakatan GJ (1982) The Effect of Probenecid on Nafcillin Disposition. *J Clin Pharmacol* **22**:482-489.
- Ward KW and Smith BR (2004) A comprehensive quantitative and qualitative evaluation of extrapolation of intravenous pharmacokinetic parameters from rat, dog, and monkey to humans. II. Volume of distribution and mean residence time. *Drug Metabolism and Disposition* **32**:612-619.
- Watanabe R, Esaki T, Kawashima H, Natsume-Kitatani Y, Nagao C, Ohashi R, and Mizuguchi K (2018) Predicting Fraction Unbound in Human Plasma from Chemical Structure: Improved Accuracy in the Low Value Ranges. *Molecular Pharmaceutics* **15**:5302-5311.
- Welker HA, Wiltshire H, and Bullingham R (1998) Clinical pharmacokinetics of mibefradil. *Clin Pharmacokinet* **35**:405-423.
- Wilkinson G and Shand D (1975 ) Commentary: A physiological approach to hepatic drug clearance, pp 377-390, *Clinical Pharmacology and Therapeutics*.

- Willis JV, Kendall MJ, and Jack DB (1980) A Study of the Effect of Aspirin on the Pharmacokinetics of Oral and Intravenous Diclofenac Sodium. *Eur J Clin Pharmacol* **18**:415-418.
- Wishart DS, Feunang YD, Guo AC, Lo EJ, Marcu A, Grant JR, Sajed T, Johnson D, Li C, Sayeeda Z, Assempour N, Iynkkaran I, Liu YF, Maciejewski A, Gale N, Wilson A, Chin L, Cummings R, Le D, Pon A, Knox C, and Wilson M (2018) DrugBank 5.0: a major update to the DrugBank database for 2018. *Nucleic Acids Res* **46**:D1074-D1082.
- Ye M, Nagar S, and Korzekwa K (2016) A physiologically based pharmacokinetic model to predict the pharmacokinetics of highly protein-bound drugs and the impact of errors in plasma protein binding. *Biopharm Drug Dispos* **37**:123-141.
- Zebisch K, Voigt V, Wabitsch M, and Brandsch M (2012) Protocol for effective differentiation of 3T3-L1 cells to adipocytes. *Analytical Biochemistry* **425**:88-90.
- Zhivkova Z (2017) Quantitative Structure - Pharmacokinetics Relationships for Plasma Protein Binding of Basic Drugs. *Journal of Pharmacy and Pharmaceutical Sciences* **20**:349-359.
- Zhivkova Z and Doytchinova I (2012a) Prediction of steady-state volume of distribution of acidic drugs by quantitative structure-pharmacokinetics relationships. *Journal of Pharmaceutical Sciences* **101**:1253-1266.
- Zhivkova Z and Doytchinova I (2012b) Quantitative structure-plasma protein binding relationships of acidic drugs. *Journal of Pharmaceutical Sciences* **101**:4627-4641.
- Zou P, Zheng N, Yang YS, Yu LX, and Sun DX (2012) Prediction of volume of distribution at steady state in humans: comparison of different approaches. *Expert Opin Drug Metab Toxicol* **8**:855-872.

## APPENDIX A: STRUCTURES OF COMPOUNDS

Table 11: Structures of probe drugs and internal standards.

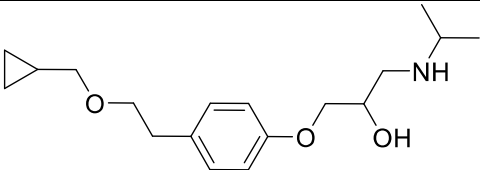
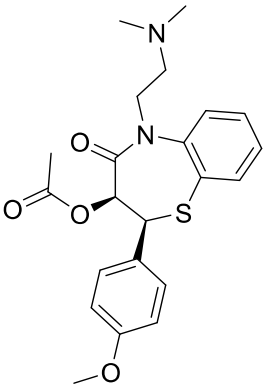
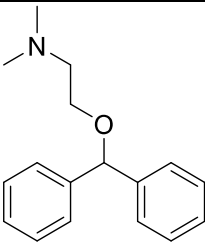
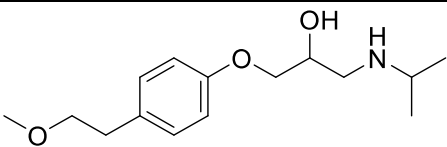
Compounds	Structures
<b>Probe drugs</b>	
Betaxolol	
Diltiazem	
Diphenhydramine	
Metoprolol	

Table 11 continued.

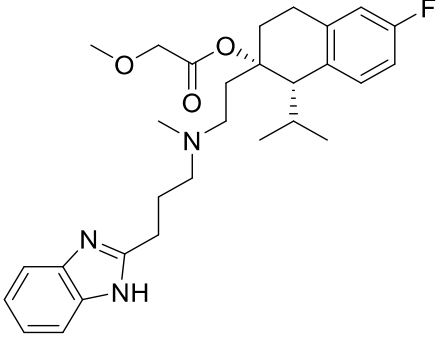
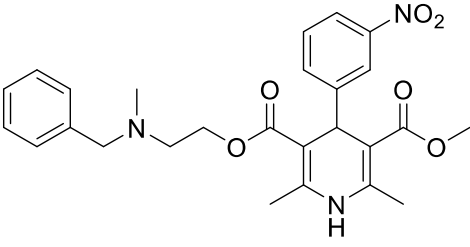
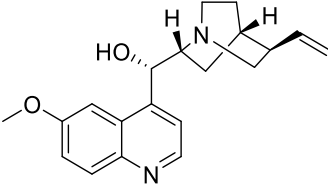
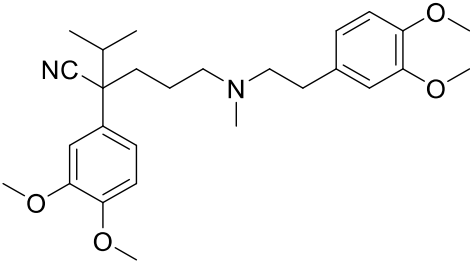
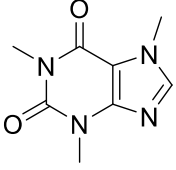
Compounds	Structures
<b>Probe drugs</b>	
Mibefradil	 <p>The structure of Mibefradil features a 1H-indazole ring system connected via a propyl chain to a tertiary amine. This amine is further linked to a side chain containing a methyl group, a chiral center with an isopropyl group, and a 4-fluorophenyl ring. The side chain also includes an ester linkage to a methoxyacetate group.</p>
Nicardipine	 <p>Nicardipine is a dihydropyridine derivative. It has a 4-nitrophenyl group at the 4-position, a methyl group at the 2-position, and a methyl ester group at the 3-position. A side chain at the 1-position consists of a propyl chain with a tertiary amine substituted with a benzyl group.</p>
Quinidine	 <p>Quinidine is a dimeric alkaloid consisting of two quinidine units. Each unit is a quinoline ring system with a methoxy group at the 8-position, linked to a quinuclidine bicyclic system. The quinuclidine system has a hydroxyl group and an allyl group attached to the nitrogen bridgehead.</p>
Verapamil	 <p>Verapamil is a 1,4-dihydropyridine derivative. It features a 3,4,5-trimethoxyphenyl group at the 4-position, a nitrile group and an isopropyl group at the 2-position, and a side chain at the 1-position consisting of a propyl chain with a tertiary amine substituted with a 3,4,5-trimethoxyphenyl group.</p>
Caffeine	 <p>Caffeine is a purine alkaloid. It consists of a fused pyrimidine and imidazole ring system with three methyl groups attached to the nitrogen atoms.</p>

Table 11 continued.

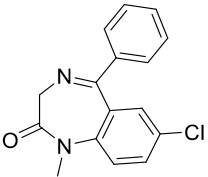
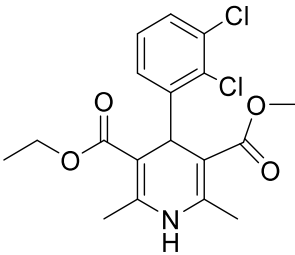
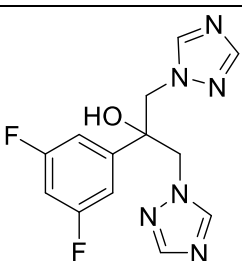
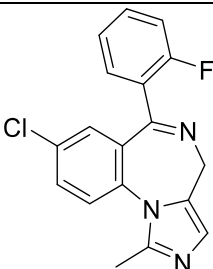
Compounds	Structures
<b>Probe drugs</b>	
Diazepam	 <p>The chemical structure of Diazepam is a 7-chloro-1-methyl-5-phenyl-1,5-dihydro-2H-1,4-benzodiazepin-2-one. It features a benzodiazepine core with a chlorine atom at the 7-position, a methyl group on the nitrogen at the 1-position, and a phenyl ring at the 5-position.</p>
Felodipine	 <p>The chemical structure of Felodipine is a 1,4-dihydropyridine derivative. It has a methyl group at the 4-position, a methyl ester at the 3-position, and a 2,6-dichlorophenyl group at the 2-position. Additionally, it has an ethyl ester at the 5-position.</p>
Fluconazole	 <p>The chemical structure of Fluconazole is a triazole derivative. It consists of a 1,2,4-triazole ring connected via a methylene group to a carbon atom. This carbon atom is also bonded to a hydroxyl group and a 2,6-difluorophenyl ring.</p>
Midazolam	 <p>The chemical structure of Midazolam is a benzodiazepine derivative. It features a benzodiazepine core with a methyl group on the nitrogen at the 1-position, a 2-fluorophenyl group at the 5-position, and a 4-chlorophenyl group at the 7-position.</p>
Phenytoin	 <p>The chemical structure of Phenytoin is a hydantoin derivative. It consists of a central carbon atom bonded to two phenyl rings and a hydantoin ring (a five-membered ring containing two nitrogen atoms and one carbonyl group).</p>

Table 11 continued.

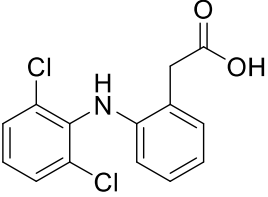
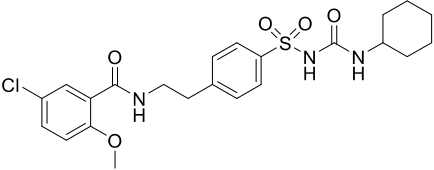
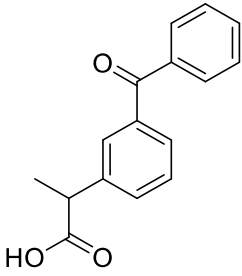
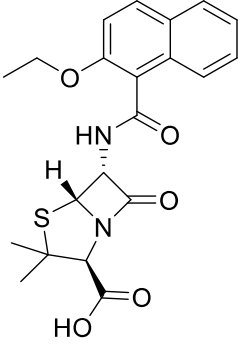
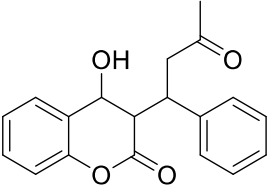
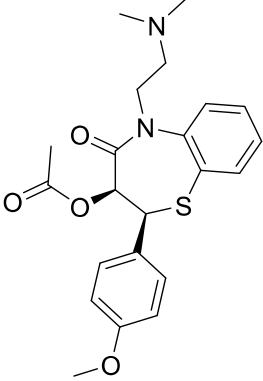
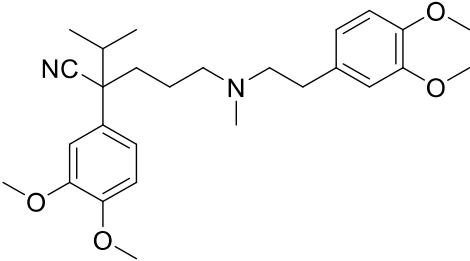
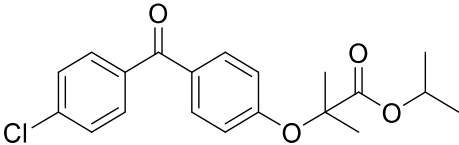
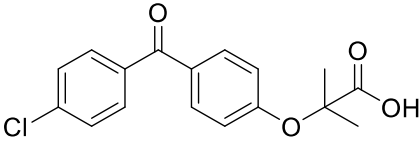
Compounds	Structures
<b>Probe drugs</b>	
Diclofenac	
Glyburide	
Ketoprofen	
Nafcillin	
Warfarin	

Table 11 continued.

Compounds	Structures
<b>Internal standards</b>	
Diltiazem	 <p>The chemical structure of Diltiazem is a 1,5-benzothiazepine derivative. It features a central seven-membered ring containing one sulfur atom and one nitrogen atom. The nitrogen atom is substituted with a dimethylaminoethyl group (-N(CH<sub>3</sub>)<sub>2</sub>CH<sub>2</sub>CH<sub>2</sub>-). The sulfur atom is bonded to a phenyl ring. The carbon atom adjacent to the sulfur in the seven-membered ring is substituted with a 4-methoxyphenyl group (-C<sub>6</sub>H<sub>4</sub>-OCH<sub>3</sub>) and a 2-oxo-1,3-dioxol-5-yl group (-C(=O)-O-CH<sub>2</sub>-O-).</p>
Verapamil	 <p>The chemical structure of Verapamil is a 1,4-dihydropyridine derivative. It consists of a six-membered dihydropyridine ring with a methyl group at the 4-position and a 1-(2,4,6-trimethoxyphenyl)ethyl group at the 2-position. The 1-position of the dihydropyridine ring is substituted with a 2-(3,4-dimethoxyphenyl)ethyl group.</p>
Fenofibrate	 <p>The chemical structure of Fenofibrate is an ester. It features a central benzophenone core (two phenyl rings connected by a carbonyl group). One phenyl ring is substituted with a chlorine atom at the para position. The other phenyl ring is substituted with a 2-(4-chlorophenyl)ethoxy group at the para position. The carbonyl carbon of the benzophenone core is also bonded to a 2-(4-chlorophenyl)ethoxy group and an isopropyl group.</p>
Fenofibric Acid	 <p>The chemical structure of Fenofibric Acid is the carboxylic acid form of Fenofibrate. It is identical to Fenofibrate, except that the isopropyl ester group is replaced by a carboxylic acid group (-COOH).</p>

APPENDIX B: REPRESENTATIVE MASS SPECTROMETRY PARAMETERS

Table 12: Representative MS parameters.

Compound	Mass Spectrometer	Collision Gas (psi)	Precursor ion and Product Ion	DP (V)	CE (V)	CXP (V)
<b>Probe Compounds</b>						
Betaxolol	API 4000	12	308.1/116.2	44	27	22
Diltiazem	API 4000 Qtrap	12	415.2/178.2	106	35	10
Diphenhydramine	API 4000	12	256.9/168.2	47	15	13
Metoprolol	API 4000 Qtrap	12	268.2/116.0	87	28	6
Mibefradil	API 4000 Qtrap	12	496.3/202.1	101	33	10
Nicardipine	API 4000 Qtrap	12	480.4/315.0	85	32	7
Quinidine	API 4000 Qtrap	12	325.3/307.12	97	31	7
Verapamil	API 4000 Qtrap	10	455.5/165.0	80	41	12
Caffeine	API 4000 Qtrap	12	195.2/138.2	16	28	13
Diazepam	API 4000 Qtrap	12	285.1/192.9	111	47	10
Felodipine	API 4000 Qtrap	10	384.21/338.1	78	30	15
Fluconazole	API 4000	12	307.1/238.1	60	24	6
Midazolam	API 4000 Qtrap	12	326.2/291.2	108	38	18
Phenytoin	API 4000 Qtrap	12	253.3/182.2	44	26	3
Diclofenac	API 4000 Qtrap	12	296.1/252.0	-60	-17	-5
Glyburide	API 4000	12	494.1/369.1	34	25	18
Ketoprofen	API 4000 Qtrap	12	255.1/209.1	98	22	17
Nafcillin	API 4000 Qtrap	12	415.3/199.2	113	22	14
Warfarin	API 4000 Qtrap	12	309.0/163.1	81	21	5
<b>Internal Standards</b>						
Fenofibrate	API 4000	12	361.1/233.1	56	23	6
Fenofibrate	API 4000 Qtrap	12	360.9/233.2	81	25	16
Fenofibric acid	API 4000 Qtrap	12	317.1/230.9	-75	-16	-19
Diltiazem	API 4000	12	415.2/178.0	46	31	28
Diltiazem	API 4000 Qtrap	12	415.2/178.2	106	35	10
Verapamil	API 4000 Qtrap	12	455.5/165.0	80	41	12

APPENDIX C: REPRESENTATIVE LC PARAMETERS

Table 13: Representative LC Parameters

Compound	Internal Standard (IS)	Gradient A/B**	Flow Rate
Betaxolol	Diltiazem	0.00: 95/5 0.50: 5/95 1.00: 5/95 1.50: 95/5 7.00: 95/5	350
Diltiazem	Verapamil	0.00: 95/5 0.50: 95/5 4.00: 5/95 4.50: 5/95 5.00: 95/5 10.00: 95/5	350
Diphenhydramine	Fenofibrate	0.00: 95/5 0.50: 5/95 3.00: 5/95 3.25: 95/5 7.00: 95/5	350
Metoprolol	Diltiazem	0.00: 95/5 0.50: 5/95 3.25: 5/95 3.50: 95/5 7.00: 95/5	350
Mibefradil	Diltiazem	0.00: 95/5 0.50: 95/5 4.00: 5/95 4.50: 5/95 5.00: 95/5 8.00: 95/5	400
Nicardipine	Diltiazem	0.00: 95/5 0.50: 95/5 4.00: 5/95 4.50: 5/95 5.00: 95/5 8.00: 95/5	400
Quinidine	Diltiazem	0.00: 98/2 0.50: 98/2 3.00: 5/95 4.50: 5/95 5.00: 98/2 10.00: 98/2	500

Table 13 continued.

<b>Compound</b>	<b>Internal Standard (IS)</b>	<b>Gradient A/B**</b>	<b>Flow Rate</b>
Verapamil	Diltiazem	0.00: 95/5 0.50: 5/95 1.50: 5/95 2.00: 95/5 8.00: 95/5	350
Caffeine	Diltiazem	0.00: 98/2 0.50: 5/95 1.50: 5/95 2.00: 98/2 7.00: 98/2	450
Diazepam	Diltiazem	0.00: 95/5 0.50: 95/5 4.00: 5/95 4.50: 5/95 5.00: 95/5 8.00: 95/5	400
Felodipine	Diltiazem	0.00: 98/2 0.50: 98/2 4.00: 5/95 4.50: 5/95 5.00: 98/2 10.00: 98/2	400
Fluconazole	Diltiazem	0.00: 90/10 0.50: 5/95 1.50: 5/95 2.00: 90/10 8.00: 90/10	450
Midazolam	Diltiazem	0.00: 95/5 0.50: 95/5 4.00: 5/95 4.50: 5/95 5.00: 95/5 10.00: 95/5	350
Phenytoin	Diltiazem	0.00: 98/2 0.50: 98/2 4.00: 5/95 4.50: 5/95 5.00: 98/2 10.00: 98/2	400

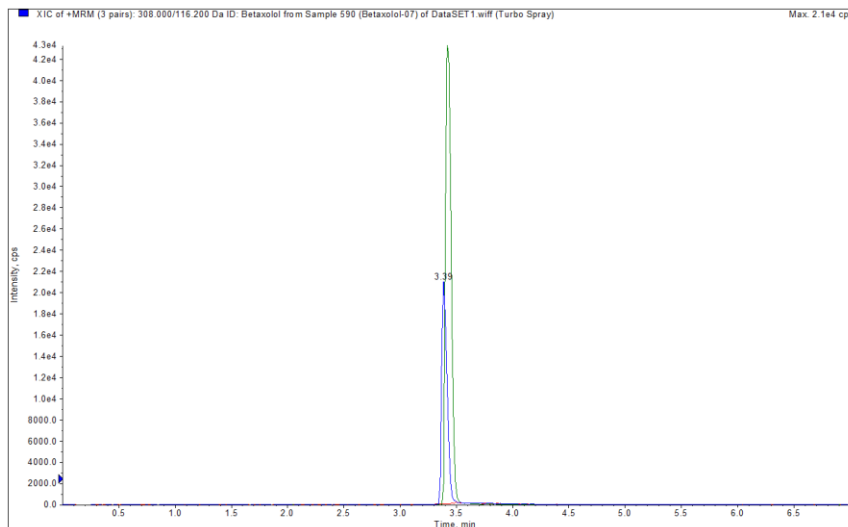
Table 13 continued.

<b>Compound</b>	<b>Internal Standard (IS)</b>	<b>Gradient A/B**</b>	<b>Flow Rate</b>
Diclofenac	Fenofibric Acid	0.00: 98/2 0.50: 5/95 1.50: 5/95 2:00: 98/2 7.00: 98/2	450
Glyburide	Fenofibrate	0.00: 90/10 0.50: 5/95 3.50: 5/95 3.75: 90/10 7.00: 90/10	400
Ketoprofen	Diltiazem	0.00: 98/2 0.50: 5/95 3.50: 5/95 3.75: 98/2 8.00: 98/2	500
Nafcillin	Diltiazem	0.00: 95/5 0.50: 95/5 4.00: 5/95 4.50: 5/95 5.00: 95/5 8.00: 95/5	400
Warfarin	Diltiazem	0.00: 98/2 0.50: 98/2 4.00: 5/95 4.50: 5/95 5.00: 98/2 10.00: 98/2	400

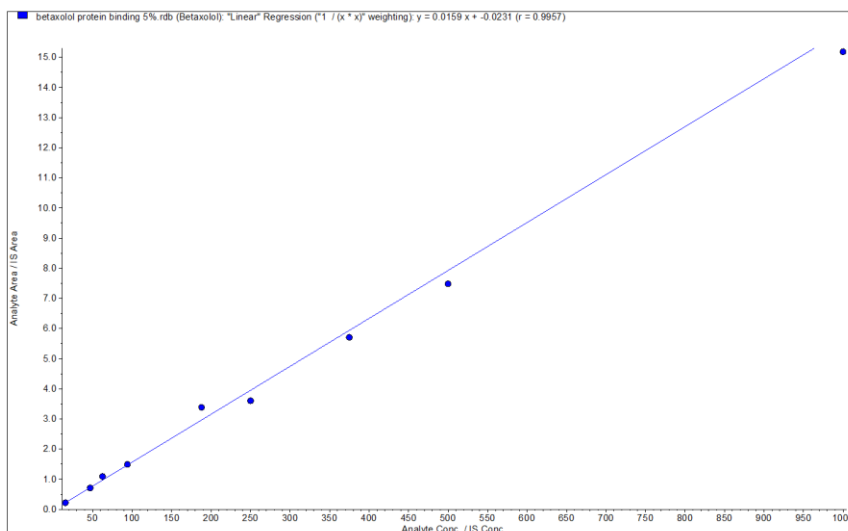
\*\*A: water with 0.1% formic acid B: acetonitrile with 0.1% formic acid

## APPENDIX D: REPRESENTATIVE LC-MS/MS CHROMATOGRAMS AND STANDARD CURVES FOR PROBE DRUGS

### Betaxolol

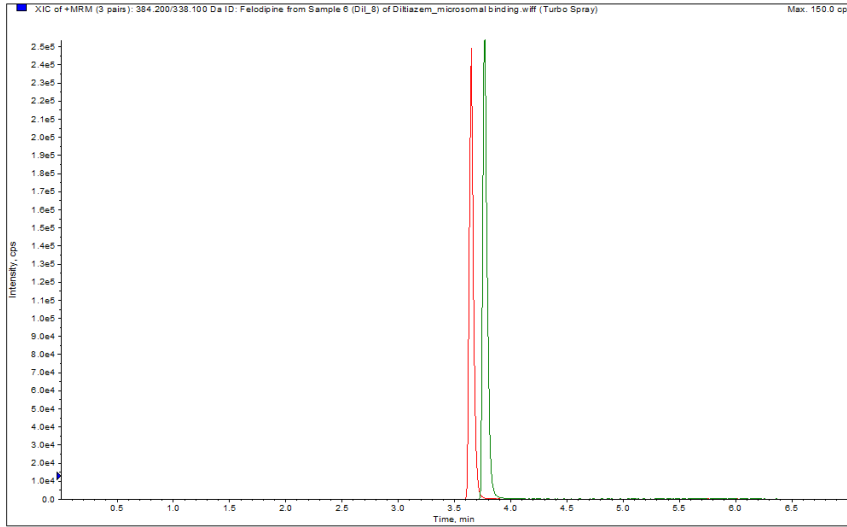


Representative chromatogram for betaxolol (blue) in RLM, with diltiazem (green) used as an internal standard.

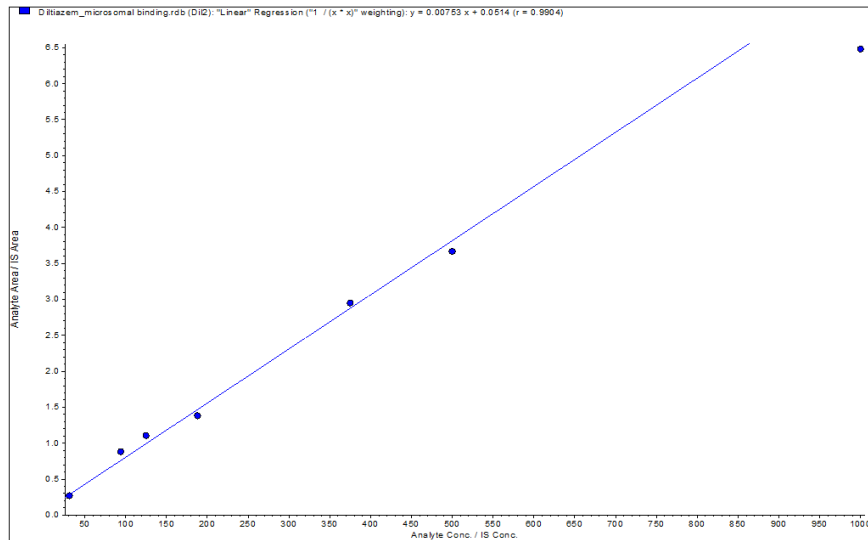


Representative standard curve for betaxolol in RLM, with diltiazem used as an internal standard.

## Diltiazem

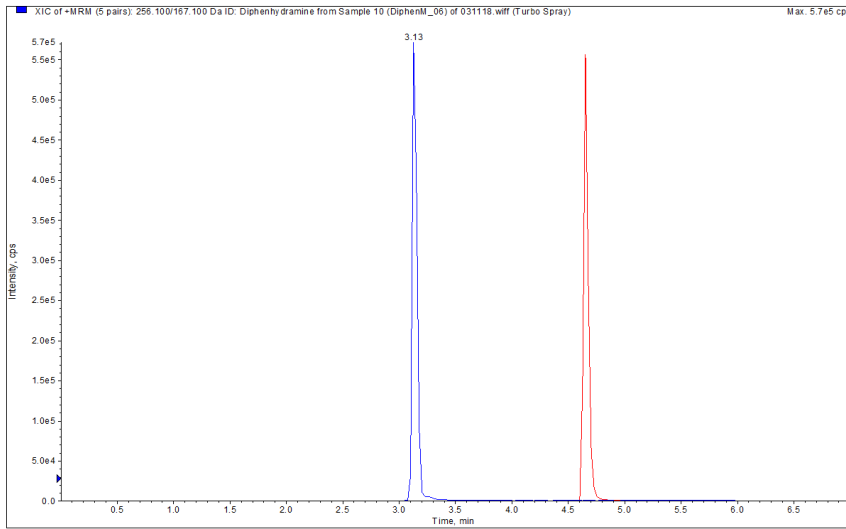


Representative chromatogram for diltiazem (red) in RLM, with verapamil (green) used as an internal standard.

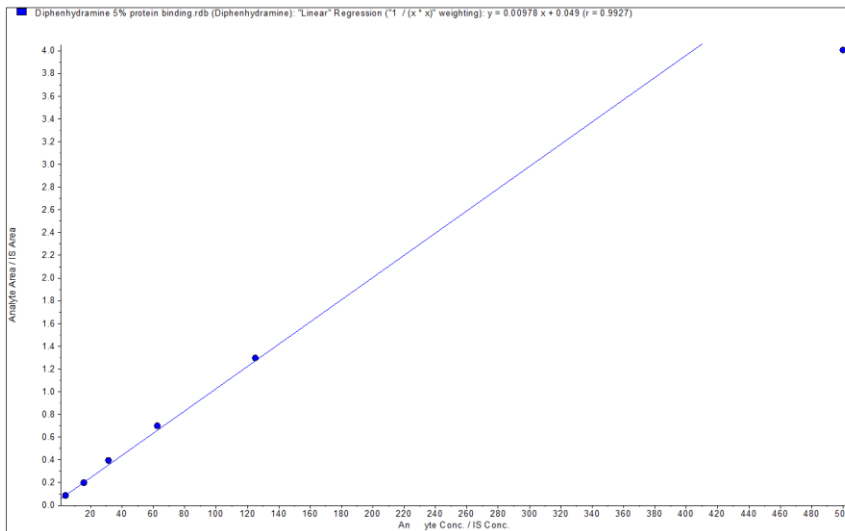


Representative standard curve for diltiazem in RLM, with verapamil used as an internal standard.

## Diphenhydramine

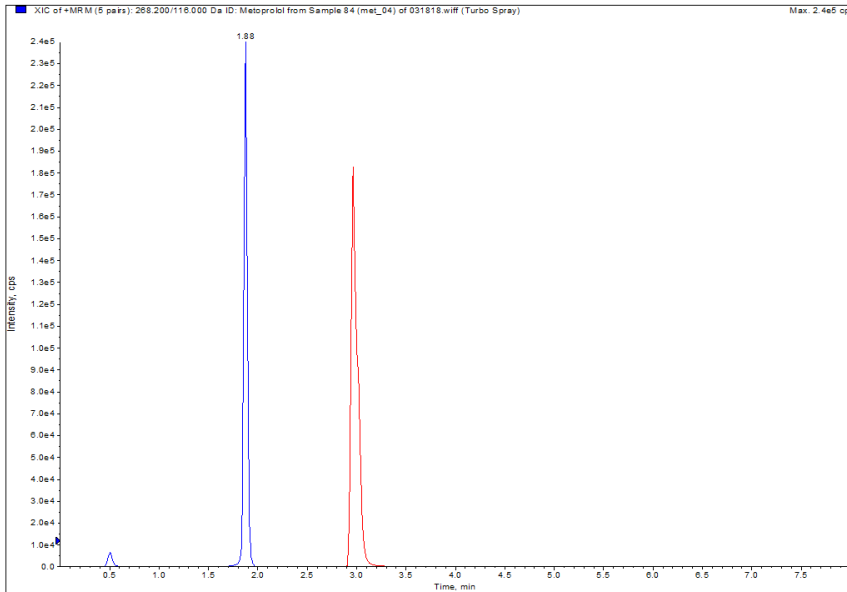


Representative chromatogram for diphenhydramine (blue) in RLM, with fenofibrate (red) used as an internal standard.

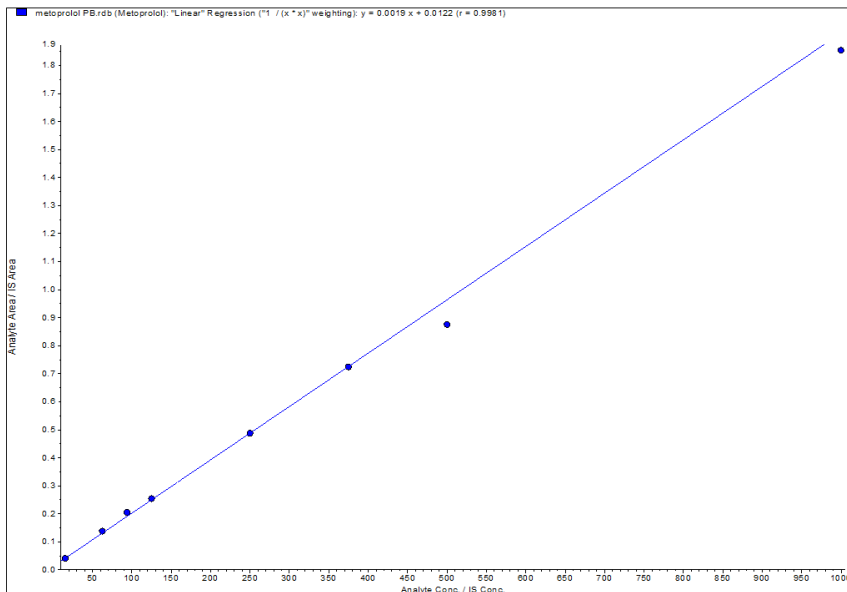


Representative standard curve for diphenhydramine in RLM, with fenofibrate used as an internal standard.

# Metoprolol

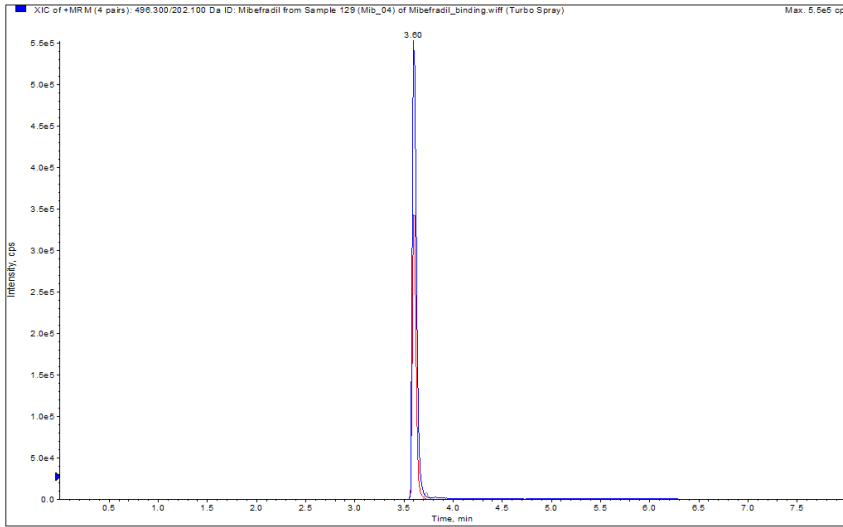


Representative chromatogram for metoprolol (blue) in human plasma, with fenofibrate (red) used as an internal standard.

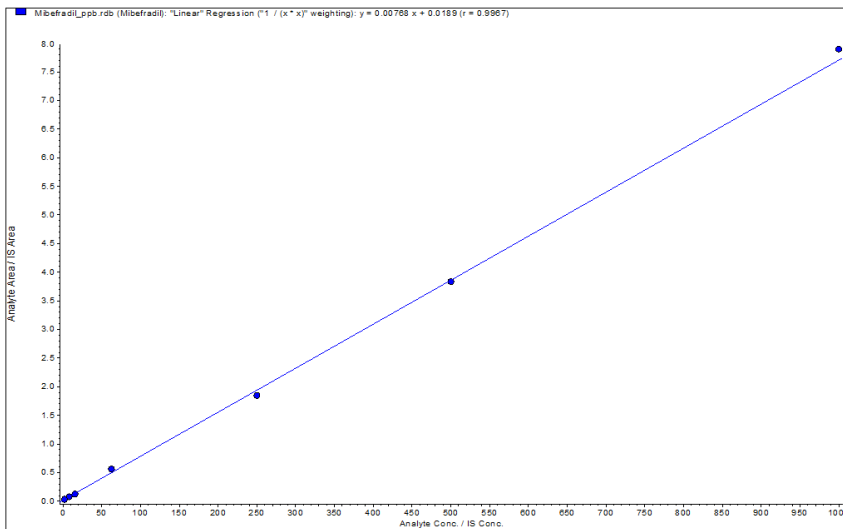


Representative standard curve for metoprolol in human plasma, with fenofibrate used as an internal standard.

# Mibefradil

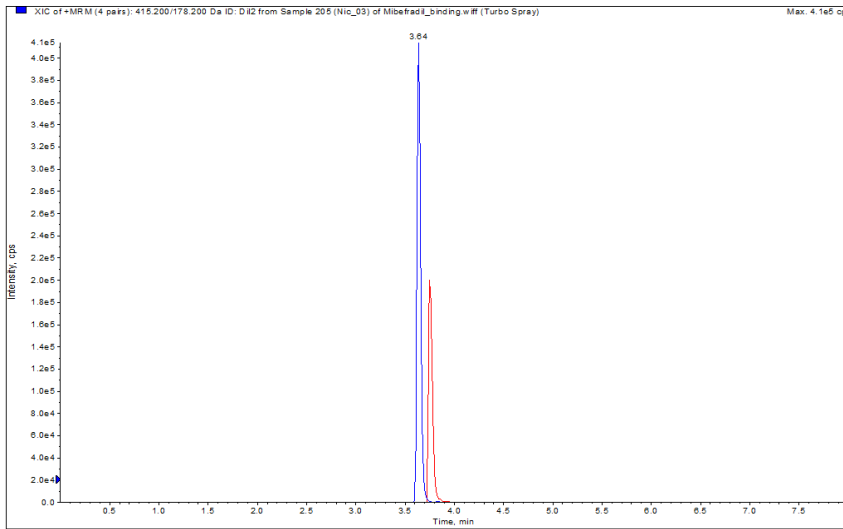


Representative chromatogram for mibefradil (blue) in human plasma, with diltiazem (red) used as an internal standard.

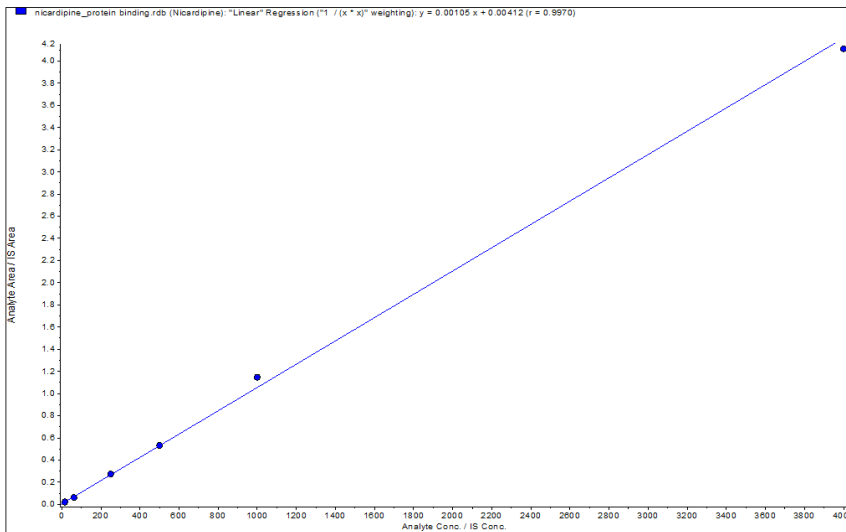


Representative standard curve for mibefradil in human plasma, with diltiazem used as an internal standard.

# Nicardipine

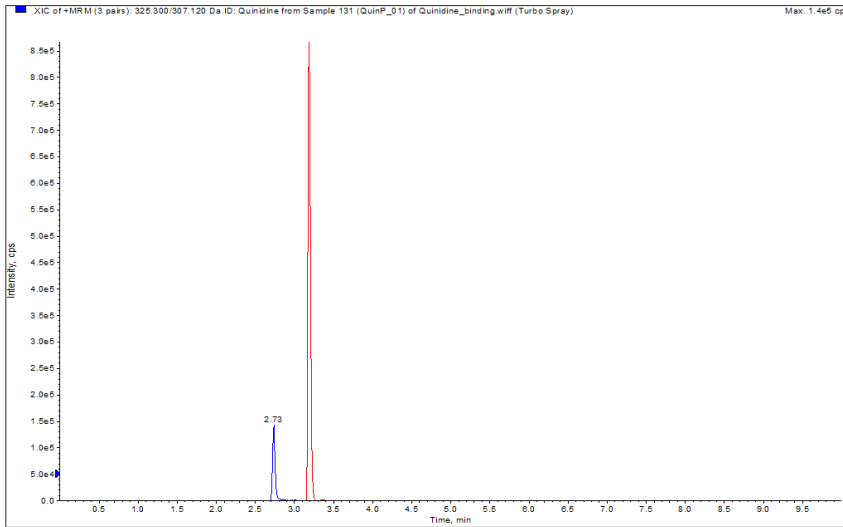


Representative chromatogram for nicardipine (red) in human plasma, with diltiazem (blue) used as an internal standard.

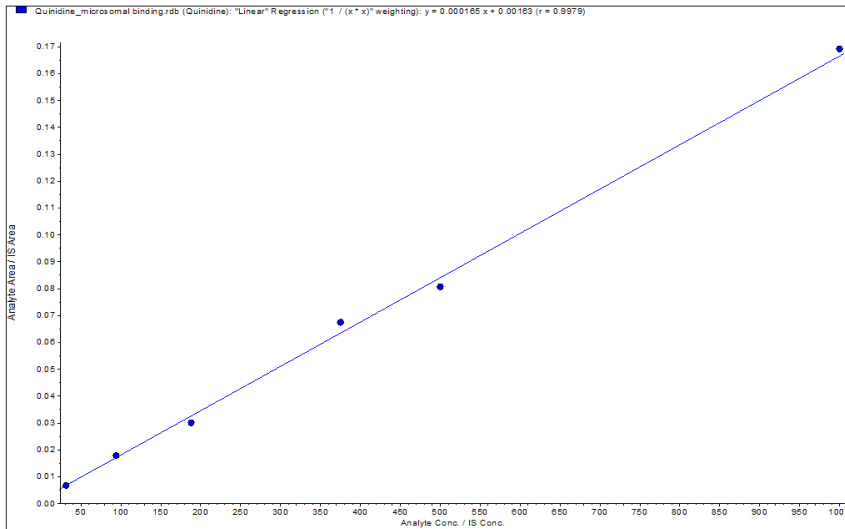


Representative standard curve for nicardipine in human plasma, with diltiazem used as an internal standard.

## Quinidine

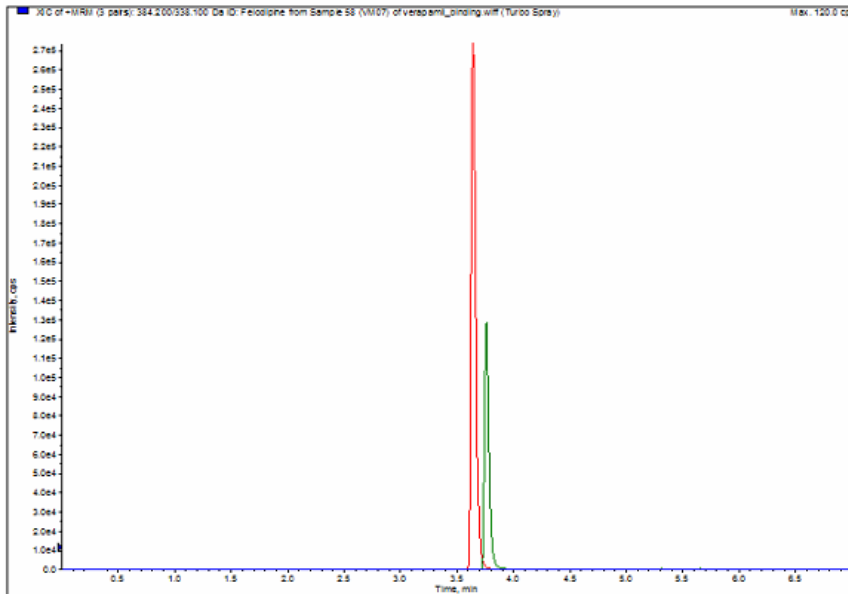


Representative chromatogram for quinidine (blue) in RLM, with diltiazem (red) used as an internal standard.

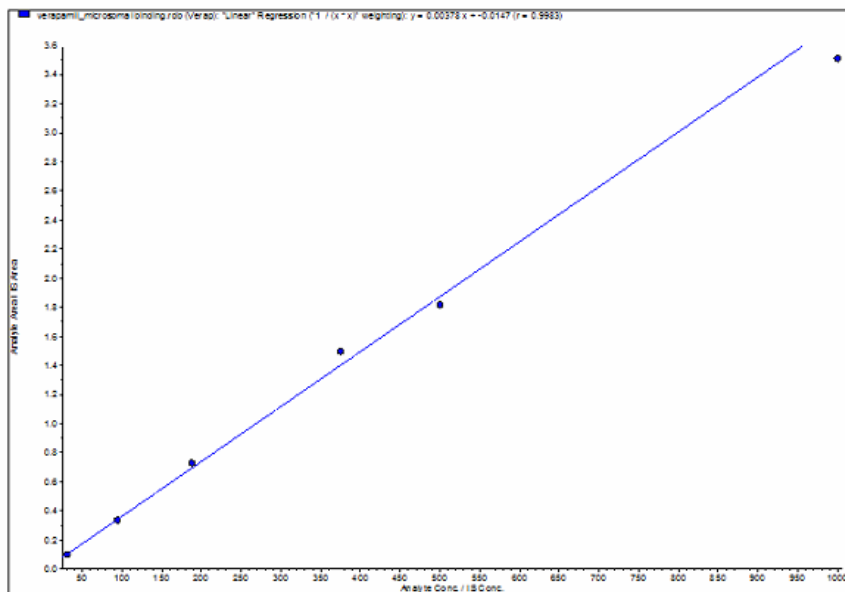


Representative standard curve for quinidine in RLM, with diltiazem used as an internal standard.

## Verapamil

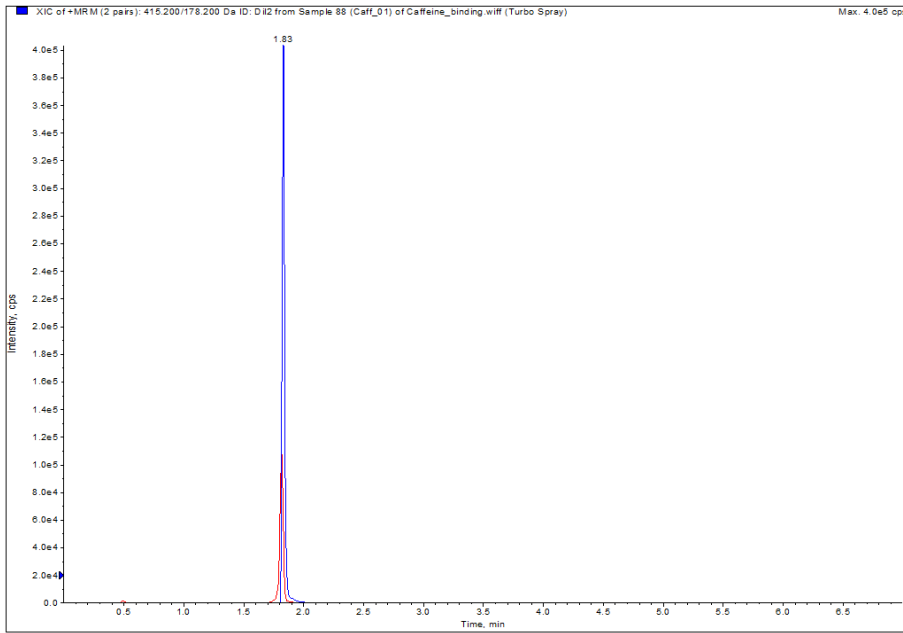


Representative chromatogram for verapamil (green) in RLM, with diltiazem (red) used as an internal standard.

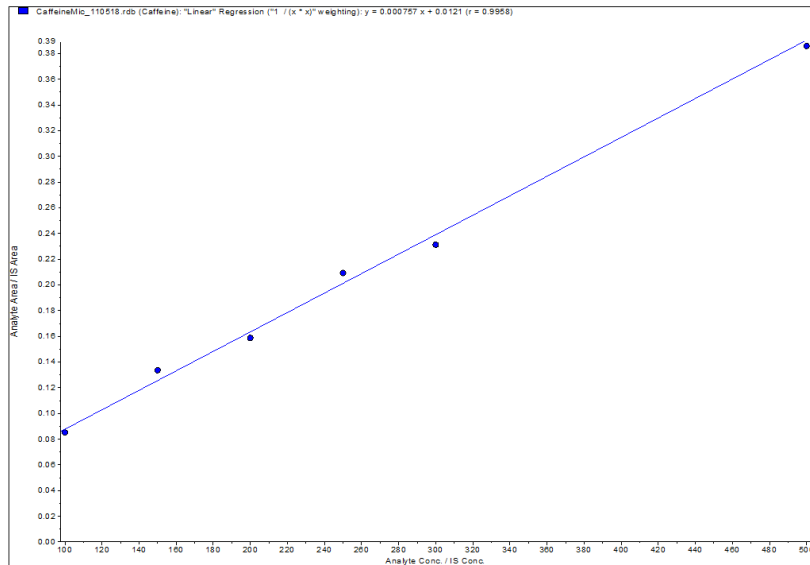


Representative standard curve for verapamil in RLM, with diltiazem used as an internal standard.

# Caffeine



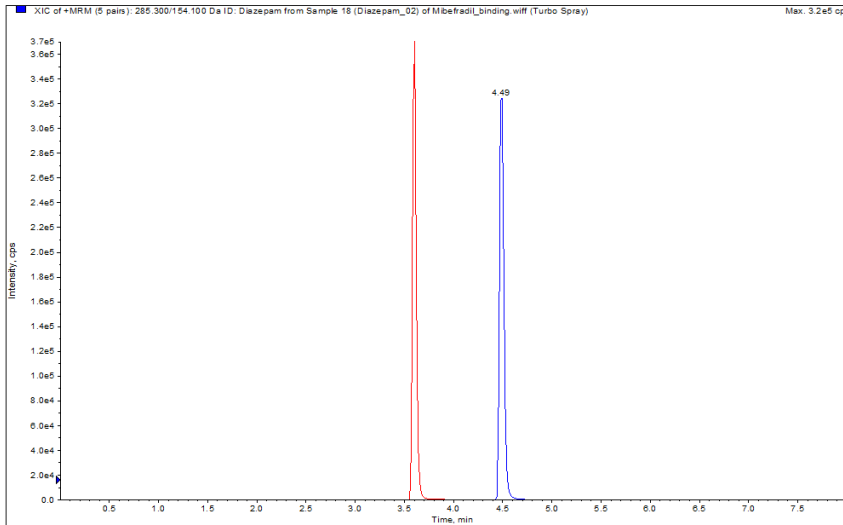
Representative chromatogram for caffeine (red) in RLM, with diltiazem (blue) used as an internal standard.



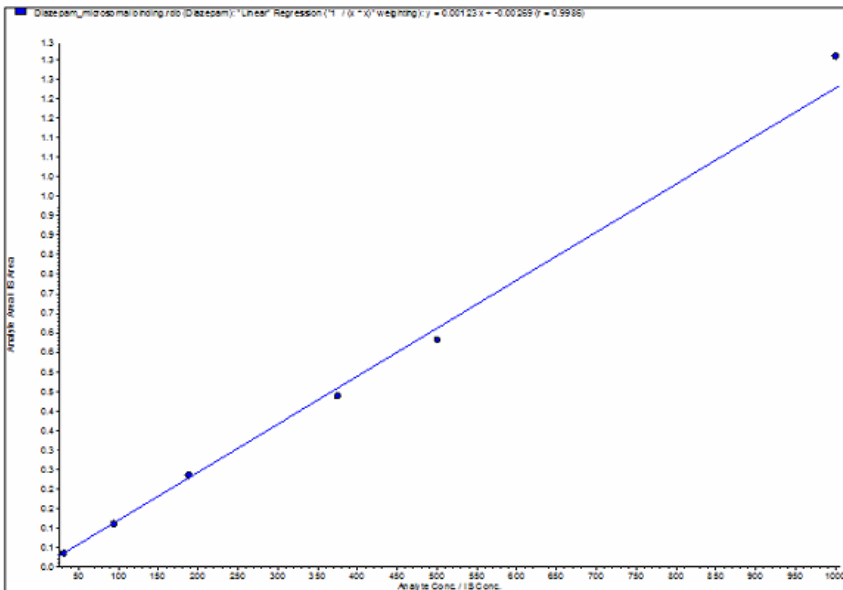
Representative standard curve for caffeine in RLM, with diltiazem used as an internal standard.

# Diazepam

## Representative chromatogram: diazepam

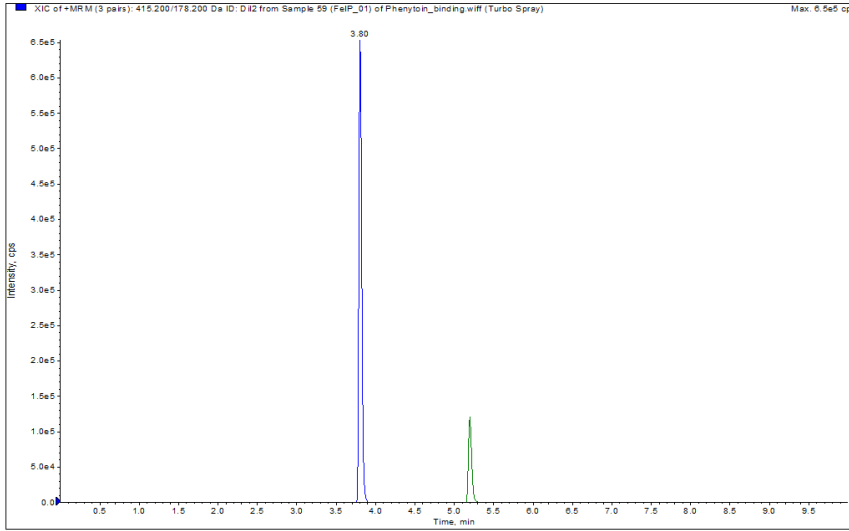


Representative chromatogram for diazepam (blue) in RLM, with diltiazem (red) used as an internal standard.

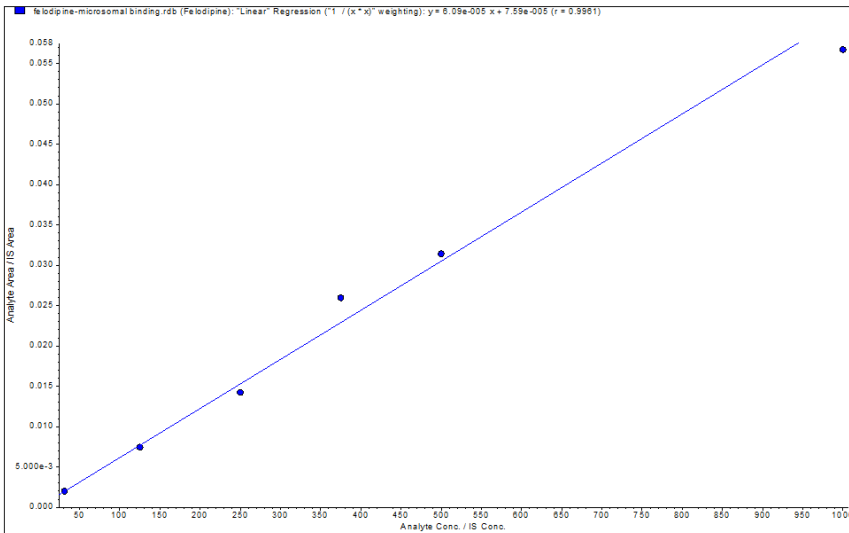


Representative standard curve for diazepam in RLM, with diltiazem used as an internal standard.

# Felodipine

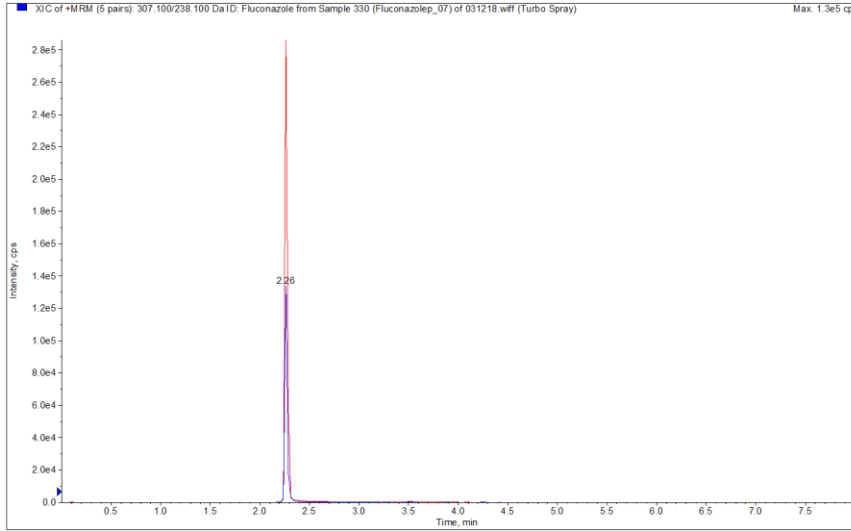


Representative chromatogram for felodipine (green) in human plasma, with diltiazem (blue) used as an internal standard.

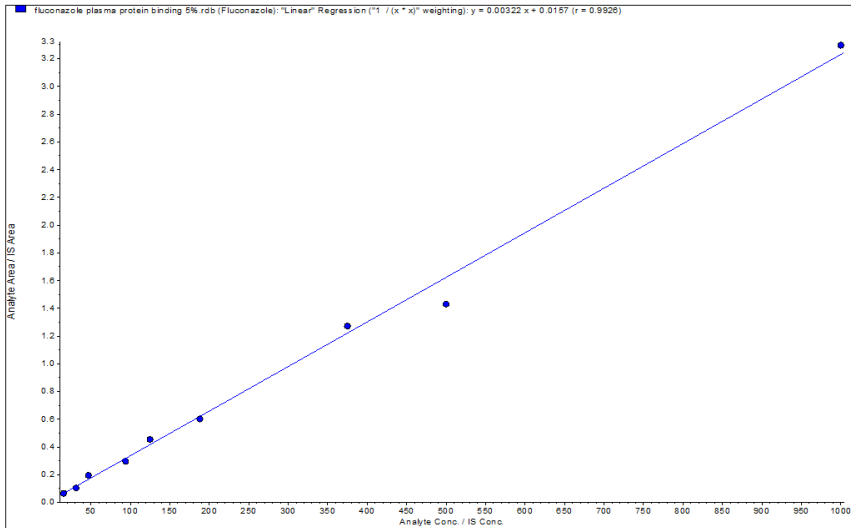


Representative standard curve for felodipine in RLM, with diltiazem used as an internal standard.

# Fluconazole

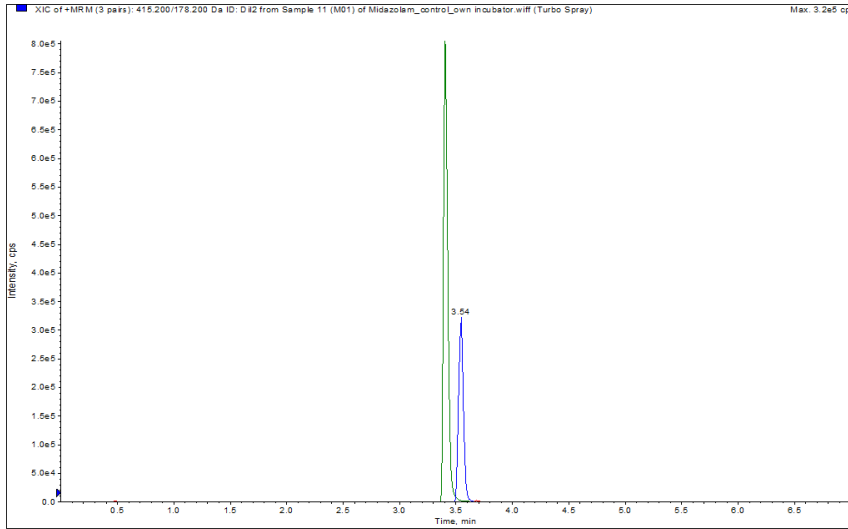


Representative chromatogram for fluconazole (blue) in human plasma, with diltiazem (red) used as an internal standard.

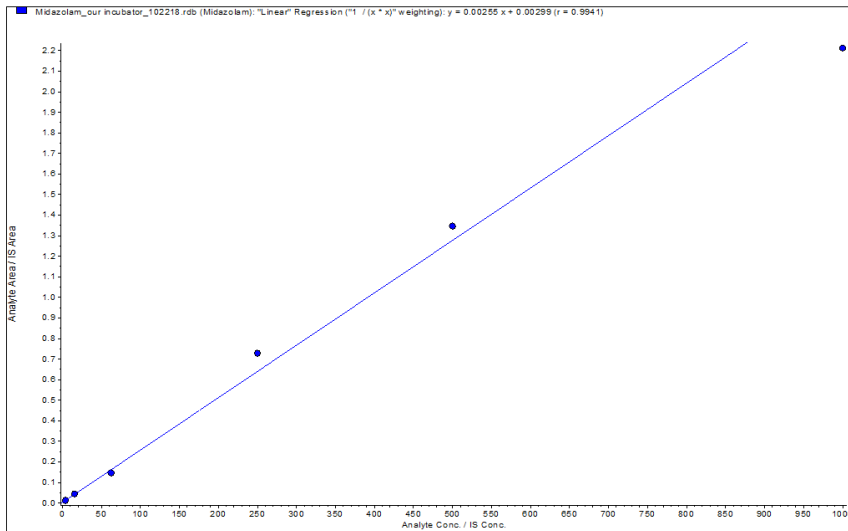


Representative standard curve for fluconazole in human plasma, with diltiazem used as an internal standard.

## Midazolam

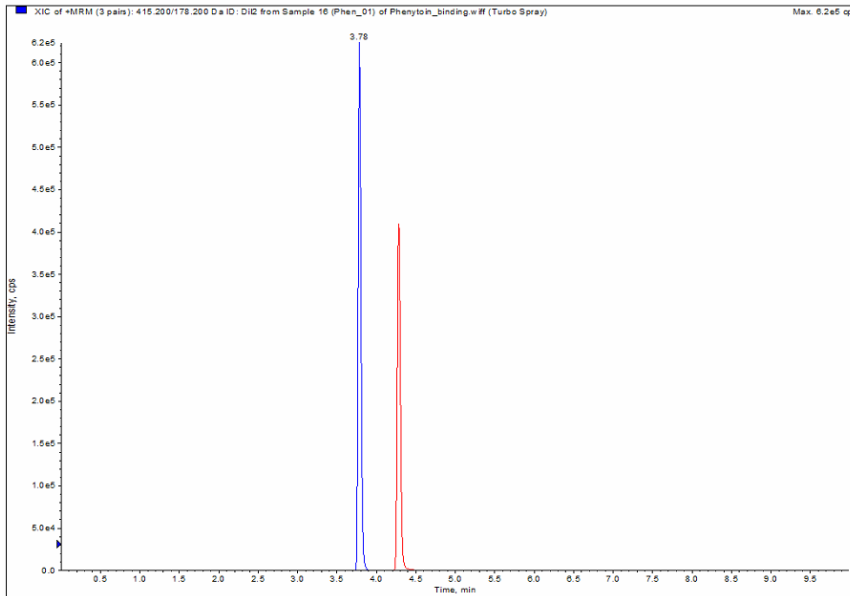


Representative chromatogram for midazolam (green) in human plasma, with diltiazem (blue) used as an internal standard.



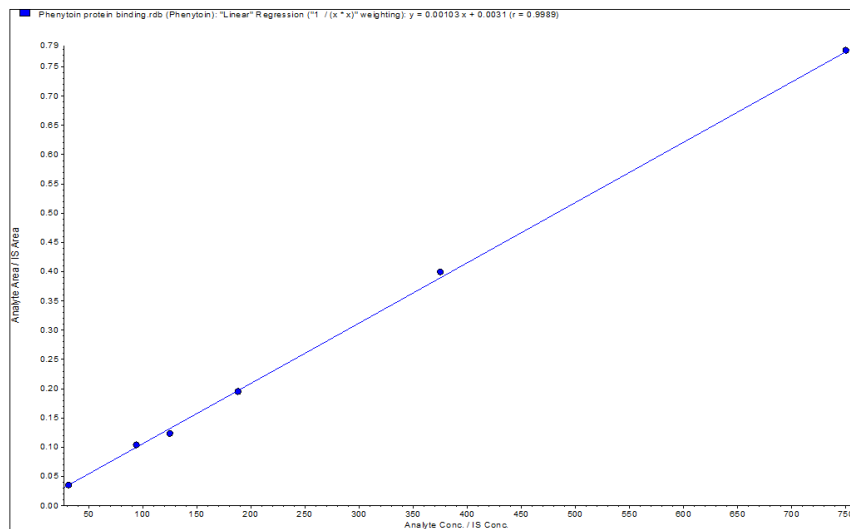
Representative standard curve for midazolam in human plasma, with diltiazem used as an internal standard.

## Phenytoin



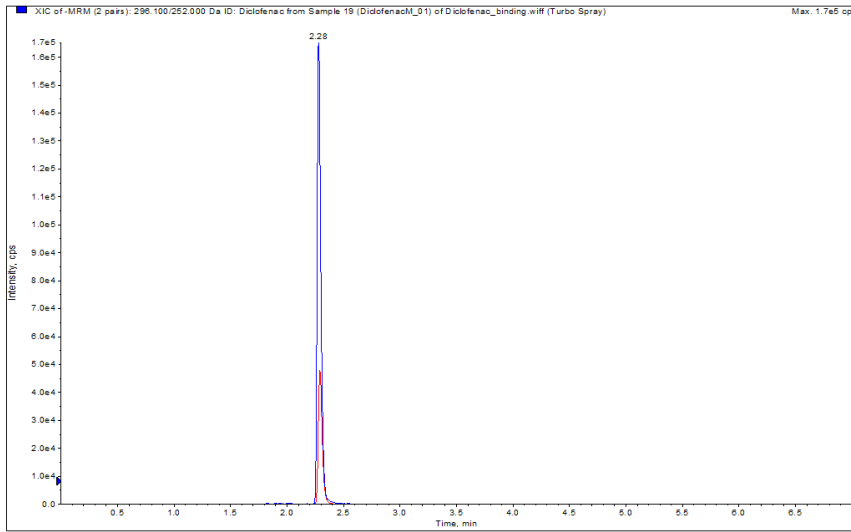
Representative chromatogram for phenytoin (red) in human plasma, with diltiazem (blue) used as an internal standard.

Representative standard curve: phenytoin

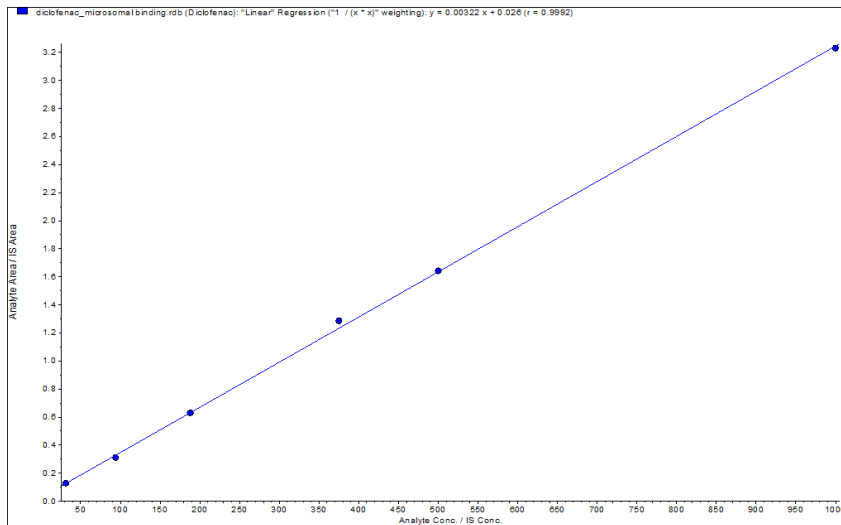


Representative standard curve for phenytoin in human plasma, with diltiazem used as an internal standard.

## Diclofenac

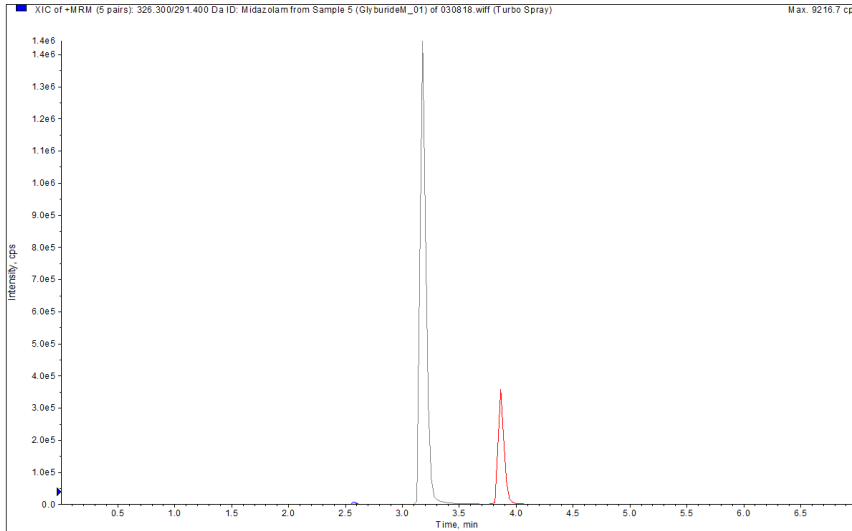


Representative chromatogram for diclofenac (blue) in RLM, with fenofibric acid (red) used as an internal standard.

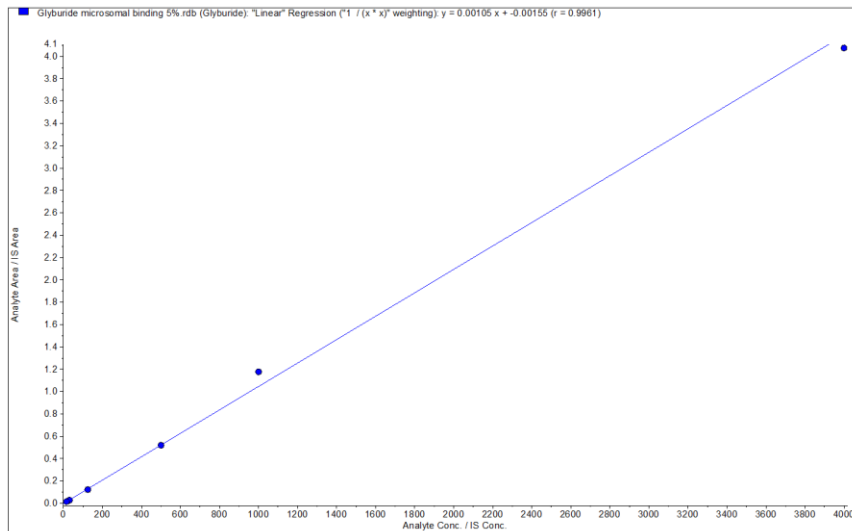


Representative standard curve for diclofenac in RLM, with fenofibric acid used as an internal standard.

## Glyburide

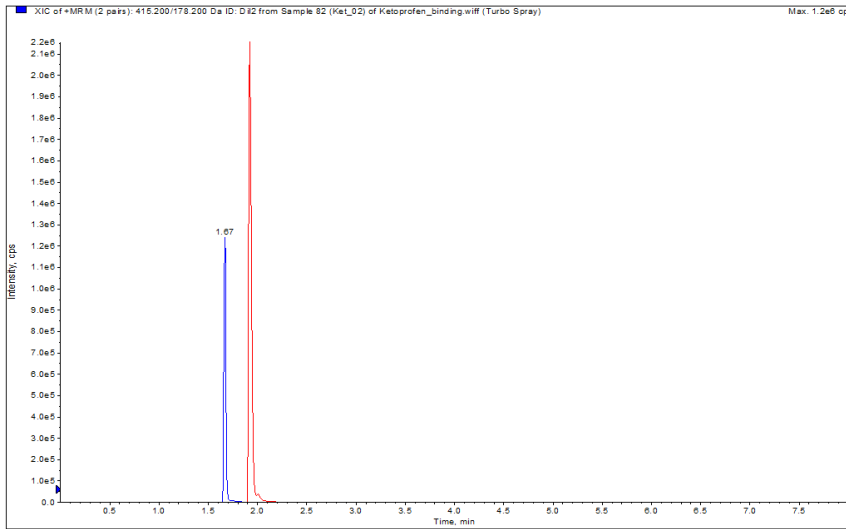


Representative chromatogram for glyburide (grey) in RLM, with fenofibrate (red) used as an internal standard.

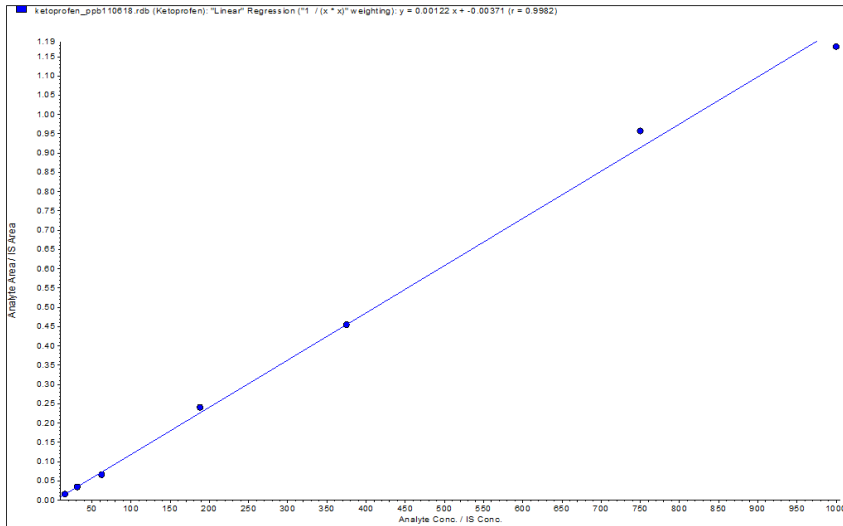


Representative standard curve for glyburide in RLM, with fenofibrate used as an internal standard.

# Ketoprofen

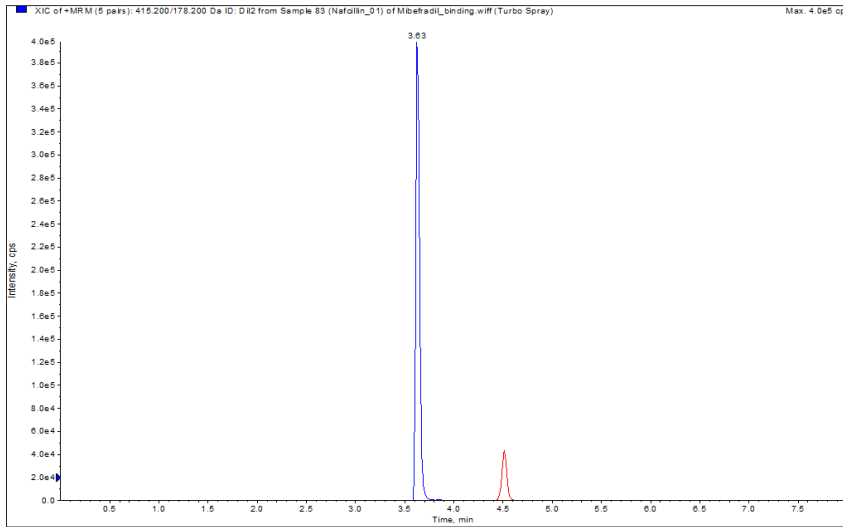


Representative chromatogram for ketoprofen (red) in human plasma, with diltiazem (blue) used as an internal standard.



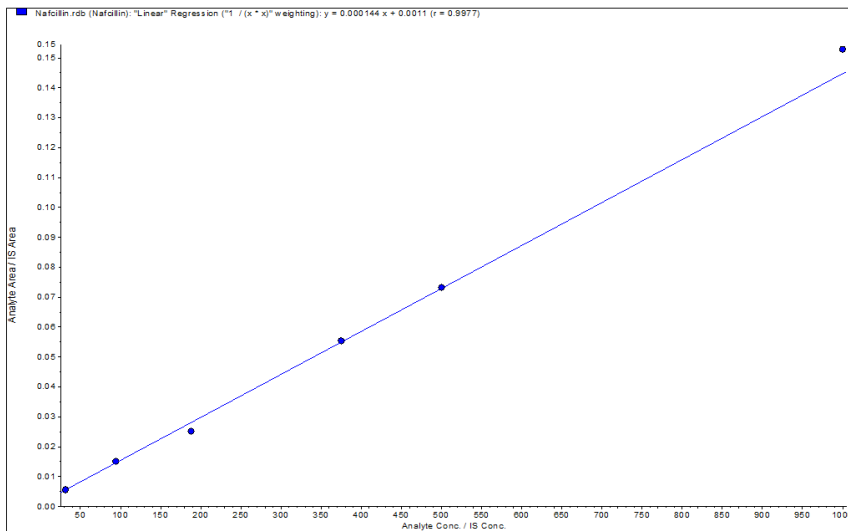
Representative standard curve for ketoprofen in human plasma, with diltiazem used as an internal standard.

## Nafcillin



Representative chromatogram for nafcillin (red) in RLM, with diltiazem (blue) used as an internal standard.

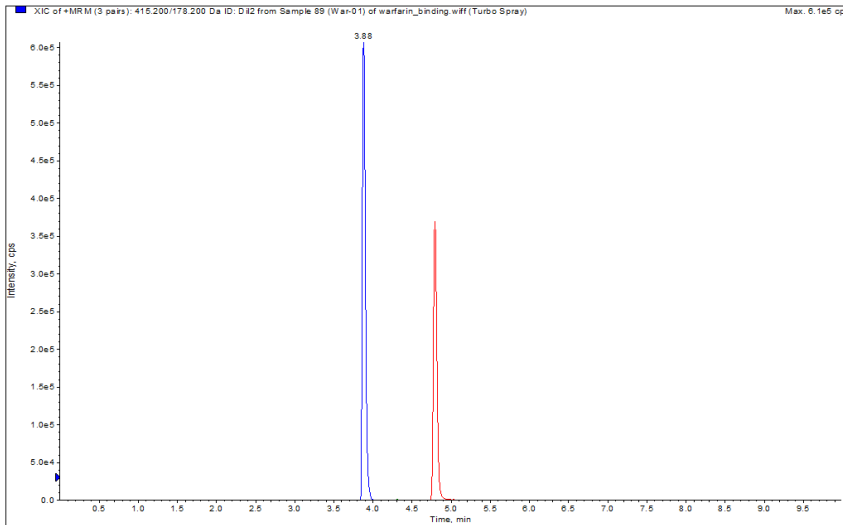
Representative standard curve (microsomes)



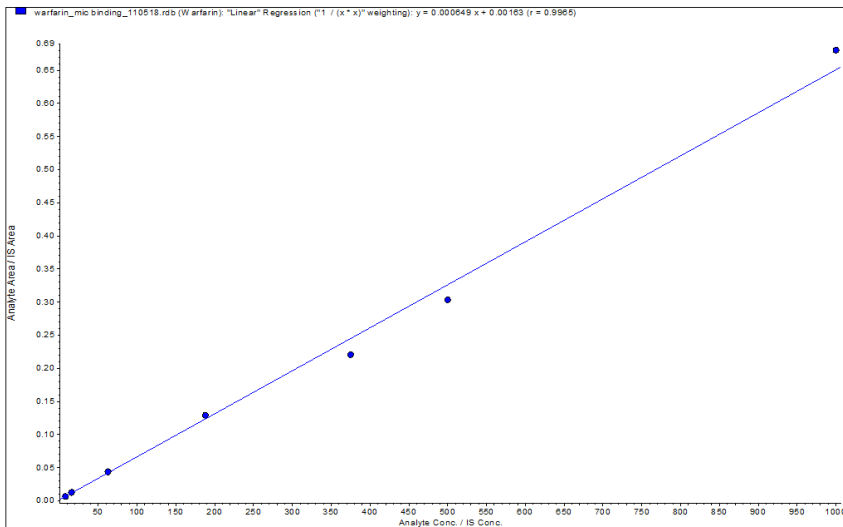
Representative standard curve for nafcillin in RLM, with diltiazem used as an internal standard.

# Warfarin

## Representative chromatogram



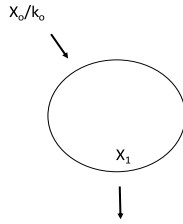
Representative chromatogram for warfarin (red) in RLM, with diltiazem (blue) used as an internal standard.



Representative standard curve for warfarin in RLM, with diltiazem used as an internal standard.

## APPENDIX E: COMPARTMENTAL MODELS

### One-compartment model



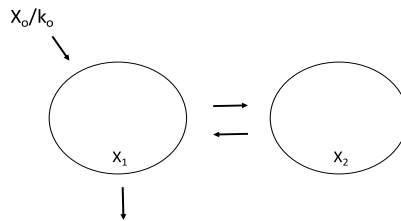
Differential Equations (IV Bolus)

$$\frac{dX_1}{dt} = -k_{10} X_1$$

Differential Equations (IV Infusion)

$$\frac{dX_1}{dt} = k_o - k_{10} X_1$$

### Two-compartment model



Differential Equations (IV Bolus)

$$\frac{dX_1}{dt} = k_{21}X_2 - (k_{12}+k_{10}) X_1$$

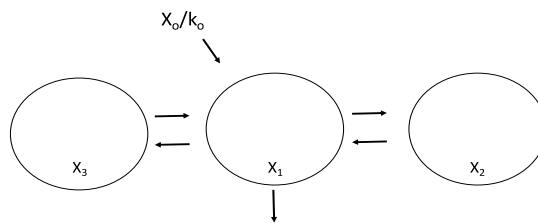
$$\frac{dX_2}{dt} = k_{12}X_1 - k_{21}X_2$$

Differential Equations (IV Infusion)

$$\frac{dX_1}{dt} = k_o - (k_{12}+k_{10}) X_1 + k_{21}X_2$$

$$\frac{dX_2}{dt} = k_{12}X_1 - k_{21}X_2$$

### Three-compartment model



Differential Equations (IV Bolus)

$$\frac{dX_1}{dt} = k_{21}X_2 + k_{31}X_3 - (k_{13} + k_{12} + k_{10}) X_1$$

$$\frac{dX_2}{dt} = k_{12}X_1 - k_{21}X_2$$

$$\frac{dX_3}{dt} = k_{13}X_1 - k_{31}X_3$$

Differential Equations (IV Infusion)

$$\frac{dX_1}{dt} = k_o - (k_{13} + k_{12} + k_{10}) X_1 + k_{21}X_2 + k_{31}X_3$$

$$\frac{dX_2}{dt} = k_{12}X_1 - k_{21}X_2$$

$$\frac{dX_3}{dt} = k_{13}X_1 - k_{31}X_3$$

## APPENDIX F: PHYSIOLOGICAL PARAMETERS

All tissue composition literature data and plasma/blood physiological parameters were obtained from the literature (Brown et al., 1997; Poulin and Theil, 2002; Fenneteau et al., 2010; Ye et al., 2016).

Table 14: Tissue composition literature data.

	Blood Flow rate (L/min)	Tissue Volume (L)	Fractional tissue volume				Intracellular water	Extracellular water	Tissue Conc. Of Acidic phospholipids (mg/g)	Albumin Ratio	Lipoprotein Ratio
			Neutral Lipids	Phospholipids	Neutral Phospholipids						
Adipose	0.296	12.46	0.853	0.002	0.00160	0.153	0.0170	0.400	0.0490	0.0680	
Bone and Rest	0.563	15.52	0.0170	0.00287	0.00170	0.100	0.346	0.670	0.100	0.0500	
Brain	0.683	1.40	0.0390	0.0019	0.00150	0.162	0.620	0.400	0.0480	0.0410	
Gut	0.967	1.20	0.0380	0.0148	0.0125	0.282	0.475	2.41	0.158	0.141	
Heart	0.228	0.330	0.0140	0.0129	0.0111	0.320	0.456	2.25	0.157	0.160	
Kidney	1.08	0.310	0.0120	0.029	0.0242	0.273	0.483	5.03	0.130	0.137	
Liver	1.42	1.82	0.0140	0.0284	0.0240	0.161	0.573	4.56	0.0860	0.161	
Lung	5.69	0.530	0.0220	0.0162	0.0128	0.336	0.446	3.91	0.212	0.168	
Muscle	1.08	28.0	0.0100	0.0093	0.00720	0.118	0.630	1.53	0.0640	0.0590	
Skin	0.330	2.59	0.0600	0.0093	0.00440	0.382	0.291	1.32	0.277	0.0960	
Spleen	0.114	0.168	0.00770	0.01388	0.0113	0.207	0.579	3.18	0.097	0.207	
Blood Cell			0.00170	0.0034	0.00290		0.603	0.5	0.500		

Table 15: Plasma and blood physiological parameters.

	value
pH plasma	7.4
pH intracellular fluid	7.0
pH blood cell	7.22
Hematocrit	0.45
Fractional tissue volume: intracellular water	0.603
Tissue Conc. Of Acidic phospholipids (mg/g)	0.5
Fractional tissue volume: neutral phospholipids	0.00290
Fractional tissue volume: neutral lipids	0.00170
Fractional tissue volume: phospholipids	0.0034
Tissue volume: arterial blood (L)	1.89
Tissue volume: venous blood (L)	3.78

APPENDIX G: DRUG SPECIFIC PARAMETERS

Reproduced with permission from *Drug Metabolism and Disposition, Prediction of tissue - plasma partition coefficients using microsomal partitioning: Incorporation into physiologically-based pharmacokinetic models and steady state volume of distribution predictions*, 47, 12, 1050-1060. Copyright 2019 The American Society for Pharmacology and Experimental Therapeutics.

Table 16: Drug specific parameters (Holt et al. 2019b).

Compound	Class <sup>a</sup>	f <sub>up</sub> (n=4) <sup>b</sup>	f <sub>um</sub> (n=4) <sup>b</sup>	logP	Pk <sub>a,a</sub>	Pk <sub>a,b</sub>	BP	LogD <sub>vo</sub>	CL (L/h)	References
Betaxolol	B	0.50 (12%)	0.77 (3%)	2.81	14	9.4	2 <sup>c</sup>	1.78	10.2	(Riddell et al., 1987; Recanatini, 1992; Rodgers and Rowland, 2007)
Diltiazem	B	0.26 (8%)	0.48 (2%)	2.7	14	7.7	1	1.88	97.5	(Rekker and Mannhold, 1992; Obach, 1999; Ishihama et al., 2002)
Diphenhydramine	B	0.44 (4%)	0.84 (4%)	3.27	14	8.98	0.74	2.30	43	(Albert et al., 1975; Sangster, 1994; Hansch et al., 1995; Obach, 1999)
Metoprolol	B	0.87 (17%)	0.80 (3%)	1.88	14	9.7	1.14	0.746	58.8	(Hansch et al., 1995; Rodgers and Rowland, 2007)
Mibefradil	B	0.031 (11%)	0.034 (15%)	3.07	14	10.2	0.64	2.07	15.5	(Welker et al., 1998; Nagar and Korzekwa, 2017)
Nicardipine	B	0.0024 (7%)	0.039 (12%)	3.82	14	8.6	0.71	2.90	31.2	(Sangster, 1993; Rodgers and Rowland, 2007)
Quinidine	B	0.15 (8%)	0.815 (10%)	3.52	14	8.94	0.92	2.07	14	(Sangster, 1994; Obach, 1999; Nagar and Korzekwa, 2017)
Verapamil	B	0.088 (20%)	0.37 (19%)	3.79	14	8.92	0.74	2.88	49	(Sangster, 1994; Hansch et al., 1995; Robinson and Mehvar, 1996; Obach, 1999)

Table 16 continued.

Compound	Class <sup>a</sup>	f <sub>up</sub> (n=4) <sup>b</sup>	f <sub>um</sub> (n=4) <sup>b</sup>	logP	PK <sub>a,a</sub>	PK <sub>a,b</sub>	BP	LogD <sub>vo</sub>	CL (L/h)	References
Caffeine	N	0.72 <sup>d</sup>	0.98 (6%)	- 0.07	14	1.04	1.01	-1.43	5.2	(Hansch et al., 1995; Rodgers and Rowland, 2007)
Diazepam	N	0.012 (9%)	0.74 (4%)	2.82	14	3.4	0.64	1.79	1.33	(Maguire et al., 1980; Sangster, 1993; O'Neil, 2006)
Felodipine	N	0.0017 (12%)	0.023 (27%)	3.86	14	5.07	0.7	2.95	41.7	(Diez et al., 1991; Uchimura et al., 2010; Pandey et al., 2013)
Fluconazole	N	0.93 (14%)	0.94 (14%)	0.8	14	1.77	1	-0.79	1.25	(Debruyne et al., 1987; Debruyne, 1997; Rodgers and Rowland, 2007)
Midazolam	N	0.033 (4%)	0.71 (4%)	3.15	14	6.01	0.53	2.16	18	(Heizmann et al., 1983; Rodgers and Rowland, 2007)
Phenytoin	N	0.18 (7%)	0.83 (3%)	2.21	8.32	1	0.61	1.11	1.61	(Stella et al., 1998; Brittain, 2007; Uchimura et al., 2010)
Diclofenac	A	0.0014 (18%)	0.78 (4%)	4.51	4.15	1	0.55	3.68	17.6	(Sangster, 1994; Obach, 1999; Avdeef, 2003)
Glyburide	A	0.0012 (16%)	0.72 (9%)	4.29	5.38	1	0.57	2.59	4.81	(Austin et al., 2002; Li et al., 2017)
Ketoprofen	A	0.0041 (9%)	0.95 (4%)	3.12	4.45	1	0.56	2.06	5.02	(Sangster, 1993; Sangster, 1994; Rodgers and Rowland, 2007; Ye et al., 2016)
Nafcillin	A	0.123 (6%)	0.94 (14%)	2.7	2.6	1	0.55 <sup>e</sup>	1.66	33.9	(Wishart et al., 2018)
Warfarin	A	0.0076 (13%)	0.98 (16%)	2.7	5.05	1	0.55	1.66	0.179	(Hiskey et al., 1962; Hansch et al., 1995; Obach, 1999)

<sup>a</sup> Bases - B, Acids - A, Neutral - N. <sup>b</sup>All experimental values unless otherwise noted. <sup>c</sup> Rat BP was used. <sup>d</sup> An average of literature values was used. <sup>e</sup>0.55 was used (1-hematocrit).

## APPENDIX H: CLINICAL DATA

Table 17: Clinical data from the literature.

Name	Class <sup>a</sup>	Type	subjects	Wt	Dose	duration	Points	V <sub>ss</sub>	CL	Reference
				kg	mg	minutes	#	L	L/h	
Betaxolol	B	infusion	n=10	73.6	8.94	30	17	360	11	(Ludden et al., 1988)
Diltiazem	B	infusion	n=12	63	15	30	13	306	97	(Hermann et al., 1983)
Diphenhydramine	B	bolus	n=8	98.0	56	n/a	12	788	43	(Scavone et al., 1990)
Metoprolol	B	infusion	n=5	66	3.9	10	20	274	59	(Regårdh et al., 1974)
Mibefradil	B	Infusion	n=6	70 <sup>c</sup>	20	30	16	187	17	(Clozel et al., 1991)
Nicardipine	B	bolus	n=6 <sup>b</sup>	67.0	10	n/a	12	62	76	(Campbell et al., 1985)
Quinidine	B	infusion	n=12 <sup>b</sup>	65.3	244	22	12	227	18.5	(Ueda et al., 1976)
Verapamil	B	infusion	n=20	70 <sup>c</sup>	10	5	15	266	49	(McAllister and Kirsten, 1982)
Caffeine	N	infusion	n=10	79.5	350	30	17	42.8	5.2	(Blanchard and Sawers, 1983)
Diazepam	N	infusion	n=24	78.1	5	1	21	89.5	1.33	(Agarwal et al., 2013)
Felodipine	N	infusion	n=10	74	2.5	30	22	320	41.7	(Edgar et al., 1985)
Fluconazole	N	infusion	n=6	70 <sup>c</sup>	50	n/a	13	59.3	1.25	(Ripa et al., 1993)
Midazolam	N	bolus	n=6	67.6	10	n/a	15	51.2	18	(Heizmann et al., 1983)
Phenytoin	N	infusion	n=6	78.1	275	6	15	38.8	1.76	(Gugler et al., 1976)
Diclofenac	A	infusion	n=6	65	46.5	2	15	9.23	17.6	(Willis et al., 1980)
Glyburide	A	infusion	n=10	77.8	2	60	19	11.78	4.88	(Debruyne et al., 1987)
Ketoprofen	A	bolus	n=7	70 <sup>c</sup>	100	n/a	12	9.9	5.02	(Debruyne et al., 1987)
Nafcillin	A	infusion	n=6	70 <sup>c</sup>	475	7	9	20.4	33.9	(Waller et al., 1982)
Warfarin	A	bolus	n=6	66.8	100	n/a	8	7.66	.179	(O'Reilly et al., 1971)

<sup>a</sup> Bases - B, Acids - A, Neutral - N; <sup>b</sup> Individual C-t not provided. C-t profile simulated from average parameters. <sup>c</sup> Individual weights not provided, and 70 kg assumed.

APPENDIX I: DIFFERENTIAL EQUATIONS FOR PBPK MODEL

$$\frac{dC_{lung}}{dt} = Q_c \frac{C_{vp} BP - C_{lung} \frac{BP}{K_{p, lung}}}{V_{t, lung}}$$

$$\frac{dC_{adipose}}{dt} = Q_{adipose} \frac{C_{ab} - C_{adipose} \frac{BP}{K_{p, adipose}}}{V_{t, adipose}}$$

$$\frac{dC_{bone}}{dt} = Q_{bone} \frac{C_{ab} - C_{bone} \frac{BP}{K_{p, bone}}}{V_{t, bone}}$$

$$\frac{dC_{brain}}{dt} = Q_{brain} \frac{C_{ab} - C_{brain} \frac{BP}{K_{p, brain}}}{V_{t, brain}}$$

$$\frac{dC_{heart}}{dt} = Q_{heart} \frac{C_{ab} - C_{heart} \frac{BP}{K_{p, heart}}}{V_{t, heart}}$$

$$\frac{dC_{kidney}}{dt} = Q_{kidney} \frac{C_{ab} - C_{kidney} \frac{BP}{K_{p, kidney}}}{V_{t, kidney}}$$

$$\frac{dC_{muscle}}{dt} = Q_{muscle} \frac{C_{ab} - C_{muscle} \frac{BP}{K_{p, muscle}}}{V_{t, muscle}}$$

$$\frac{dC_{spleen}}{dt} = Q_{spleen} \frac{C_{ab} - C_{spleen} \frac{BP}{K_{p, spleen}}}{V_{t, spleen}}$$

$$\frac{dC_{gut}}{dt} = Q_{gut} \frac{C_{ab} - C_{gut} \frac{BP}{K_{p, gut}}}{V_{t, gut}}$$

$$\frac{dC_{skin}}{dt} = Q_{skin} \frac{C_{ab} - C_{skin} \frac{BP}{K_{p, skin}}}{V_{t, skin}}$$

$$\frac{dC_{rob}}{dt} = Q_{rob} \frac{C_{ab} - C_{rob} \frac{BP}{K_{p,rob}}}{V_{t,rob}}$$

$$\frac{dC_{ab}}{dt} = Q_c \frac{C_{lung} \frac{BP}{K_{p,lung}} - C_{ab}}{V_{t,ab}}$$

$$\begin{aligned} \frac{dC_{vp}}{dt} BP = & (Q_{adipose} C_{adipose} \frac{BP}{K_{p,adipose}} + Q_{bone} C_{bone} \frac{BP}{K_{p,bone}} + Q_{brain} C_{brain} \frac{BP}{K_{p,brain}} \\ & + Q_{heart} C_{heart} \frac{BP}{K_{p,heart}} + Q_{kidney} C_{kidney} \frac{BP}{K_{p,kidney}} \\ & + Q_{muscle} C_{muscle} \frac{BP}{K_{p,muscle}} + Q_{rob} C_{rob} \frac{BP}{K_{p,rob}} + Q_{liver} C_{liver} \frac{BP}{K_{p,liver}} \\ & + Q_{skin} C_{skin} \frac{BP}{K_{p,skin}} + k_0 - Q_c C_{vp}) / V_{t,vp} \end{aligned}$$

APPENDIX J: BODIPY QUANTITATION METHODS

Table 18: BODIPY quantitation method 1.

Compound**	Cell Type*	Quantitation Method 1		
		Intensity Cytoplasm Neutral Lipids Mean - Mean per Well	Cell Region Area [ $\mu\text{m}^2$ ] - Mean per Well	Mean Intensity * Area
Q	undiff_cell	2.10E+03	2.32E+03	4.85E+06
Q	undiff_cell	1.58E+03	6.89E+03	1.09E+07
Q	undiff_cell	1.78E+03	1.15E+04	2.05E+07
Q	undiff_cell	1.58E+03	7.77E+03	1.23E+07
B	undiff_cell	1.61E+03	5.18E+03	8.34E+06
C	undiff_cell	1.80E+03	6.93E+03	1.25E+07
C	undiff_cell	2.36E+03	3.15E+03	7.45E+06
C	diff_cell	4.48E+03	1.10E+05	4.93E+08
C	diff_cell	4.38E+03	1.11E+05	4.88E+08
C	diff_cell	4.32E+03	1.07E+05	4.61E+08
C	diff_cell	4.90E+03	1.08E+05	5.29E+08
C	undiff_cell	2.06E+03	6.11E+03	1.26E+07
C	undiff_cell	2.16E+03	6.17E+03	1.33E+07
F	diff_cell	4.37E+03	1.04E+05	4.57E+08
F	diff_cell	4.18E+03	1.07E+05	4.47E+08
F	diff_cell	3.96E+03	1.06E+05	4.20E+08
F	diff_cell	4.50E+03	1.02E+05	4.57E+08
F	undiff_cell	1.72E+03	9.95E+03	1.72E+07
F	undiff_cell	1.92E+03	8.52E+03	1.63E+07
D	diff_cell	4.52E+03	1.06E+05	4.82E+08
D	diff_cell	4.59E+03	1.11E+05	5.08E+08
D	diff_cell	4.74E+03	1.06E+05	5.00E+08
D	diff_cell	5.20E+03	1.06E+05	5.52E+08
F	undiff_cell	1.83E+03	1.07E+04	1.95E+07
F	undiff_cell	1.81E+03	1.36E+04	2.46E+07
M	diff_cell	4.21E+03	1.02E+05	4.31E+08

Table 18 continued.

Compound**	Cell Type*	Quantitation Method 1		
		Intensity Cytoplasm Neutral Lipids Mean - Mean per Well	Cell Region Area [ $\mu\text{m}^2$ ] - Mean per Well	Mean Intensity * Area
M	diff_cell	4.47E+03	1.03E+05	4.58E+08
M	diff_cell	4.38E+03	1.07E+05	4.68E+08
M	diff_cell	4.73E+03	1.01E+05	4.77E+08
D	undiff_cell	1.87E+03	1.84E+04	3.44E+07
D	undiff_cell	1.81E+03	1.44E+04	2.60E+07
Q	diff_cell	4.23E+03	1.02E+05	4.32E+08
Q	diff_cell	4.04E+03	1.01E+05	4.06E+08
Q	diff_cell	4.23E+03	9.69E+04	4.10E+08
Q	diff_cell	4.18E+03	1.04E+05	4.35E+08
D	undiff_cell	1.75E+03	1.11E+04	1.93E+07
D	undiff_cell	1.63E+03	1.83E+04	2.99E+07
B	diff_cell	4.10E+03	1.02E+05	4.18E+08
M	undiff_cell	1.96E+03	4.36E+03	8.57E+06
M	undiff_cell	1.86E+03	5.13E+03	9.54E+06
M	undiff_cell	3.09E+03	1.39E+03	4.29E+06
M	undiff_cell	1.47E+03	8.11E+03	1.19E+07

\*diff\_cell: differentiated 3T3-L1 cells, undiff\_cell: undifferentiated 3T3-L1 cells.  
 \*\*M: midazolam, C: caffeine, B: blank, D: diclofenac, Q: quinidine, F: felodipine

Table 19: BODIPY quantitation method 2.

Compound**	Cell Type*	Quantitation Method 2		
		Intensity Cytoplasm Neutral Lipids Mean - Mean per Well	Cell Region Area [ $\mu\text{m}^2$ ] - Mean per Well	Mean Intensity * Area
Q	undiff_cell	9.98E+02	3.79E+04	3.78E+07
Q	undiff_cell	9.23E+02	6.29E+04	5.81E+07
Q	undiff_cell	1.01E+03	8.60E+04	8.71E+07
Q	undiff_cell	9.77E+02	5.08E+04	4.96E+07
B	undiff_cell	8.68E+02	6.76E+04	5.86E+07
C	undiff_cell	9.61E+02	7.48E+04	7.18E+07
C	undiff_cell	1.16E+03	3.48E+04	4.04E+07
C	diff_cell	3.14E+03	2.61E+05	8.21E+08
C	diff_cell	3.08E+03	2.62E+05	8.06E+08
C	diff_cell	3.00E+03	2.51E+05	7.55E+08
C	diff_cell	3.42E+03	2.44E+05	8.35E+08
C	undiff_cell	1.07E+03	6.46E+04	6.91E+07
C	undiff_cell	1.09E+03	5.61E+04	6.13E+07
F	diff_cell	3.00E+03	2.61E+05	7.83E+08
F	diff_cell	2.95E+03	2.53E+05	7.45E+08
F	diff_cell	2.73E+03	2.57E+05	7.02E+08
F	diff_cell	3.18E+03	2.35E+05	7.48E+08
F	undiff_cell	1.02E+03	7.62E+04	7.74E+07
F	undiff_cell	1.10E+03	7.36E+04	8.12E+07
D	diff_cell	3.13E+03	2.52E+05	7.90E+08
D	diff_cell	3.28E+03	2.45E+05	8.04E+08
D	diff_cell	3.30E+03	2.39E+05	7.88E+08
D	diff_cell	3.77E+03	2.24E+05	8.44E+08
F	undiff_cell	1.02E+03	8.84E+04	9.00E+07
F	undiff_cell	1.04E+03	9.83E+04	1.03E+08
M	diff_cell	2.85E+03	2.63E+05	7.47E+08
M	diff_cell	3.18E+03	2.34E+05	7.43E+08
M	diff_cell	3.10E+03	2.48E+05	7.70E+08
M	diff_cell	3.40E+03	2.26E+05	7.68E+08

Table 19 continued.

Compound**	Cell Type*	Quantitation Method 2		
		Intensity Cytoplasm Neutral Lipids Mean - Mean per Well	Cell Region Area [ $\mu\text{m}^2$ ] - Mean per Well	Mean Intensity * Area
D	undiff_cell	1.11E+03	1.06E+05	1.18E+08
D	undiff_cell	1.07E+03	9.43E+04	1.01E+08
Q	diff_cell	2.95E+03	2.50E+05	7.38E+08
Q	diff_cell	2.84E+03	2.48E+05	7.04E+08
Q	diff_cell	2.87E+03	2.43E+05	6.95E+08
Q	diff_cell	2.98E+03	2.48E+05	7.37E+08
D	undiff_cell	1.08E+03	5.99E+04	6.45E+07
D	undiff_cell	9.95E+02	8.57E+04	8.52E+07
B	diff_cell	2.77E+03	2.58E+05	7.13E+08
M	undiff_cell	9.79E+02	4.69E+04	4.59E+07
M	undiff_cell	9.60E+02	5.68E+04	5.46E+07
M	undiff_cell	1.51E+03	1.79E+04	2.71E+07
M	undiff_cell	8.74E+02	7.12E+04	6.22E+07

\*diff\_cell: differentiated 3T3-L1 cells, undiff\_cell: undifferentiated 3T3-L1 cells.

\*\*M: midazolam, C: caffeine, B: blank, D: diclofenac, Q: quinidine, F: felodipine

Table 20: BODIPY quantitation method 3.

Compound**	Cell Type*	Quantitation Method 3		
		Intensity Cytoplasm Neutral Lipids Mean - Mean per Well	Cell Region Area [ $\mu\text{m}^2$ ] - Mean per Well	Mean Intensity * Area
Q	undiff_cell	4.48E+03	1.10E+05	4.93E+08
Q	undiff_cell	4.38E+03	1.11E+05	4.88E+08
Q	undiff_cell	4.32E+03	1.07E+05	4.61E+08
Q	undiff_cell	4.90E+03	1.08E+05	5.29E+08
B	undiff_cell	4.37E+03	1.04E+05	4.57E+08
C	undiff_cell	4.18E+03	1.07E+05	4.47E+08
C	undiff_cell	3.96E+03	1.06E+05	4.20E+08
C	diff_cell	4.50E+03	1.02E+05	4.57E+08
C	diff_cell	4.52E+03	1.06E+05	4.82E+08
C	diff_cell	4.59E+03	1.11E+05	5.08E+08
C	diff_cell	4.74E+03	1.06E+05	5.00E+08
C	undiff_cell	5.20E+03	1.06E+05	5.52E+08
C	undiff_cell	4.21E+03	1.02E+05	4.31E+08
F	diff_cell	4.47E+03	1.03E+05	4.58E+08
F	diff_cell	4.38E+03	1.07E+05	4.68E+08
F	diff_cell	4.73E+03	1.01E+05	4.77E+08
F	diff_cell	4.23E+03	1.02E+05	4.32E+08
F	undiff_cell	4.04E+03	1.01E+05	4.06E+08
F	undiff_cell	4.23E+03	9.69E+04	4.10E+08
D	diff_cell	4.18E+03	1.04E+05	4.35E+08
D	diff_cell	4.10E+03	1.02E+05	4.18E+08
D	diff_cell	9.98E+02	3.79E+04	3.78E+07
D	diff_cell	9.23E+02	6.29E+04	5.81E+07
F	undiff_cell	1.01E+03	8.60E+04	8.71E+07
F	undiff_cell	9.77E+02	5.08E+04	4.96E+07
M	diff_cell	8.68E+02	6.76E+04	5.86E+07
M	diff_cell	9.61E+02	7.48E+04	7.18E+07
M	diff_cell	1.16E+03	3.48E+04	4.04E+07
M	diff_cell	1.07E+03	6.46E+04	6.91E+07

Table 20 continued.

Compound**	Cell Type*	Quantitation Method 3		
		Intensity Cytoplasm Neutral Lipids Mean - Mean per Well	Cell Region Area [ $\mu\text{m}^2$ ] - Mean per Well	Mean Intensity * Area
D	undiff_cell	1.09E+03	5.61E+04	6.13E+07
D	undiff_cell	1.02E+03	7.62E+04	7.74E+07
Q	diff_cell	1.10E+03	7.36E+04	8.12E+07
Q	diff_cell	1.02E+03	8.84E+04	9.00E+07
Q	diff_cell	1.04E+03	9.83E+04	1.03E+08
Q	diff_cell	1.11E+03	1.06E+05	1.18E+08
D	undiff_cell	1.07E+03	9.43E+04	1.01E+08
D	undiff_cell	1.08E+03	5.99E+04	6.45E+07
B	diff_cell	9.95E+02	8.57E+04	8.52E+07
M	undiff_cell	9.79E+02	4.69E+04	4.59E+07
M	undiff_cell	9.60E+02	5.68E+04	5.46E+07
M	undiff_cell	1.51E+03	1.79E+04	2.71E+07
M	undiff_cell	8.74E+02	7.12E+04	6.22E+07

\*diff\_cell: differentiated 3T3-L1 cells, undiff\_cell: undifferentiated 3T3-L1 cells.

\*\*M: midazolam, C: caffeine, B: blank, D: diclofenac, Q: quinidine, F: felodipine